Gene therapy of Malignant Gliomas

Maarten ter Horst

Gene therapy of Malignant Gliomas

Gentherapie voor maligne gliomen

Proefschrift

ter verkrijging van de graad van doctor aan de
Erasmus Universiteit Rotterdam
op gezag van de
rector magnificus

Prof.dr. S.W.J. Lamberts

en volgens besluit van het College voor Promoties.

De openbare verdediging zal plaatsvinden op

woensdag 9 januari 2008 om 15.45 uur

door

Maarten ter Horst

geboren te Enschede

Promotiecommissie

Promotoren: Prof.dr. P.A.E. Sillevis Smitt
Prof.dr.ir. M. Hendriks-de Jong

Overige leden: Prof.dr. C.M.F. Dirven
Prof.dr. R.C. Hoeben
Prof.dr. E.P. Krenning

Copromotor: Dr. H.C.G.M. de Leeuw

Voor Manon

Contents

PART 1

Preface

CHAPTER 1

Introduction

1.1 Gliomas

Gliomas are the most frequent primary brain tumors in adults with an annual incidence of 5-10 per 100,000[1]. Three main types can be distinguished based on histological features: astrocytomas, oligodendrogliomas and mixed oligoastrocytomas. Analysis of the most malignant region of the tumor allows tumor grading (low grade or WHO grades I and II versus high grade or malignant, WHO grade III and IV) depending on the presence of increased cellularity, distinct nuclear atypia, marked mitotic activity, microvascular proliferation and necrosis[2]. The highest grade (WHO grade IV) is known as glioblastoma multiforme (GBM). In general, malignant gliomas are treated by a combination of surgery, radiation therapy, and chemotherapy. Despite advances in all these treatment modalities, the overall median survival of patients remains less than 1 year and fewer than 5% survive for 5 years or longer[3,4]. Recently, a phase 3 trial in GBM showed that the addition of concomitant and adjuvant temozolomide to initial radiotherapy significantly increased the 2-year survival from 10 to 27%[5]. However, eventually all malignant gliomas will recur after initial treatment. Because m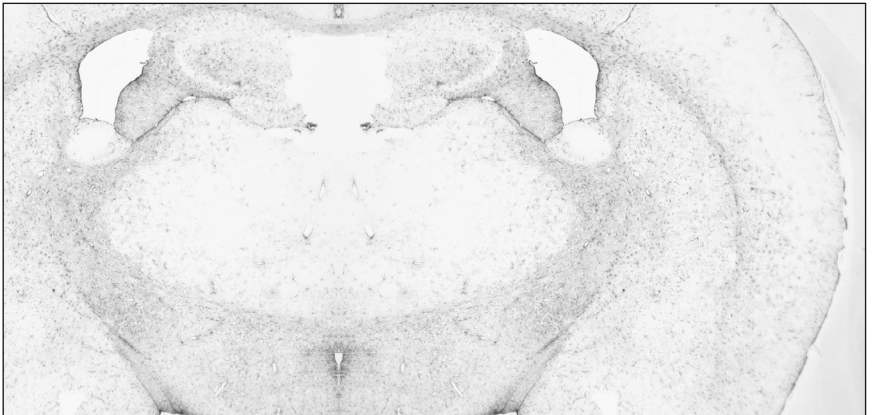ore than 80% of these tumors recur within a 2-3 cm margin of the original lesion[6], loco-regional treatment strategies, such as gene therapy, can possibly prolong survival and improve quality of life.

1.2 Gene Therapy

Gene therapy intends to deliver and express exogenous genetic material in cells, for therapeutic purposes and for basic scientific studies. Interest in gene therapy expanded with the identification of diseases caused by defects in single genes and the application of recombinant DNA technology to genetically modify viruses[7]. Indeed, the first clinical gene therapy trials focused on viral delivery of genes into human cells, affected by single-gene defects, such as ADA-SCID[8], cystic fibrosis, hemophilia, muscular dystrophy and sickle cell anemia[7].

In general, gene delivery can be accomplished by viral and non-viral vectors. Advantages of non-viral vectors include low cytotoxicity, low immunogenicity, no size limit and ease of preparation and scale-up[9,10]. However, the efficacy of non-viral delivery is severely hampered by poor cellular uptake[11], inefficient trafficking through the cytoplasm and crossing of the nuclear membrane and rapid nuclease-mediated degradation. In order to improve cellular uptake, non-viral vectors can be combined with carriers such as liposomes, proteins, nanoparticles or synthetic agents that mask the strong negative charge of the DNA and facilitate uptake over membranes[12].

In clinical gene therapy, the main advantages of viral over non-viral vector systems are the high level of gene transfer and the high expression levels of the transgenes that can be accomplished by the former. However, viral vector systems are much more difficult and expensive to produce and they raise greater safety issues. Attributable to the efficient gene transfer, viral vectors are most commonly used in clinical trials, in particular adenoviral and retroviral vectors[13]. Other vectors used for gene therapy, mainly in preclinical studies, include the Herpes Simplex virus type 1 (HSV-1)[14], adeno-associated virus (AAV)[15], New Castle disease virus[16], Semliki Forest virus[17], vaccinia virus[18], poliovirus[19], reovirus[20] and myxomavirus[21].

In cancer gene therapy, many therapeutic genes have been applied. Following transfection of malignant cells and subsequent expression, most of these transgenes will increase the susceptibility of the malignant cell to any form of destruction or will restore a normal growth pattern. Therapeutic genes that have been used in experimental and clinical studies include genes encoding for cytokines (e.g. tumor necrosis factor (TNF), granulocyte macrophage colony stimulating factor (GM-CSF), interleukine-2 (IL-2), interleukine-4 (IL-4))[14], tumor suppressor genes (e.g. p53)[22] and suicide genes (e.g. herpes simplex virus- thymidine kinase (HSV-tk), cytosine deaminase (CD), nitroreductase or cytochrome P450)[23]. In malignant glioma the most commonly used transgene in clinical trials so far is HSV-tk. Tumor cells transduced with the HSV-tk gene will express the thymidine kinase enzyme leading to the selective phosphorylation of several nucleoside analogues including ganciclovir (GCV). After phosphorylation of GCV to its monophosphate form (GCV-MP), it is further phosphorylated by cellular kinases to diphosphate (GCV-DP) and triphosphate (GCV-TP). GCV-TP inhibits DNA polymerase I and is incorporated into the elongating DNA strand resulting in chain termination and cell death[24-26].

The efficacy of HSV-tk 'suicide' gene therapy is enhanced by the bystander effect, whereby non-transduced tumor cells are also killed by transfer of toxic metabolites through gap junctions[27], induction of apoptosis[28], killing of tumor endothelial cells[29] and activation of a host immune response[30].

In the mid 1990s, the first clinical gene therapy trials in malignant gliomas were initiated, using replication-deficient retroviruses to introduce the HSV-tk suicide gene into glioma cells. After this approach appeared save, a large phase 3 study was conducted in newly diagnosed GBM patients[31]. Patients received either standard therapy (surgical resection followed by radiotherapy) or standard therapy plus adjuvant gene therapy during surgery. No significant difference was found between the two groups, probably due to very low transduction efficiency in vivo[32,33]. Based on these results, no further retrovirus mediated HSV-tk gene therapy trials have been conducted in malignant glioma patients.

Adenovirus is another commonly used vector for gene therapy. Advantages of adenoviral vectors in cancer gene therapy include the relatively easy production of high titer batches for clinical use, large insert capacity (7-30 kb, depending on the adenoviral vector used), the ability to transduce dividing and non-dividing cells, lack of integration into the host genome and favorable safety profile in terms of both mild patient toxicity and limited if any shedding[34]. These features have led to adenoviral-mediated gene therapy for several cancers including gliomas, ovarian, prostate, head and neck, and bladder cancer and other tumors[35-37].

1.2.1 Adenoviral gene therapy in malignant glioma

After encouraging results in preclinical studies, several phase I-II clinical trials were conducted with adenovirus serotype 5 (Ad5)-mediated HSV-tk suicide gene therapy in malignant gliomas[35,38-42] (Table 1). These trials have clearly demonstrated the feasibility and safety of this approach. Taking six[35,38-42] studies together, twenty-six of 70 patients (39%) lived one year or more, indicating some efficacy, although patient selection bias cannot be excluded.

Despite the excellent safety record of adenoviral vectors and preliminary evidence of some efficacy, several hurdles have been identified that limit their efficacy. First, the expression level of the Coxsackie Adenovirus receptor (CAR), the high-affinity receptor for adenoviral

Table 1. Clinical adenovirus mediated gene therapy trials in malignant gliomas.

Authors and phase study	No. of patients	Treatment gene and dose	Main adverse events	Treatment response	Median survival (months)
Sandimar[41] Phase IIa	21	HSV-tk, 3×10^{10} pfu/10ml	↑ anti-Ad antibody and seizures; low grade fever	↑ Ad.HSV-tk survival time 2 fold (p<0.012)	14
Trask[40] Phase I	12	HSV-tk, up to 2×10^{12} vp, 1 ml	↑confusion, seizures; hyponatremia	3 responders, survival ≥25 months	4
Eck[38] Phase I	13	HSV-tk, 2×10^{8}-10^{11} pfu	↑intracranial pressure with headache; altered mental status	5 responders, survival ≥12 months	10
Germano[39] Phase I	11	HSV-tk, up to 9×10^{11} vp, 1 ml	none	2 responders, tumor control in MRI ≥12 months	10.4
Sillevis Smitt[35] Phase I	14	HSV-tk, up to 4.6×10^{11} vp/ 10 ml	none	No anti-tumor respons	4
Immonen[42] Phase IIb	36	HSV-tk, 3×10^{10} pfu/ 10 ml	↑ anti-Ad antibody; local postoperative edema	↑ Ad.HSV-tk survival time 81% (p<0.0095)	14.4
Lang[44] Phase I	15	p53, up to 3×10^{12} vp, 1-5 ml	Mild headache, fatigue, and fever	5 responders tumor control in MRI ≥6 months	10
Chiocca[48] Phase I	24	Replication selective mutant (ONYX-015), 10^{7}-10^{10} pfu, 1 ml	none	No definitive anti-tumor response	6.2

cell binding, is reduced on glioma cells in vivo resulting in low transduction efficiency[43]. Secondly, following injection into a brain tumor the lateral spread of adenoviral vectors into the surrounding brain is limited to on average 5 mm from the catheter tract[44]. Finally, the high prevalence of neutralizing antibodies (NAb) against Ad5 hampers the infection efficiency following systemic and local administration[45-47].

In order to enhance adenoviral-mediated gene therapy several advances have been made that resulted in animal models in a) improvement of infection efficiency by retargeting the virus to other receptors than CAR; b) improvement of lateral spread and direct oncolytic effect by creation of selectively replicating adenoviruses; and c) development of alternative routes of adenoviral delivery.

1.2.2   Retargeting

Adenovirus infection is mediated by binding of the fiber knob region to the receptor of the target cell, which is CAR for most serotypes, including the most commonly used serotype 5 (Ad5)[49]. Internalization of the virus is mediated by the interaction of a penton-base Arg-Gly-Asp (RGD) motif and cellular $\alpha_V\beta$ integrins[49], which leads to endocytosis of the virion via clathrin-coated pits (Fig. 1). After endocytosis the vesicular pH drops due to the acidification by proton pumps and at pH 6.0, the virus penetrates the endosomal membrane, escapes to the cytosol[50] and translocates along microtubule tracks to the nucleus where viral genes or transgenes are transcribed. Recently, it has been suggested that expression of CAR is a rate limiting factor for the infectivity with Ad5[51]. Tumor cells expressing low levels of CAR are resistant to Ad5 infection and to efficient oncolysis by replicating Ad5[52]. Gliomas, like many other tumors express low levels of CAR[43,47,53]. Therefore, modifications in adenoviruses are required to improve the infection efficiency. Currently, it is possible to use targeted viral
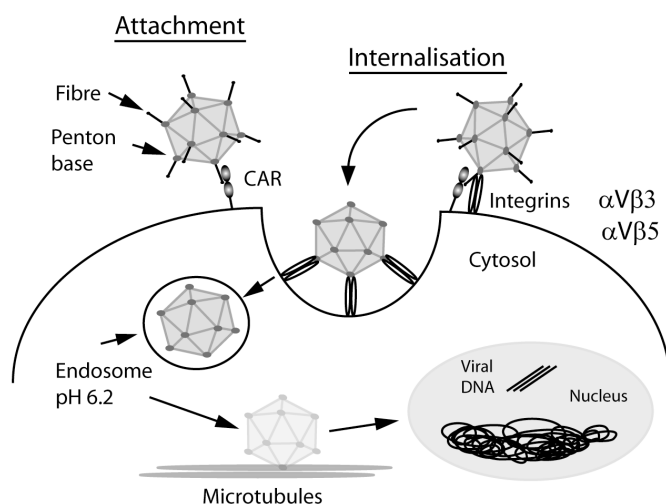
Fig. 1 Cell binding and entry of adenovirus serotype 5 (Ad5)

vectors to direct gene transfer to specific receptors. The use of targeted adenoviruses is likely to increase safety and efficacy, reduce toxicity and even permit systemic administration of these vectors[54].

One of the first successful genetic modifications of adenoviral tropism was the insertion of the RGD motif into the hexon protein, HI loop or C-terminus of the viral fiber protein[55-58]. This strategy improved adenoviral entry into cells, independent of CAR expression, but it did not enhance cancer specificity. Further attempts are being made to target adenovirus to receptors which are highly expressed on gliomas like epidermal growth factor receptor (EGFR), fibroblast growth factor receptor (FGFR) or urokinase-type plasminogen activator receptor (uPAR)[59-61].

Another strategy is the generation of chimeric adenoviral vectors by removing the fiber of Ad5 followed by the insertion of a PCR amplified DNA encoding for a fiber derived from an alternative serotype[62,63]. At present, 51 human Ad serotypes have been identified that are grouped into six species: A, B (subdivided in B1 and B2), C, D, E and F[64,65]. The association between serotype and clinical syndrome[66] suggests that diverse organs are targets for different serotypes. Although many adenoviral serotypes infect cells through CAR, other receptors have been described. Recently, CD46 was found to be the common receptor for subgroup B adenoviruses[67,68]. Since CD46 expression is very low on neurons[69] and because B-group adenoviral vectors infect glioma cells more efficiently than Ad5[47,70], several chimeric adenoviral vectors, carrying B-serogroup fibers have been examined for the treatment of brain tumors. Ulasov et al.[71] infected glioma cells with a chimeric Ad5/3 adenovirus, possessing the receptor binding fiber knob domain of Ad3 in the Ad5 capsid retargeting the virus to CD46, and showed increased transduction efficiency compared to Ad5 in glioma cells. Similarly, Brouwer et al. found increased transduction efficiency of Ad5-based chimeric vectors carrying B-serogroup fibers, following infection of primary glioma cells[47].

1.2.3   Conditionally Replicating Adenovirus (CRAds)

The first application of viral therapy goes back to the beginning of the 20th century. In 1904 Dock et al.[72] described the use of rabies virus vaccination in patients to treat cervical cancers. In 1953, adenovirus was isolated and three years later used for local injections into cervical cancers[73]. However, a low efficiency/toxicity ratio led to the abandonment of viral therapy in the 1970's. In the 1990's interest in gene therapy and viral vectors revived and expanded. Adenoviruses used in the initial clinical gene therapy trials carried a deletion in the E1 region which rendered the viral replication defective and heterologous genes were cloned instead of the E1 genes, usually under the control of a heterologous promoter[74]. In addition, viruses were constructed and clinically applied that were replication competent[75,76]. Those vectors necessarily contained and expressed the E1 region, either in its 'natural position'[75] or cloned elsewhere into the genome[77]. The theoretical advantages of viral therapy using

replication competent recombinant adenoviral vectors include a) a direct cytolytic effect on infected cells; b) subsequent lateral spread of virus to neighbouring cells, resulting in further tumor/tissue penetration; c) enhanced immune response; and d) because of the replication of adenovirus DNA, higher levels of expression of the therapeutic gene are achieved.

Conditionally replicative adenoviruses (CRAds) are replication competent adenoviral vectors generally designed to replicate selectively in tumor cells. Selective replication in tumor cells will not only increase the oncolytic efficacy but also limit toxicity to normal tissues, in particular the liver. Most CRAds are created by genetic engineering of the early-1 (E1) genes and/or their promoters. The major task of E1 proteins is to induce expression of subsequent viral genes, and to modify the cellular gene expression and protein activity to favor viral replication. Two strategies have been used to restrict virus replication to tumor cells and spare normal cells; a) mutation-type CRAds; and b) promoter-controlled-type CRAds.

Mutation-type CRAds have for instance deletions in the retinoblastoma gene (Rb)-binding region of E1A (e.g. the delta24 adenovirus[78]) or in the p53 binding and inactivation region of E1B (e.g. ONYX-015)[79,80] in order to increase the tumor specificity of viral replication. Delta24 is an adenovirus that contains a deletion of amino acids 122-129 in the conserved region (CR)2 of the E1A protein, comprising a 24 bp region in the viral genome and replicates specifically in cells with G1-checkpoint dysfunction due to inactivation of the Rb system[81]. ONYX-015 is an adenovirus that contains a 827 bp deletion in the E1B region (E1B55K coding region) and a point mutation at codon 2022 that generates a stop codon preventing expression of a truncated protein from residual portions of the E1B region. ONYX-015 can replicate in both tumor and non-cancer cells that lack functional p53, resulting in a cytopathic effect in tissues expressing an abnormal *TP53* gene, without damaging normal tissue. However, the mutations in the E1 genes generally decrease the efficiency of viral replication[78,82]. In addition, the stringency of replication control in these CRAds is still under discussion[83,84]. This approach will not further be addressed in this thesis.

Another approach is the use of tissue or tumor specific promoters (TTSP) to drive viral genes critical for replication, such as E1A, E1B or E4. Many well-characterized TTSP have been investigated in CRAds for cancer gene therapy[51,54,82]. Several CRAds controlled by TTSP have been examined in malignant glioma cells lines. These include the midkine (MK)[85], the cyclooxygenase-2 (COX-2)[86] and the hypoxia / hypoxia inducible factor (HIF) responsive promoters[87].

In this thesis the use of the glial fibrillary acidic protein (GFAP) promoter in an adenoviral context will be examined. GFAP is an intermediate-filament protein expressed abundantly and almost exclusively in glial cells of the central nervous system. A 2.2 kb 5'-flanking segment of the human GFAP gene, termed the gfa2 promoter, is sufficient to drive expression predominantly in astrocytes in transgenic mice[88]. We constructed gfa2-based promoters that carry additional copies of either the B region or of the co joined A, B and D regions

(ABD)[89]. Either one or three copies of these enhancer elements was placed just upstream of the basal promoter in gfa2 to yield the gfa2(B)$_1$, gfa2(B)$_3$, gfa2(ABD)$_1$ and gfa2(ABD)$_3$ promoters. We found that the gfa2 'super' promoters are useful for production of short-term, astrocyte-specific and high expression levels of therapeutic genes in an adenoviral context[89].

1.3 Delivery

In most current glioma gene therapy trials, viral vectors are delivered by direct intratumoral or wound bed injections[13,90]. The major obstacle is the limited tissue distribution following direct injections[44] caused by the rapid cellular uptake of vectors and their relatively large size (20-150 nm). In addition, small volumes and slow infusions are required to avoid compression damage[91]. Several strategies have been developed that may improve vector distribution.

1.3.1 Convection enhanced delivery

Convection enhanced delivery (CED) is based on continuous infusion of drugs via intracranial catheters, enabling convective distribution of high drug concentrations over large volumes of the target tissue[92]. CED has been successfully applied in clinical glioma trials to administer large molecules such as immunotoxins[93,94]. CED has also been used to deliver viral vectors to the brain.

   In experimental models, CED-mediated delivery resulted in improved transduction of the brain by adenovirus[95,96], AAV[97,98], and herpes simplex virus[99]. However, improved transduction was mainly related to an increase of the total amount of injected virus as compared to single injection.

   In this thesis adenoviral vector distribution by CED was compared with single injection and multiple injections at a constant virus titer[100].

1.3.2 Stem cells

In addition to totipotent embryonic stem cells, which can generate all cell types, tissue restricted stem cells have been identified in a variety of organs (e.g. brain, bone marrow, skin)[101]. Migration of stem cells may circumvent the limited tissue distribution of adenovirus. Bone-marrow derived mesenchymal stem cells and neural stem cells had prominent tropism for glioma cells following systemic injection[102-104]. Furthermore, when these cells are transfected with viral vectors to express antitumor transgenes, they migrated through brain parenchyma and reached glioma cells that otherwise would be inaccessible to therapy[103-105]. The use of stem cells as delivery vehicle for the treatment of malignant gliomas remains confined to the basic science laboratory though several groups are committed to translate this technology into clinical trials for patients with central nervous system neoplasms[106].

1.3.3 Opening BBB

Several groups have tried to improve the delivery of viral vectors by systemic administration in combination with disruption of the blood-brain barrier (BBB) or, more selectively, the blood-tumor barrier (BTB). Beside the limitations of the intact BBB and BTB, systemic vector delivery raises several important concerns including the accumulation of viral vectors in normal tissues (e.g. liver and lung) and immunogenic responses[107] that are beyond the scope of this thesis.

Global BBB disruption can be accomplished by administration of hypertonic agents, such as mannitol[106]. Liu et al.[108] studied intracarotid injection of oncolytic herpes simplex vectors after osmotic BBB disruption for the treatment of metastatic brain tumors in mice. They showed a significantly longer (p<0.02) survival of mice injected with HSV after BBB disruption with mannitol (mean survival 17.4 days) than HSV without BBB disruption (mean survival 14.1 days). Selective BTB disruption can be achieved by several vasoactive molecules including bradykinin and bradykinin analogues. Intracarotid injection of adenoviral vectors in 9L brain tumor bearing rats resulted in enhanced transgene expression following opening of the BTB with bradykinine[109]. Without BTB disruption, 3-9% of the tumors cells expressed the transgene in large tumor foci while after bradykinine administration expression was noticed in 12-32% (p<0.001).

1.4 Imaging

Over the last decade, molecular imaging techniques have achieved major improvements in gene expression imaging. Direct evaluation of gene expression is possible with, for example, contrast agents that bind directly to a specific target (e.g. receptor). Indirect evaluation may be achieved by using specific substrate probes for a target enzyme. Gene expression imaging will facilitate the monitoring and evaluation of gene therapy in vivo by defining the location, magnitude and persistence of gene expression in time[110]. The main gene imaging techniques will be discussed.

1.4.1 Radionuclide imaging

Positron emission tomography (PET) and single-photon emission computed tomography (SPECT) are based on non-invasive imaging of radionuclides. They are highly sensitive for the imaging probe (picomolar concentration) and are valuable for detecting protein markers with low expression levels[111]. PET can detect positron emitting radionuclides such as ^{11}C, ^{124}I or ^{18}F. Positrons emitted by the radionuclide are annihilated in tissue by merging with an electron. This merging results in emission of two high-energy photons which are detected by the PET detector array and used to reconstruct volumetric images of the concentration of

the positron-emitting probe[112]. SPECT acquires information on the concentration of single gamma ray emitting radionuclides such as ^{111}In, ^{123}I or ^{99m}Tc using a photon detector array similar to PET. One of the most significant differences between PET and SPECT is that position detection of the photons in SPECT does not convey adequate information about its origin or the direction it was traveling, resulting in a sensitivity that is typically several orders of magnitude lower than in a PET system[113]. In 'molecular imaging' of gene transfer, radiolabeled tracers are selectively retained as a result of expression of marker genes such as the human somatostatin receptor subtype 2 (sst$_2$)[100,114], genes encoding transporter proteins including the sodium/iodide symporter[115], or genes encoding enzymes that selectively metabolize the probe resulting in intracellular sequestration such as the herpes simplex virus type 1 thymidine kinase (HSV1-tk) gene[116-119].

Jacobs et al. used PET in combination with ^{124}I-labelled 2'-fluoro-2'-deoxy-1b-D-arabino-furanosyl-5-iodo-uracil ([^{124}I]-FIAU)-a specific marker substrate for gene expression of HSV-1-tk-to identify HSV-1-tk gene expression in a phase I/II clinical trial of gene therapy for recurrent GBM in five patients. The location, magnitude, and extent of vector-mediated HSV-1-tk gene expression could be monitored non-invasively by PET and seemed to predict the therapeutic response. Application of SPECT/PET in preclinical gene therapy studies in malignant gliomas, e.g. HSV1-tk imaging in small animals, provides in vivo response information and may reduce the number of animals required[120-122].

Furthermore, several radiolabeled tracers like 2-[^{18}F]fluoro-2 deoxy-D-glucose ([^{18}F]FDG), methyl-[^{11}C]-L-methionine ([^{11}C]MET) and 3'-[^{18}F]fluoro-L-thymidine ([^{18}F]FLT) are used for PET imaging in the clinic to assess quantitative information on the metabolic state of gliomas. These radiotracers are being incorporated into proliferating gliomas depending on their tumor grade as a reflection of increased activity of membrane transporters for glucose ([^{18}F]FDG), amino acids ([^{11}C]MET), and nucleosides ([^{18}F]FLT) as well increased expression of cellular hexokinase ([^{18}F]FDG) and thymidine kinase ([^{18}F]FLT)[123]. As surrogate markers for proliferation and tumor cell density they can be used to identify the biological active tumor portion and respons to therapy.

1.4.2 Optical imaging

Advantages of optical in vivo imaging include its "low cost" when compared to other approaches such as SPECT, PET or MRI and the high sensitivity (detection of probes in the picomolar range). Optical imaging visualizes reporter genes based on fluorescent or bioluminescent properties. In fluorescent approaches [e.g., green fluorescent protein (GFP)], an external light source is required for exciting the reporter protein. In contrast, the bioluminescent reporter protein (e.g. luciferase) generates light by catalyzing the appropriate administered substrate (e.g. luciferin). The biological use of cooled charge-coupled device

(CCD) cameras has subsequently enabled imaging of the very low levels of visible light emitted from internal body organs of rodents[124-128]. To date, Firefly luciferase, Renilla luciferase, bacterial luciferase, GFP and red fluorescent protein (RFP) are the reporter proteins that have been used most regularly for optical reporter gene imaging studies in living rodents[129,130].

Following injection of stably transfected and RFP-expressing tumor xenografts, optical computed and emission tomography could provide high-resolution 3D images in vivo, providing information on a variety of aspects of tumor structure and function[131]. So far, the application of optical imaging cannot be used as a general technique in humans due to attenuation of low-energy photons[132]. This, however, may change with the advent of near-infrared fluorescence (NIRF) imaging. NIRF imaging uses wavelengths in the 700- to 900-nm range, where the absorbance and autofluorescence spectra for water and biomolecules is minimal, thus allowing for efficient photon penetration of tissue with minimal intratissue light scattering. NIRF can propagate significant distances via multiple scattering, enabling imaging of deep (> 1 cm) tissues[133]. Recent advances have shown that NIRF imaging can be used to effectively monitor a variety of molecular targets including antigens[134] and cell surface receptors (e.g. EGFr binding EGF-Cy5.5 optical probe or $\alpha_v\beta$ integrins binding Cy5.5-linked cyclic arginine-glycine-aspartic acid (RGD) peptide)[135,136]

1.4.3 MRI

MRI has the advantage of very high spatial resolution (10-100µm in small animals), but offers only a milli- to micromolar sensitivity to most contrast agents. Therefore, amplification strategies are required for the detection of agents in the nanomolar concentration range.

For example, MRI imaging of expression of the transferrin receptor can be achieved by endocytotic internalization of supramagnetic substances, such as monocristalline iron oxide nanoparticles (MION)[137]. Genove et al. stereotactically injected an adenovirus encoding the transferrin receptor into mouse brain and observed robust contrast in virus-transduced neurons and glia for several weeks due to endogenous iron uptake[138]. MRI visualizes iron accumulation as low signal on T2 weighted images.

Besides imaging of contrast binding to receptors, recent progress in nanotechnology opened up new avenues for smart contrast agents to target enzymes as well[139].

A recent study[140] also reports the synthesis of two novel gadolinium bisamides, which were designed as enzyme-activated contrast agents for MRI. In the presence of peroxidases the gadolinium bisamides polymerize resulting in increased relaxivity and subsequent enhanced in vitro signal uptake on T1 weighted images. In vivo applications of the novel gadolinium bisamides are currently investigated.

References

1 Legler JM, Ries LA *et al.* Cancer surveillance series [corrected]: brain and other central nervous system cancers: recent trends in incidence and mortality. *J Natl Cancer Inst 1999*; **91:** 1382-1390.

2 Kleihues P, Cavenee WK (eds). *World Health Organization Classification of Tumours. Pathology and Genetics of Tumours of the Nervous System*. IARC Press: Lyon, 2000.

3 Surawicz TS, Davis F *et al.* Brain tumor survival: results from the National Cancer Data Base. *J Neurooncol 1998*; **40:** 151-160.

4 McLendon RE, Halperin EC. Is the long-term survival of patients with intracranial glioblastoma multiforme overstated? *Cancer 2003*; **98:** 1745-1748.

5 Stupp R, Mason WP *et al.* Radiotherapy plus concomitant and adjuvant temozolomide for glioblastoma. *N Engl J Med 2005*; **352:** 987-996.

6 Massey V, Wallner KE. Patterns of second recurrence of malignant astrocytomas. *Int J Radiat Oncol Biol Phys 1990*; **18:** 395-398.

7 Selkirk SM. Gene therapy in clinical medicine. *Postgrad Med J 2004*; **80:** 560-570.

8 Blaese RM, Culver KW *et al.* T lymphocyte-directed gene therapy for ADA- SCID: initial trial results after 4 years. *Science 1995*; **270:** 475-480.

9 Lee M, Kim SW. Polyethylene glycol-conjugated copolymers for plasmid DNA delivery. *Pharm Res 2005*; **22:** 1-10.

10 Li SD, Huang L. Gene therapy progress and prospects: non-viral gene therapy by systemic delivery. *Gene Ther 2006*; **13:** 1313-1319.

11 Lv H, Zhang S *et al.* Toxicity of cationic lipids and cationic polymers in gene delivery. *J Control Release 2006*; **114:** 100-109.

12 Evans CH, Gouze E *et al.* Gene therapeutic approaches-transfer in vivo. *Adv Drug Deliv Rev 2006*; **58:** 243-258.

13 Pulkkanen KJ, Yla-Herttuala S. Gene therapy for malignant glioma: current clinical status. *Mol Ther 2005*; **12:** 585-598.

14 Varghese S, Rabkin SD. Oncolytic herpes simplex virus vectors for cancer virotherapy. *Cancer Gene Ther 2002*; **9:** 967-978.

15 Mizuno M, Yoshida J, Colosi P, Kurtzman G. Adeno-associated virus vector containing the herpes simplex virus thymidine kinase gene causes complete regression of intracerebrally implanted human gliomas in mice, in conjunction with ganciclovir administration. *Jpn J Cancer Res 1998*; **89:** 76-80.

16 Russell SJ. RNA viruses as virotherapy agents. *Cancer Gene Ther 2002*; **9:** 961-966.

17 Ren H, Boulikas T *et al.* Immunogene therapy of recurrent glioblastoma multiforme with a liposomally encapsulated replication-incompetent Semliki forest virus vector carrying the human interleukin-12 gene--a phase I/II clinical protocol. *J Neurooncol 2003*; **64:** 147-154.

18 Timiryasova TM, Chen B, Haghighat P, Fodor I. Vaccinia virus-mediated expression of wild-type p53 suppresses glioma cell growth and induces apoptosis. *Int J Oncol 1999*; **14:** 845-854.

19 Gromeier M, Lachmann S *et al.* Intergeneric poliovirus recombinants for the treatment of malignant glioma. *Proc Natl Acad Sci U S A 2000*; **97:** 6803-6808.

20 Wilcox ME, Yang W *et al.* Reovirus as an oncolytic agent against experimental human malignant gliomas. *J Natl Cancer Inst 2001*; **93:** 903-912.

21 Lun X, Yang W *et al.* Myxoma virus is a novel oncolytic virus with significant antitumor activity against experimental human gliomas. *Cancer Res 2005*; **65:** 9982-9990.

22 Swisher SG, Roth JA *et al.* Induction of p53-regulated genes and tumor regression in lung cancer patients after intratumoral delivery of adenoviral p53 (INGN 201) and radiation therapy. *Clin Cancer Res 2003*; **9:** 93-101.

23 Dachs GU, Tupper J, Tozer GM. From bench to bedside for gene-directed enzyme prodrug therapy of cancer. *Anticancer Drugs 2005*; **16:** 349-359.

24 Cheng YC, Grill SP *et al.* Metabolism of 9-(1,3-dihydroxy-2-propoxymethyl)guanine, a new anti-herpes virus compound, in herpes simplex virus-infected cells. *J Biol Chem 1983*; **258:** 12460-12464.

25 Frank KB, Chiou JF, Cheng YC. Interaction of herpes simplex virus-induced DNA polymerase with 9-(1,3-dihydroxy-2-propoxymethyl)guanine triphosphate. *J Biol Chem 1984*; **259:** 1566-1569.

26 Tomicic MT, Thust R, Kaina B. Ganciclovir-induced apoptosis in HSV-1 thymidine kinase express-ing cells: critical role of DNA breaks, Bcl-2 decline and caspase-9 activation. *Oncogene 2002*; **21:** 2141-2153.

27 Touraine RL, Ishii-Morita H, Ramsey WJ, Blaese RM. The bystander effect in the HSVtk/ganciclovir system and its relationship to gap junctional communication. *Gene Ther 1998*; **5:** 1705-1711.

28 Hamel W, Magnelli L, Chiarugi VP, Israel MA. Herpes simplex virus thymidine kinase/ganciclovir-mediated apoptotic death of bystander cells. *Cancer Res 1996*; **56:** 2697-2702.

29 Ram Z, Walbridge S *et al.* The effect of thymidine kinase transduction and ganciclovir therapy on tumor vasculature and growth of 9L gliomas in rats. *J Neurosurg 1994*; **81:** 256-260.

30 Vile RG, Castleden S *et al.* Generation of an anti-tumour immune response in a non-immunogenic tumour: HSVtk killing in vivo stimulates a mononuclear cell infiltrate and a Th1-like profile of intra-tumoural cytokine expression. *Int J Cancer 1997*; **71:** 267-274.

31 Rainov NG. A phase III clinical evaluation of herpes simplex virus type 1 thymidine kinase and ganciclovir gene therapy as an adjuvant to surgical resection and radiation in adults with previously untreated glioblastoma multiforme. *Hum Gene Ther 2000*; **11:** 2389-2401.

32 Rainov NG, Ren H. Clinical trials with retrovirus mediated gene therapy--what have we learned? *J Neurooncol 2003*; **65:** 227-236.

33 Kay MA, Glorioso JC, Naldini L. Viral vectors for gene therapy: the art of turning infectious agents into vehicles of therapeutics. *Nat Med 2001*; **7:** 33-40.

34 Wu Q, Moyana T, Xiang J. Cancer gene therapy by adenovirus-mediated gene transfer. *Curr Gene Ther 2001*; **1:** 101-122.

35 Smitt PS, Driesse M *et al.* Treatment of relapsed malignant glioma with an adenoviral vector containing the herpes simplex thymidine kinase gene followed by ganciclovir. *Mol Ther 2003*; **7:** 851-858.

36 van der Linden RR, Haagmans BL *et al.* Virus specific immune responses after human neoadjuvant adenovirus-mediated suicide gene therapy for prostate cancer. *Eur Urol 2005*; **48:** 153-161.

37 Rocconi RP, Numnum TM *et al.* Targeted gene therapy for ovarian cancer. *Curr Gene Ther 2005*; **5:** 643-653.

38 Eck SL, Alavi JB *et al.* Treatment of recurrent or progressive malignant glioma with a recombinant adenovirus expressing human interferon-beta (H5.010CMVhIFN-beta): a phase I trial. *Hum Gene Ther 2001*; **12:** 97-113.

39 Germano IM, Fable J, Gultekin SH, Silvers A. Adenovirus/herpes simplex-thymidine kinase/ganci-clovir complex: preliminary results of a phase I trial in patients with recurrent malignant gliomas. *J Neurooncol 2003*; **65:** 279-289.

40 Trask TW, Trask RP *et al.* Phase I study of adenoviral delivery of the HSV-tk gene and ganciclovir administration in patients with current malignant brain tumors. *Mol Ther 2000*; **1:** 195-203.

41 Sandmair AM, Loimas S *et al.* Thymidine kinase gene therapy for human malignant glioma, using replication-deficient retroviruses or adenoviruses. *Hum Gene Ther 2000*; **11:** 2197-2205.

42 Immonen A, Vapalahti M *et al.* AdvHSV-tk gene therapy with intravenous ganciclovir improves sur-vival in human malignant glioma: a randomised, controlled study. *Mol Ther 2004*; **10:** 967-972.

43 Miller CR, Buchsbaum DJ *et al.* Differential susceptibility of primary and established human glioma cells to adenovirus infection: targeting via the epidermal growth factor receptor achieves fiber receptor-independent gene transfer. *Cancer Res 1998*; **58:** 5738-5748.

44 Lang FF, Bruner JM *et al.* Phase I trial of adenovirus-mediated p53 gene therapy for recurrent glioma: biological and clinical results. *J Clin Oncol 2003*; **21:** 2508-2518.

45 Vogels R, Zuijdgeest D *et al.* Replication-deficient human adenovirus type 35 vectors for gene transfer and vaccination: efficient human cell infection and bypass of preexisting adenovirus immunity. *J Virol 2003*; **77:** 8263-8271.

46 Nagao S, Kuriyama S *et al.* Adenovirus-mediated gene transfer into tumors: evaluation of direct readministration of an adenoviral vector into subcutaneous tumors of immunocompetent mice. *Int J Oncol 2001*; **18:** 57-65.

47 Brouwer E, Havenga MJ *et al.* Human adenovirus type 35 vector for gene therapy of brain cancer: improved transduction and bypass of pre-existing anti-vector immunity in cancer patients. *Cancer Gene Ther 2007*; **14:** 211-219.

48 Chiocca EA, Abbed KM *et al.* A phase I open-label, dose-escalation, multi-institutional trial of injection with an E1B-Attenuated adenovirus, ONYX-015, into the peritumoral region of recurrent malignant gliomas, in the adjuvant setting. *Mol Ther 2004*; **10:** 958-966.

49 Wickham TJ. Targeting adenovirus. *Gene Ther 2000*; **7:** 110-114.

50 Medina-Kauwe LK. Endocytosis of adenovirus and adenovirus capsid proteins. *Adv Drug Deliv Rev 2003*; **55:** 1485-1496.

51 Rein DT, Breidenbach M, Curiel DT. Current developments in adenovirus-based cancer gene therapy. *Future Oncol 2006*; **2:** 137-143.

52 Douglas JT, Kim M *et al.* Efficient oncolysis by a replicating adenovirus (ad) in vivo is critically dependent on tumor expression of primary ad receptors. *Cancer Res 2001*; **61:** 813-817.

53 Fuxe J, Liu L *et al.* Expression of the coxsackie and adenovirus receptor in human astrocytic tumors and xenografts. *Int J Cancer 2003*; **103:** 723-729.

54 Jiang H, McCormick F *et al.* Oncolytic adenoviruses as antiglioma agents. *Expert Rev Anticancer Ther 2006*; **6:** 697-708.

55 Reynolds P, Dmitriev I, Curiel D. Insertion of an RGD motif into the HI loop of adenovirus fiber protein alters the distribution of transgene expression of the systemically administered vector. *Gene Ther 1999*; **6:** 1336-1339.

56 Vigne E, Mahfouz I *et al.* RGD inclusion in the hexon monomer provides adenovirus type 5-based vectors with a fiber knob-independent pathway for infection. *J Virol 1999*; **73:** 5156-5161.

57 Einfeld DA, Brough DE *et al.* Construction of a pseudoreceptor that mediates transduction by adenoviruses expressing a ligand in fiber or penton base. *J Virol 1999*; **73:** 9130-9136.

58 Wickham TJ, Tzeng E *et al.* Increased in vitro and in vivo gene transfer by adenovirus vectors containing chimeric fiber proteins. *J Virol 1997*; **71:** 8221-8229.

59 van Beusechem VW, Mastenbroek DC *et al.* Conditionally replicative adenovirus expressing a targeting adapter molecule exhibits enhanced oncolytic potency on CAR-deficient tumors. *Gene Ther 2003*; **10:** 1982-1991.

60 Rancourt C, Rogers BE *et al.* Basic fibroblast growth factor enhancement of adenovirus-mediated delivery of the herpes simplex virus thymidine kinase gene results in augmented therapeutic benefit in a murine model of ovarian cancer. *Clin Cancer Res 1998*; **4:** 2455-2461.

61 Drapkin PT, O'Riordan CR *et al.* Targeting the urokinase plasminogen activator receptor enhances gene transfer to human airway epithelia. *J Clin Invest 2000*; **105:** 589-596.

62 Shayakhmetov DM, Lieber A. Dependence of adenovirus infectivity on length of the fiber shaft domain. *J Virol 2000*; **74:** 10274-10286.

63 Havenga MJ, Lemckert AA *et al.* Exploiting the natural diversity in adenovirus tropism for therapy and prevention of disease. *J Virol 2002*; **76:** 4612-4620.

64 Wigand R, Mauss M, Adrian T. Chimpanzee adenoviruses are related to four subgenera of human adenoviruses. *Intervirology 1989*; **30:** 1-9.

65 De Jong JC, Wermenbol AG *et al.* Adenoviruses from human immunodeficiency virus-infected individuals, including two strains that represent new candidate serotypes Ad50 and Ad51 of species B1 and D, respectively. *J Clin Microbiol 1999*; **37:** 3940-3945.

66 Hierholzer JC. Adenoviruses in the immunocompromised host. *Clin Microbiol Rev 1992*; **5:** 262-274.

67 Gaggar A, Shayakhmetov DM, Lieber A. CD46 is a cellular receptor for group B adenoviruses. *Nat Med 2003*.

68 Segerman A, Atkinson JP *et al.* Adenovirus type 11 uses CD46 as a cellular receptor. *J Virol 2003*; **77:** 9183-9191.

69 Singhrao SK, Neal JW *et al.* Spontaneous classical pathway activation and deficiency of membrane regulators render human neurons susceptible to complement lysis. *Am J Pathol 2000*; **157:** 905-918.

70 Skog J, Edlund K *et al.* Efficient internalization into low-passage glioma cell lines using adenoviruses other than type 5: an approach for improvement of gene delivery to brain tumours. *J Gen Virol 2004*; **85:** 2627-2638.

71 Ulasov IV, Tyler MA *et al.* CD46 represents a target for adenoviral gene therapy of malignant glioma. *Hum Gene Ther 2006*; **17:** 556-564.

72 Dock G. Rabies Virus vaccination in a patient with cervical carcinoma. *Amer. J. Med. Sci. 1904*; **127:** 563.

73 Huebner RJ, Rowe WP *et al.* Studies on the use of viruses in the treatment of carcinoma of the cervix. *Cancer 1956*; **9:** 1211-1218.

74 Brody SL, Crystal RG. Adenovirus-mediated in vivo gene transfer. *Ann N Y Acad Sci 1994*; **716:** 90-101.

75 Berkner KL. Expression of heterologous sequences in adenoviral vectors. *Curr Topics Microbiol Immunol 1992*; **158:** 39-66.

76 Tacket CO, Losonsky G *et al.* Initial safety and immunogenicity studies of an oral recombinant adenohepatitis B vaccine. *Vaccine 1992*; **10:** 673-676.

77 Levrero M, Barban V *et al.* Defective and nondefective adenovirus vectors for expressing foreign genes in vitro and in vivo. *Gene 1991*; **101:** 195-202.

78 Fueyo J, Alemany R *et al.* Preclinical characterization of the antiglioma activity of a tropism-enhanced adenovirus targeted to the retinoblastoma pathway. *J Natl Cancer Inst 2003*; **95:** 652-660.

79 Bischoff JR, Kirn DH *et al.* An adenovirus mutant that replicates selectively in p53-deficient human tumor cells. *Science 1996*; **274:** 373-376.

80 Yew PR, Berk AJ. Inhibition of p53 transactivation required for transformation by adenovirus early 1B protein. *Nature 1992*; **357:** 82-85.

81 Fueyo J, Gomez-Manzano C *et al.* A mutant oncolytic adenovirus targeting the Rb pathway produces anti-glioma effect in vivo. *Oncogene 2000*; **19:** 2-12.

82 Kruyt FA, Curiel DT. Toward a new generation of conditionally replicating adenoviruses: pairing tumor selectivity with maximal oncolysis. *Hum Gene Ther 2002*; **13:** 485-495.

83 Edwards SJ, Dix BR *et al.* Evidence that replication of the antitumor adenovirus ONYX-015 is not controlled by the p53 and p14(ARF) tumor suppressor genes. *J Virol 2002*; **76:** 12483-12490.

84 Heise C, Hermiston T *et al.* An adenovirus E1A mutant that demonstrates potent and selective systemic anti-tumoral efficacy. *Nat Med 2000*; **6:** 1134-1139.

85 Kohno S, Nakagawa K *et al.* Midkine promoter-based conditionally replicative adenovirus for malignant glioma therapy. *Oncol Rep 2004*; **12:** 73-78.

86 Ahmed A, Thompson J *et al.* A conditionally replicating adenovirus targeted to tumor cells through activated RAS/P-MAPK-selective mRNA stabilization. *Nat Biotechnol 2003*; **21:** 771-777.

87 Post DE, Van Meir EG. A novel hypoxia-inducible factor (HIF) activated oncolytic adenovirus for cancer therapy. *Oncogene 2003*; **22:** 2065-2072.

88 Brenner M, Kisseberth WC *et al.* GFAP promoter directs astrocyte-specific expression in transgenic mice. *J Neurosci 1994*; **14:** 1030-1037.

89 de Leeuw B, Su M *et al.* Increased glia-specific transgene expression with glial fibrillary acidic protein promoters containing multiple enhancer elements. *J Neurosci Res 2006*; **83:** 744-753.

90 Driesse MJ, Vincent AJ *et al.* Intracerebral injection of adenovirus harboring the HSVtk gene combined with ganciclovir administration: toxicity study in nonhuman primates. *Gene Ther 1998*; **5:** 1122-1129.

91 Hsich G, Sena-Esteves M, Breakefield XO. Critical issues in gene therapy for neurologic disease. *Hum Gene Ther 2002*; **13:** 579-604.

92 Mardor Y, Rahav O *et al.* Convection-enhanced drug delivery: increased efficacy and magnetic resonance image monitoring. *Cancer Res 2005*; **65:** 6858-6863.

93 Husain SR, Puri RK. Interleukin-13 receptor-directed cytotoxin for malignant glioma therapy: from bench to bedside. *J Neurooncol 2003*; **65:** 37-48.

94 Laske DW, Youle RJ, Oldfield EH. Tumor regression with regional distribution of the targeted toxin TF-CRM107 in patients with malignant brain tumors. *Nat Med 1997*; **3:** 1362-1368.

95 Betz AL, Shakui P, Davidson BL. Gene transfer to rodent brain with recombinant adenoviral vectors: effects of infusion parameters, infectious titer, and virus concentration on transduction volume. *Exp Neurol 1998*; **150:** 136-142.

96 Brust D, Feden J *et al.* Radiosensitization of rat glioma with bromodeoxycytidine and adenovirus expressing herpes simplex virus-thymidine kinase delivered by slow, rate-controlled positive pressure infusion. *Cancer Gene Ther 2000*; **7:** 778-788.

97 Bankiewicz KS, Eberling JL *et al.* Convection-enhanced delivery of AAV vector in parkinsonian monkeys; in vivo detection of gene expression and restoration of dopaminergic function using pro-drug approach. *Exp Neurol 2000*; **164:** 2-14.

98 Sanftner LM, Sommer JM *et al.* AAV2-mediated gene delivery to monkey putamen: evaluation of an infusion device and delivery parameters. *Exp Neurol 2005*; **194:** 476-483.

99 Muldoon LL, Nilaver G *et al.* Comparison of intracerebral inoculation and osmotic blood-brain barrier disruption for delivery of adenovirus, herpesvirus, and iron oxide particles to normal rat brain. *Am J Pathol 1995*; **147:** 1840-1851.

100 Ter Horst M, Verwijnen SM *et al.* Locoregional Delivery of Adenoviral Vectors. *J Nucl Med 2006*; **47:** 1483-1489.

101 Fan X, Salford LG, Widegren B. Glioma stem cells: Evidence and limitation. *Semin Cancer Biol 2006*.

102 Lee J, Elkahloun AG *et al.* Cellular and genetic characterization of human adult bone marrow-derived neural stem-like cells: a potential antiglioma cellular vector. *Cancer Res 2003*; **63:** 8877-8889.

103 Nakamizo A, Marini F *et al.* Human bone marrow-derived mesenchymal stem cells in the treatment of gliomas. *Cancer Res 2005*; **65:** 3307-3318.

104 Aboody KS, Brown A *et al.* Neural stem cells display extensive tropism for pathology in adult brain: evidence from intracranial gliomas. *Proc Natl Acad Sci U S A 2000*; **97:** 12846-12851.

105 Benedetti S, Pirola B *et al.* Gene therapy of experimental brain tumors using neural progenitor cells. *Nat Med 2000*; **6:** 447-450.

106 Badruddoja MA, Black KL. Improving the delivery of therapeutic agents to CNS neoplasms: a clinical review. *Front Biosci 2006*; **11:** 1466-1478.

107 Wang Y, Yuan F. Delivery of viral vectors to tumor cells: extracellular transport, systemic distribution, and strategies for improvement. *Ann Biomed Eng 2006*; **34:** 114-127.

108 Liu R, Martuza RL, Rabkin SD. Intracarotid delivery of oncolytic HSV vector G47Delta to metastatic breast cancer in the brain. *Gene Ther 2005*; **12:** 647-654.

109 Rainov NG, Ikeda K *et al.* Intraarterial delivery of adenovirus vectors and liposome-DNA complexes to experimental brain neoplasms. *Hum Gene Ther 1999*; **10:** 311-318.

110 Tjuvajev JG, Stockhammer G *et al.* Imaging the expression of transfected genes in vivo. *Cancer Res 1995*; **55:** 6126-6132.

111 Rome C, Couillaud F, Moonen CT. Gene expression and gene therapy imaging. *Eur Radiol 2006*.

112 Reader AJ, Zweit J. Developments in whole-body molecular imaging of live subjects. *Trends Pharmacol Sci 2001*; **22:** 604-607.

113 Chatziioannou AF. Instrumentation for molecular imaging in preclinical research: Micro-PET and Micro-SPECT. *Proc Am Thorac Soc 2005*; **2:** 533-536, 510-511.

114 Zinn KR, Buchsbaum DJ *et al.* Noninvasive monitoring of gene transfer using a reporter receptor imaged with a high-affinity peptide radiolabeled with 99mTc or 188Re. *J Nucl Med 2000*; **41:** 887-895.

115 Carlin S, Akabani G, Zalutsky MR. In vitro cytotoxicity of (211)at-astatide and (131)I-iodide to glioma tumor cells expressing the sodium/iodide symporter. *J Nucl Med 2003*; **44:** 1827-1838.

116 Tjuvajev JG, Finn R *et al.* Noninvasive imaging of herpes virus thymidine kinase gene transfer and expression: a potential method for monitoring clinical gene therapy. *Cancer Res 1996*; **56:** 4087-4095.

117 Haubner R, Avril N *et al.* In vivo imaging of herpes simplex virus type 1 thymidine kinase gene expression: early kinetics of radiolabelled FIAU. *Eur J Nucl Med 2000*; **27:** 283-291.

118 Gambhir SS, Barrio JR *et al.* Imaging of adenoviral-directed herpes simplex virus type 1 thymidine kinase reporter gene expression in mice with radiolabeled ganciclovir. *J Nucl Med 1998*; **39:** 2003-2011.

119 de Vries EF, van Waarde A *et al.* [(11)C]FMAU and [(18)F]FHPG as PET tracers for herpes simplex virus thymidine kinase enzyme activity and human cytomegalovirus infections. *Nucl Med Biol 2000*; **27:** 113-119.

120 Choi SR, Zhuang ZP *et al.* SPECT imaging of herpes simplex virus type1 thymidine kinase gene expression by [(123)I]FIAU(1). *Acad Radiol 2005*; **12:** 798-805.

121 Cho SY, Ravasi L *et al.* Evaluation of (76)Br-FBAU as a PET reporter probe for HSV1-tk gene expression imaging using mouse models of human glioma. *J Nucl Med 2005*; **46:** 1923-1930.

122 Jacobs AH, Rueger MA *et al.* Imaging-guided gene therapy of experimental gliomas. *Cancer Res 2007*; **67:** 1706-1715.

123 Jacobs AH, Voges J *et al.* Imaging in gene therapy of patients with glioma. *J Neurooncol 2003*; **65:** 291-305.

124 Honigman A, Zeira E *et al.* Imaging transgene expression in live animals. *Mol Ther 2001*; **4:** 239-249.

125 Wu JC, Sundaresan G, Iyer M, Gambhir SS. Noninvasive optical imaging of firefly luciferase reporter gene expression in skeletal muscles of living mice. *Mol Ther 2001*; **4:** 297-306.

126 Lipshutz GS, Gruber CA *et al.* In utero delivery of adeno-associated viral vectors: intraperitoneal gene transfer produces long-term expression. *Mol Ther 2001*; **3:** 284-292.

127 Contag PR, Olomu IN, Stevenson DK, Contag CH. Bioluminescent indicators in living mammals. *Nat Med 1998*; **4:** 245-247.

128 Contag CH, Spilman SD *et al.* Visualizing gene expression in living mammals using a bioluminescent reporter. *Photochem Photobiol 1997*; **66:** 523-531.

129 Bhaumik S, Gambhir SS. Optical imaging of Renilla luciferase reporter gene expression in living mice. *Proc Natl Acad Sci U S A 2002*; **99:** 377-382.

130 Katz MH, Takimoto S *et al.* An imageable highly metastatic orthotopic red fluorescent protein model of pancreatic cancer. *Clin Exp Metastasis 2004*; **21:** 7-12.

131 Oldham M, Sakhalkar H *et al.* Three-dimensional imaging of xenograft tumors using optical computed and emission tomography. *Med Phys 2006*; **33:** 3193-3202.

132 Penuelas I, Haberkorn U, Yaghoubi S, Gambhir SS. Gene therapy imaging in patients for oncological applications. *Eur J Nucl Med Mol Imaging 2005*; **32 Suppl 2:** S384-403.

133 Gurfinkel M, Ke S *et al.* Near-infrared fluorescence optical imaging and tomography. *Dis Markers 2003*; **19:** 107-121.

134 Ballou B, Fisher GW, Hakala TR, Farkas DL. Tumor detection and visualization using cyanine fluorochrome-labeled antibodies. *Biotechnol Prog 1997*; **13:** 649-658.

135 Ke S, Wen X *et al.* Near-infrared optical imaging of epidermal growth factor receptor in breast cancer xenografts. *Cancer Res 2003*; **63:** 7870-7875.

136 Hsu AR, Hou LC *et al.* In vivo near-infrared fluorescence imaging of integrin alphavbeta3 in an orthotopic glioblastoma model. *Mol Imaging Biol 2006*; **8:** 315-323.

137 Weissleder R, Moore A *et al.* In vivo magnetic resonance imaging of transgene expression. *Nat Med 2000*; **6:** 351-355.

138 Genove G, DeMarco U *et al.* A new transgene reporter for in vivo magnetic resonance imaging. *Nat Med 2005*; **11:** 450-454.

139 Yang X, Atalar E. MRI-guided gene therapy. *FEBS Lett 2006*; **580:** 2958-2961.

140 Querol M, Chen JW, Weissleder R, Bogdanov A, Jr. DTPA-bisamide-based MR sensor agents for peroxidase imaging. *Org Lett 2005*; **7:** 1719-1722.

PART 2

Transcriptional targeting of adenoviral vectors
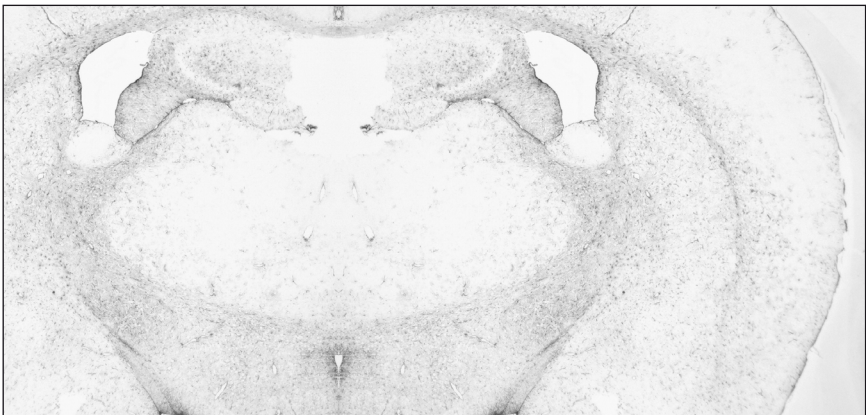
CHAPTER 2.1

Increased Glia-Specific Transgene Expression with Glial Fibrillary Acidic Protein Promoters Containing Multiple Enhancer Elements

Bertie de Leeuw[1], Mu Su[2], Maarten ter Horst[1], Shingo Iwata[2], Mark Rodijk[1], Rob C. Hoeben[3], Albee Messing[4], Peter Sillevis Smitt[1], and Michael Brenner[2]

[1]Department of Neurology, Erasmus University Medical Center, Rotterdam, The Netherlands, [2]Department of Neurobiology and the Civitan International Research Center, University of Alabama at Birmingham, Birmingham, AL, USA, [3]Department of Molecular Cell Biology, Leiden University Medical Center, Leiden, The Netherlands and [4]Waisman Center, University of Wisconsin, WI, USA
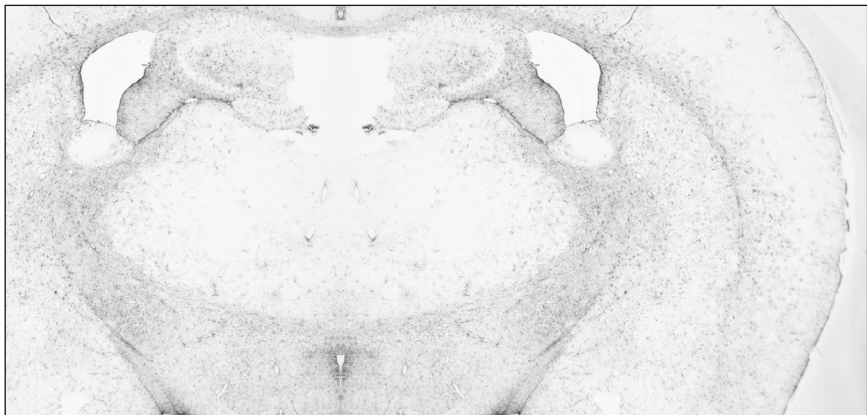
Abstract

The ability to direct transgene expression to astrocytes has become increasingly important as the roles for these cells continue to expand. Promoters consisting of the 5'-flanking region of the human or mouse glial fibrillary acidic protein (GFAP) gene have generally proved satisfactory. However, a more powerful promoter would be advantageous for several applications, such as expression of dominant negative RNAs or proteins, or for gene therapy. We investigated the possibility of increasing the transcriptional activity of the human GFAP promoter by inserting into it one or three additional copies of putative GFAP enhancer regions. The promoters enhanced with three additional copies gave 75-fold higher LacZ expression levels upon plasmid transfection into GFAP-expressing U251 cells than the parental gfa2 promoter. Surprisingly, in a transgenic mouse model, the enhanced promoters resulted in no or only very low expression of marker genes, probably caused by toxicity. When various cell lines were infected with replication deficient adenoviral vectors, the enhanced promoters gave LacZ expression levels that were approximately 10-fold higher than those with the parental gfa2 promoter, while retaining specificity for GFAP-expressing cells. Injection of the adenoviral vectors carrying the enhanced promoters into nude mouse brain showed that LacZ expression was limited to GFAP-positive cells. We conclude that gfa2 enhanced promoters are useful for production of short-term, glia-specific, high expression levels of genes in an adenoviral context. Adenoviral vectors containing these enhanced promoters may be useful in glioma gene therapy.

Introduction

Astrocytes are being increasingly recognized as playing critical roles in the development and maintenance of the CNS[1-3]. Interest in these cells has led to demand for a promoter that permits targeted astrocyte expression of transgenes in mice in order to study their functions further, as well as for developing disease models and for gene therapy. The mouse or human glial fibrillary acidic protein (GFAP) promoter has been used widely for these purposes (for review see Su et al.[4]). For many studies, these standard GFAP promoters have proved sufficient, but for certain applications, such as production of dominant negative proteins, RNAi or gene therapy, it is desirable to obtain higher levels of expression. To this end, we have modified the standard human GFAP promoter, gfa2, to try to increase its expression level. Transient transfection studies have suggested the presence of three important enhancer regions within the 2.2-kb gfa2 promoter segment. The A and B enhancer regions are located about 1,500 bp upstream of the transcription start site, whereas the D region is immediately upstream of the basal promoter[5]. Among these sequences, the B region appeared particularly potent. We constructed gfa2-based promoters that carry additional copies of either the B region or the cojoined A, B and D regions (ABD). Either one or three copies of these enhancer elements were placed just upstream of the basal promoter in gfa2 to yield the gfa2(B)$_1$, gfa2(B)$_3$, gfa2(ABD)$_1$ and gfa2(ABD)$_3$ promoters. We report here that these promoters are up to 75 times more active than the parental gfa2 when the corresponding plasmids are transiently transfected into GFAP expressing glioma cell lines and over 10 times more active when transfected in the context of a replication-deficient adenoviral vector. Although many tissue-specific promoters lose their selectivity in an adenoviral context, specificity of the adenoviral enhanced promoter constructs for GFAP-positive cells was at least as great as that of the adenoviral vector carrying the parental gfa2 promoter in vitro. These observations led us to test the enhanced promoters in transgenic mice and by adenovirus vector gene transfer into the adult brain. The enhanced promoters did not yield any marker gene expression in transgenic mice. However, injection of an adenoviral construct containing the gfa2(B)$_3$ enhanced promoter resulted in specific expression of β-galactosidase in astrocytes.

Materials and Methodes

Cell Culture and GFAP Expression

Cell lines used (tumor type, GFAP protein expression determined by Western blotting after loading 30 μg of protein per lane, origin): U251 (Glioblastoma multiforme, GFAP+, P Körnblith NIH); GOS3 (Anaplastic oligo-astrocytoma, GFAP+, Deutsche Sammlung von Mikroorganismen und Zellkulturen= DSMZ); 10.278 (Glioblastoma multiforme, GFAP+, ErasmusMC); U373 (Glioblastoma multiforme, GFAP+, European Collection of Cell Cultures= ECACC);

SNB19 (Glioblastoma multiforme, GFAP+, DSMZ); U87MG (Glioblastoma multiforme, GFAP-, Promochem in partnership with the American Type Tissue Collection= ATCC); A172 (Glioblastoma multiforme, GFAP-, ATCC); T98G (Glioblastoma multiforme, GFAP-, ATCC); U118MG (Glioblastoma multiforme, GFAP-, ATCC); U138 (Glioblastoma multiforme, GFAP-, DSMZ); MG-42-BA (Glioblastoma multiforme, GFAP-, DSMZ); A549 (Non-small cell lung carcinoma, GFAP-, ATCC); SK-BR3 (Breast adenocarcinoma, metastasis, GFAP-, ATCC); SK-MEL-2 (Melanoma, GFAP-, ATCC); Caov-3 (Ovary adenocarcinoma, GFAP-, ATCC); DU 145 (Prostate carcinoma, brain metastasis, GFAP-, ATCC); DLD-1 (Colorectal adeno-carcinoma, GFAP-, ATCC); NCI-H1299 (Non-small cell lung carcinoma, GFAP-, ATCC); NCI-H28 (Mesothelioma, GFAP-, ATCC); NIH:OVCAR-3 (Ovary adenocarcinoma; GFAP-, ATCC); Detroit 562 (Pharynx carcinoma, metastasis, GFAP-, ATCC); CAMA1 (Breast adeno-carinoma, metastasis, GFAP-, ATCC); PC3 (Prostate adenocarcinoma, metastasis, GFAP-, ATCC); NT2 (Embryonal carcinoma, GFAP-, ATCC); Hep2 (Larynx epidermoid carcinoma [HELA contaminant], GFAP-, ATCC).

Unless stated otherwise, all cell lines were cultured on DMEM (Life Technologies, Paisley, Scotland, UK) with 10% heat inactivated (30 min 56°C) FBS (Life technologies) and passaged 1:20 (37°C; 5% CO2). Normal fibroblasts were derived from breast tissue and cultured in DMEM 10% FBS (see above). The E1-transformed embryonal retina cell line 911 was cultured in the same medium with extra glucose (3 g/l) and passaged 1:5.

GFAP expression was determined by Western blotting and by immunohistochemistry. For Western blotting, cells were trypsinized, washed twice with PBS and the pellet resuspended in 8M urea 0.1M $NaPO_4$ (pH7.5) and sonicated. Then 30μg of protein (BCA method; Pierce, Rockford, IL) was mixed 1:1 with sample buffer and run on an 11% acrylamide gel. Gels were blotted onto Hybond-C-super membrane (Amersham Biosciences, UK), blocked in sterile low fat milk, dried and stored at –20°C. For detection of GFAP, monoclonal mouse anti-human GFAP (1:200, ICN, Aurora, OH) was incubated at RT for 30 min., washed and followed by alkaline phosphatase conjugated rabbit anti-mouse antibody (1:500, DAKO,

Tabel 1 Adenoviral Promoter Constructs

Relative expression strength	LacZ ratio	SEM
Adgfa2(B)3nLac/Adgfa2nLac	12,9	3,6
Adgfa2(ABD)3nLac/Adgfa2nLac	6,4	3,4
Adgfa2(B)3nLac/AdCMVnLac	0,3	0,1
Adgfa2(ABD)3nLac/AdCMVnLac	0,2	0,1
Adgfa2nLac/AdCMVnLac	0,02	0,004

Relative expression specificity (GFAP+/GFAP- cell Lines)	SI	P
Adgfa2(ABD)3nLac	28.8	0.0002
Adgfa2(B)3nLac	7.5	0.0018
Adgfa2nLac	6.8	0.0005

Glostrup, Denmark, 30 min. RT). The color reaction was developed with the Biorad AP Conjugate Substrate kit (Hercules, CA).

For immunohistochemistry, cell lines were cultured for one day on 4 chamber slides (Lab-Tek chamber slides, Nalgene Nunc International, Naperville, IL). After fixation in 10% buffered formalin, cells were incubated 30 min at RT with polyclonal rabbit anti-cow GFAP (1:800; DAKO) and incubated with biotin conjugated goat anti-rabbit IgG (1:200; Vector Laboratories, Burlingame, CA). Slides were washed and incubated with avidin-AP (Vectastain AP-standard, Vector Laboratories). Alkaline phosphatase activity was detected using chromogen (0.3 mg/ml Naphthol AS-MX, 0.01% new Fuchsine, 0.01% $NaNO_2$, 0.2M Tris/HCl pH8, 0.3 mg/ml Levamisol) and counterstained with Mayer solution.

Plasmid Construction

Fragments containing either the GFAP B region (bp -1627 to -1504 relative to the protein start site at +1) or the ABD sequence (bp -1772 to -1504 joined directly to bp -147 to -72) were generated by PCR using as template the gfa28 promoter present in pGfa28-CAT (Besnard et al., 1991). This template contains the GFAP A, B and D regions as contiguous sequences immediately flanked 5' by a Bgl II site (contributed by the vector) and 3' by a Sma I site (naturally present in the GFAP promoter). For synthesis of the ABD fragment, PCR was performed with primers lying outside these sites. For synthesis of the B fragment, the 5' primer contained a Bgl II site immediately before commencing B region homology, and the 3' primer contained a Sma I site. The sequences of these latter two primers, with the restriction sites shown in **bold** and B-region homology in *italics*, were as follows: sense = CCAACCAACC**AGATCT***TCCTCTTCATGCCCAGTGAATGA*; antisense = ATGCAG**CCCG-GG***CCTGCTCAATGGGCTTCTC*. The PCR products containing either the ABD or B region were digested with Bgl II and Sma I, the Bgl II site filled in, and the fragment cloned into the unique Sma I site of pGfa2nLac (Brenner et al., 1994), regenerating a Sma I site at the 3' end of the inserted fragment. This places the inserts at bp -71, which is the junction between the D segment and the GFAP basal promoter. The orientation and proper sequence of the inserts were verified by DNA sequencing. Repetition of this procedure produced the plasmids with 3 inserts. The beginning and ending sequences of the inserted B region fragments are contained within the PCR primer sequences provided above. The beginning of each ABD fragment is **GATCT**AACATATCCTGGTGT and the end of each sequence (also the sense strand) is GGGTGTTGCCAGGGGCACCC, with the filled in Bgl II site indicated in **bold**. The entire sequences of the segments may be obtained either from Besnard et al. (1991) or GenBank accession #M67446, or the complete plasmid sequences are available on request to M.B. Homologous plasmids carrying the chloramphenicol acetyltransferase (CAT) reporter gene were made by deleting the lacZ coding region by digestion with BamH I and replacing it with the CAT sequence, which was obtained by digestion of the pCAT3-control vector (Promega, Madison, WI) with Hind III and Xba I. Both the recipient and insert

were blunt ended by filling in prior to ligation. Proper joining of the fragments was confirmed by sequencing.

Transfection With gfa2 Enhanced Promoter Plasmids

U251 cells were plated into 6-well plates at $6x10^4$ cells/well in 2 ml of DMEM containing 10% FBS. Transfections were performed 4 days later using the calcium phosphate method. Amounts of DNA used, based on preliminary experiments to determine levels in the linear range for signal production, were 1250 ng for pGfa2nLac and 312 ng for each of the gfa2 enhanced promoters and for the positive control pSVβGal plasmid, and 12.5 ng for the luciferase expression vector, pGL3 (Promega), which was cotransfected with each of the nLac reporter plasmids to adjust for transfection efficiency. The total amount of DNA transfected was kept constant at 1.5 μg by addition of pUC19 (Fermentas Life Sciences, Hanover, MD). Cells were harvested 48 hours after transfection. LacZ expression was detected by the Galacto-Light Plus™ system (Applied Biosystems, Bedford, MA) and luciferase expression by the Luciferase Assay System (Promega) using a Monolight 2010 luminometer (Analytical Luminescence Laboratories, San Diego, CA). Three independent experiments were performed, each with duplicate samples. LacZ activity was normalized to luciferase activity, adjusted for the ng of DNA used in the transfection, and expressed relative to that of the parental pGfa2nLac plasmid.

For long-term tests of gfa2 enhanced promoter activity in transfected cells, U251 cells were plated and transfected as above, except the amount of each of the test plasmids used was 2,360 ng, and each was cotransfected with 125 ng of pcDneo[6] and 12.5 ng of pGL3. One day after transfection, 0.40 mg/ml of G418 sulfate (Cellgro, Herndon, VA) was added to the medium to select for transfected cells, and the next day each well was harvested and replated into 2 wells, with continued G418 selection. Duplicate wells were harvested on days 2, 4, 9, 14 and 21 after transfection. Cells were assayed for β-galactosidase and luciferase as described above, for CAT activity using a CAT ELISA kit (Roche Diagnostics GmbH, Mannheim, Germany), and for protein by the BCA method (Pierce). Because luciferase activity declined to near background levels about day 9, reporter gene activity was instead normalized to protein.

Construction of Adenoviral Vectors

We constructed E1- and E3-deleted adenoviral vectors containing the nLac reporter gene driven by the gfa2, gfa2(B)$_3$ or gfa2(ABD)$_3$ promoter (Fig. 1). The promoter-nLac sequences from plasmids pGfa2nLac, pGfa2(B)$_3$nLac and pGfa2(ABD)$_3$nLac (BglII-HindIII fragment) were cloned into pShuttle (digested with BglII-HindIII) and were recombined after PmeI digestion with the AdEasyI backbone plasmid in *E. coli* BJ5183[7] (Fig. 1). The viral DNA plasmids were then linearized with PacI and transfected into 911 cells[8] using the calcium-phosphate technique[9]. Resulting plaques were picked and propagated on PER.C6 cells[10] until about
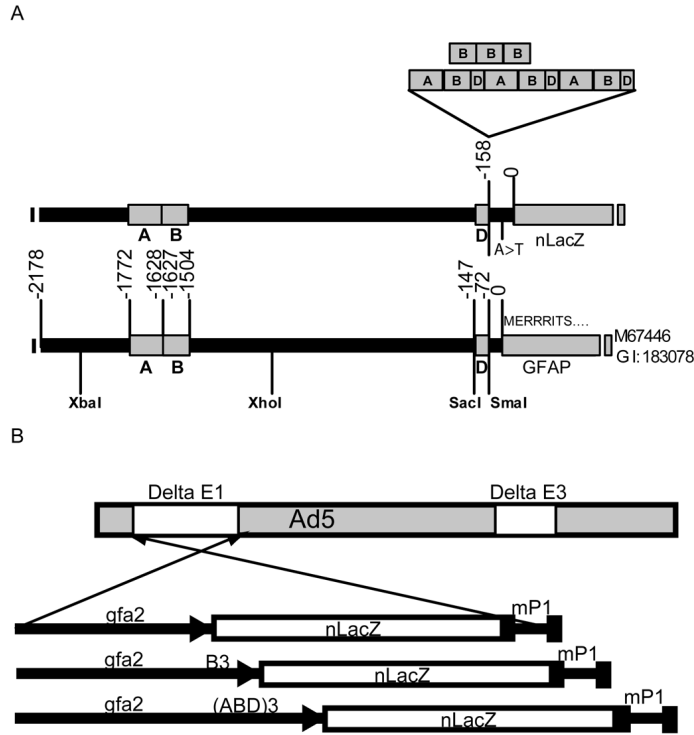
Fig. 1 Schematic of the adenoviral vectors used in this study. **A**: Promoter region of pGfa2nLac and enhanced variants relative to Genbank sequence M67446. The gfa2 promoter extends from 2,178 bp upstream to 32 bp downstream of the normal GFAP protein start site. Positions of the A, B and D enhancer regions are indicated. To form the enhanced promoters, one or three copies of the B region or the AB and D regions were inserted into the SmaI site immediately 3' of the D region. The nLacZ reporter is present in a multicloning sequence following GFAP bp 32. The natural initiating GFAP ATG has been changed to TTG so that protein synthesis commences with the nLacZ coding sequence.
B: Adenoviral vectors used. Adgfa2nLac contains the regular GFAP promoter while Adgfa2(B)$_3$nLac and Adgfa2(ABD)$_3$nLac harbor the gfa2 enhanced promoters followed by an nLacZ reporter gene. The nLacZ reporter sequence is followed by a segment from the mouse protamine 1 gene (mP1), which provides an intron, stabilizing 3'UTR and polyadenylation signal. The promoter-nLacZ-mP1 sequences were inserted in the inverse orientation compared to wild-type E1 transcription.
Delta E1 and delta E3 indicate deletion of the adenoviral E1 and E3 regions.

10^6 pfu/ml were reached. Ten independent clones of each construct were selected and used for plaque assays on A549, U251 and 911 cells, after which plaques were stained using X-gal.

Vectors giving rise to blue plaques on U251 but not on A549 cells and the control vector AdCMVnLac[11] were propagated to high titers on PER.C6 cells, CsCl gradient purified, dialysed and stored at -80°C in sucrose buffer (140 mM NaCl, 5 mM Na$_2$HPO$_4$, 1.5mM KH$_2$PO$_4$, 20 mM MgCl$_2$ and 5% sucrose). All batches were screened for replication competent

adenovirus (RCA)[12] and met the criterium of less than 1 plaque forming unit (pfu) of E1 containing virus per 10^7 pfu of E1-deleted vector. Titrations were performed on 911 cells and are presented as plaque forming units per ml[8]. The titers ranged from $3x10^8$ to $3x10^{11}$ pfu/ml.

Strength and Selectivity of Enhanced gfa2 Promoters in an Adenoviral Context

Cells were plated into 24 well plates at a density of $2x10^5$ cells/well in 1 ml DMEM containing 10% FBS and incubated overnight at 37°C. After changing the medium, the Adgfa2 constructs and the control virus (AdCMVnLac) were added in triplicate at a concentration of 100 pfu/cell with reduced FBS (6%). The medium was changed two hours after starting the incubation to normal DMEM 10% FBS. After 48 hours of incubation at 37°C the medium was removed, the cells were washed with PBS and assayed for β-galactosidase activity by the Galacto-Light Plus™ system (Applied Biosystems) using a Packard Top Count NXT luminometer (PerkinElmer Life sciences, Meriden, Conneticut). LacZ activity was normalized to protein determined with the BCA protein assay kit (Pierce).

The selectivity index (SI) was defined as the ratio of the mean β-galactosidase concentration in GFAP-positive cell lines divided by the mean β-galactosidase concentration in GFAP-negative cell lines, 48 hours after infection with the respective adenoviral vectors. For calculation of SI values and promoter ratios, β-galactosidase activity was expressed relative to that of AdCMVnLacZ, to correct for adenoviral cell entry, after background subtraction.

For X-gal staining, cells were washed twice with PBS (MgCl$_2$), fixed in ice cold 2% formaldehyde 0.8% glutaraldehyde in PBS (MgCl$_2$) for 5 min, washed again with PBS (MgCl$_2$) and stained overnight at 37°C in FIFO (5 mM potassiumferricyanide, 5mM potassiumferrocyanide, 2 mM MgCl$_2$ in PBS) containing 1mg/ml X-gal (Sigma, St. Louis, MO)[13]. Fixed and washed brain slices (see below) were stained overnight at 37°C with X-gal, washed in PBS, and postfixed in cold 4% paraformaldehyde until embedded in paraffin. 4 μm paraffin sections were aged o/n at 50ºC, deparaffinized and counterstained 5 minutes at RT using 0.1% nuclear fast red (Merck, Darmstadt, Germany) dissolved in 75 mM Al$_2$(SO$_4$)$_3$.

Transgenic Mice

All experimental protocols were approved by the Institutional Animal Care and Use Committees of the Erasmus University Medical Center, the University of Alabama at Birmingham and the University of Wisconsin, Madison, in compliance with the Guide for the Care and Use of Laboratory Animals. Injection fragments were obtained and transgenic mice produced as previously described[14]. Mice carrying the transgenes were identified by PCR of DNA obtained from tail biopsies, and adult founder mice assayed for transgene activity. LacZ reporter activity was assayed by β-galactosidase solution assays as described above and by X-gal staining of brain hemispheres[14].CAT reporter activity was assayed with the CAT

ELISA kit and with a CAT histochemical staining kit (Roche Diagnostics, GmbH, Mannheim, Germany).

Adenovirus Injection into Mouse Brain

Young adult female nu/nu BALB/c mice (Charles River, Les Oncins, France) were injected with 1.0×10^5 pfu of Adgfa2nLac, Adgfa2(B)$_3$nLac or AdCMVnLac in a total volume of 1 µl. A stereotactic frame (David Kopf Instruments, Tajuga, CA) was used to inject the adenoviral vectors into the median temporal lobe, close to the basal ganglia. Three days after injection, the animals were euthanized by isoflurane and perfused with paraformaldehyde. The brains were taken out, cut into 0.5 cm slices and postfixed in 4% paraformaldehyde 2 hours at 4°C. After 3 washes in 0.5mM MgCl$_2$ in PBS, pH7.3 [PBS (MgCl$_2$)] brain slices were stained with X-gal as described above.

Immunohistochemistry for GFAP was performed on X-gal stained formalin-fixed, paraffin-embedded, 4 µm sections. The slides were deparaffinized and endogenous peroxidase activity was blocked with 3.0% hydrogen peroxide in methanol, followed by antigen retrieval by incubation for 10 min at 37ºC with 0.1% pronase (Sigma-Aldrich, St Louis, Missouri, USA) in PBS. All incubations were performed in a humidifying chamber. Primary antibody was rabbit anti-cow GFAP (1:200; DAKO). Signal was detected using a horseradish peroxidase (HRP)-labeled second step according to the suppliers' recommendations (Envision™ rabbit kit; K4007; DAKO).

Statistical Analysis

Data were analysed using GraphPad Prism version 4.0 software (GraphPad Software, Inc., San Diego, CA, 2002). ANOVA was used to analyse the differences in mean β-galactosidase expression between the adenoviral gfa2 and enhanced promoter constructs. The difference in β-galactosidase expression between GFAP-positive and GFAP-negative cell lines was analysed with student's t-test. Before statistical analyses the data were corrected for background β-galactosidase activity by subtracting the value of the no-virus control, and for infection efficiency by dividing by the mean of the AdCMVnLac value for the same cell line. All tests were carried out two-sided and $p<0.05$ was considered statistically significant.

Results

Expression Level of Enhanced gfa2 Promoter Plasmids in U251 Cells

The GFAP-positive human glioma cell line U251 was transiently transfected with the standard and enhanced gfa2 promoter constructs as an initial test of their relative strengths. As shown in Fig. 2, the gfa2 enhanced promoters indeed have greatly increased activity. In three independent experiments, the activity compared with gfa2 averaged 6-fold higher for
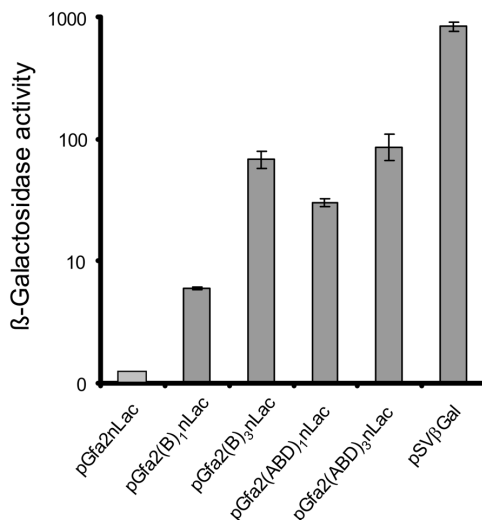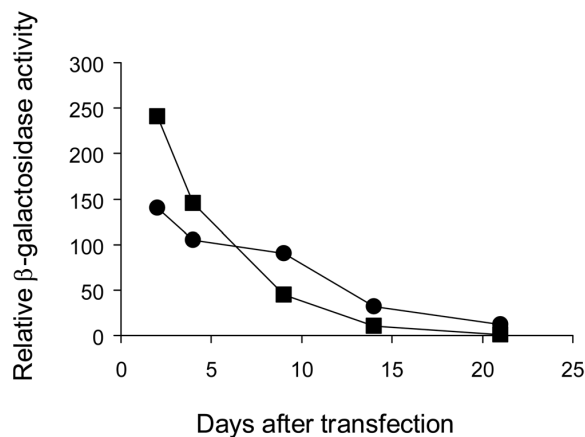
Fig. 2 Relative activity of enhanced gfa2 promoters in transiently transfected U251 cells. Cells were transfected with plasmids in which the nLac gene is driven by the natural gfa2 promoter, the enhanced gfa2 promoters or the SV40 promoter. Cells were harvested 48 hours later and β-galactosidase expression was detected by the Galacto-Light Plus system. LacZ activity was normalized to luciferase activity, adjusted for the nanograms of DNA used in the transfection. Data are averages ± SEM of three independent experiments performed in duplicate, and are expressed relative to the activity of the pGfa2nLac plasmid, whose value is set at 1.0 (p<0.001 for all differences between the enhanced gfa2 promoters and the gfa2 standard).

gfa2(B)$_1$, 30-fold for gfa2(ABD)$_1$, 68-fold for gfa2(B)$_3$, and 84-fold for gfa2(ABD)$_3$. The latter was about 10% that obtained with the pSVβgal positive control plasmid.

Expression of Enhanced gfa2 Promoters in Transgenic Mice

A series of transgenic mice was made to determine whether the enhanced gfa2 promoters could also be used to produce long-term, high levels of transgene expression in astrocytes. A total, 11 lines of mice were analyzed, three carrying the gfa2(B)$_1$nLac transgene, three with gfa2(ABD)$_1$nLac, and four with gfa2(ABD)$_3$nLac. No activity was found for any of these gfa2 enhanced promoter transgenics except for a few of the gfa2(B)$_1$nLac lines, and even those activities were well below what is typically seen for the unmodified gfa2 promoter (data not shown). In contrast, about 50% of mice carrying a gfa2-nLac transgene express at substantial levels.

A possible explanation for the negative results with the enhanced gfa2 promoters in transgenic mice is that a significant increase in the already robust activity of the gfa2 promoter for an extended time is toxic[15]. To test this hypothesis, we stably transfected U251 cells with the standard pGfa2nLac plasmid, the enhanced gfa2 pGfa2(ABD)$_3$nLac or the highly active pSVβGal as a positive control. The initial high levels of β-galactosidase activity produced by

Fig. 3 Effect of time in culture on activity of enhanced gfa2 promoters. U251 cells were cotransfected with the indicated plasmids and pcDneo and starting 1 day later subjected to continuous selection with G418 (see Methods for details). Samples were taken 2, 4, 9, 14 and 21 days after transfection, and β-galactosidase activity determined and normalized to protein. Data shown are averages of duplicate samples relative to that for pGfa2nLac (absolute values for pGfa2nLac in arbitrary units/mg protein were 3947, 4163, 361, 695, and 6745 for the 2, 4, 9, 14 and 21 day time points, respectively). A similar outcome was observed in an independent experiment.

the pGfa2(ABD)$_3$nLac and pSVβGal plasmids decreased over time in culture to near that produced by the standard pGfa2nLac plasmid (Fig. 3).

To test whether the observed decay was peculiar to the nLac reporter gene, we also examined the chloramphenicol acetyltransferase (CAT) reporter in stably transfected cells and in mice. Results for stably transfected cells were similar to those obtained with the nLac reporter gene (data not shown). No activity was found in three lines of mice carrying a gfa2(B)$_1$CAT transgene or one with a gfa2(ABD)$_3$CAT transgene.

Strength of the Enhanced gfa2 Promoters in an Adenoviral Context

Apparently, the enhanced gfa2 promoter constructs are not useful when long-term, high level, astrocyte-specific expression is required. However, these strong and tissue-specific promoters may be advantageous when short-term, high-level expression is preferred, as in adenoviral cancer gene therapy applications. Therefore, we selected the two highest expressing constructs, gfa2(B)$_3$nLac and gfa2(ABD)$_3$nLac, and cloned these into a nonreplicating adenoviral vector to drive the LacZ marker gene. We then compared the strength of these enhanced gfa2-nLacZ promoter constructs with similar gfa2-nLacZ and CMV-nLacZ promoter constructs in an adenoviral context.

Fig. 4A illustrates X-gal staining in four GFAP positive cell lines (U251, GOS3, U373 and SNB19) and two GFAP negative cell lines (NCI-H1299 and SK-BR3). After infection with Adgfa2nLac, Adgfa2(B)$_3$nLac and Adgfa2(ABD)$_3$nLac, the GFAP positive cell lines had high to intermediate (>10%) percentages of β-galactosidase positive cells. The gfa2 enhanced
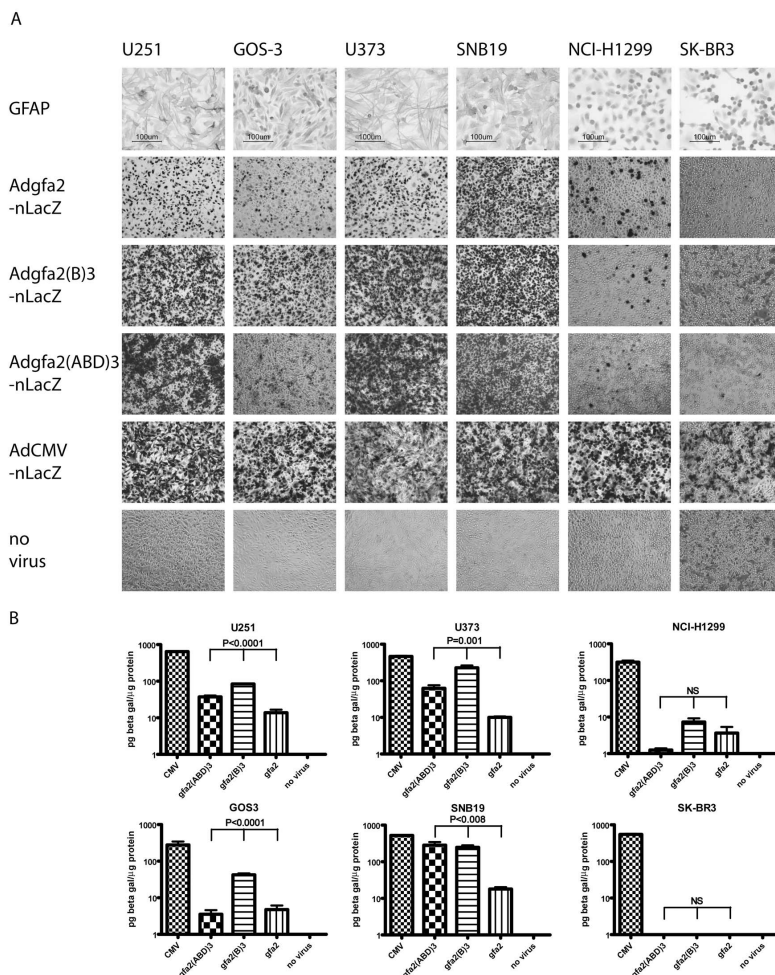
Fig. 4 Activity of gfa2 and enhanced promoters in an adenoviral context. **A:** X-gal staining 48 hours after infection with either adenoviral gfa2 or enhanced promoter constructs at a concentration of 100 pfu/cell. Infection with AdCMVnLac resulted in clear blue staining in all cell lines, indicating good and comparable viral entry. Infection of the GFAP-positive cell lines (U251, GOS3, U373 and SNB-19; see upper panel for GFAP staining at the time of the experiment) with the adenoviral enhanced constructs Adgfa2(B)$_3$nLac and Adgfa2(ABD)$_3$nLac yielded higher percentages of β-galactosidase expressing cells compared with the regular Adgfa2nLac. In the GFAP-negative cell lines (H1299 and SK-BR3), only sporadic β-galactosidase expressing cells were detected following infection with any of the gfa2 or enhanced promoter constructs. **B:** The β-galactosidase expression, following infection with the adenoviral vectors, was then measured by the Galacto-Light method. In the four GFAP positive cell lines (U251, GOS3, U373 and SNB19), the β-galactosidase expression levels obtained by Adgfa2(B)$_3$nLac and Adgfa2(ABD)$_3$nLac are almost always significantly higher than those obtained by Adgfa2nLac (ANOVA, P values indicated above brackets). The β-galactosidase concentration following infection with the enhanced promoter constructs is about 20-30% of the β-galactosidase concentration after infection by AdCMVnLac. In the two GFAP negative cell lines (SK-BR3 and H1299) β-galactosidase concentrations are much lower and do not differ significantly among the three constructs. Experiments were carried out in triplicate and bars indicate SEM. See Color figures, p. 153.

promoters tended to produce significantly higher β-galactosidase activity than the gfa2 parental promoter. The difference in X-gal staining between GFAP-positive and -negative cells was not due to a difference in adenoviral entry. After infection with the positive control AdCMVnLac virus, all cell lines showed 10-100% β-galactosidase positive cells.

We then measured and compared the β-galactosidase concentrations in the different cell lines (Fig. 4B). The mean β-galactosidase concentrations following infection of the GFAP positive cell lines with Adgfa2(ABD)$_3$nLac and Adgfa2(B)$_3$nLac were approximately 10-fold higher than with Adgfa2nLac (Table 1). The difference in β-galactosidase expression between Adgfa2(ABD)$_3$nLac and Adgfa2(B)$_3$nLac was not statistically significant. The average β-galactosidase expression levels in GFAP positive cell lines obtained with the adenoviral gfa2 enhanced promoter constructs were 20-30% of that of the strong CMV promoter construct AdCMVnLac. In the two GFAP-negative cell lines β-galactosidase concentrations were much lower and did not differ significantly among the three constructs.
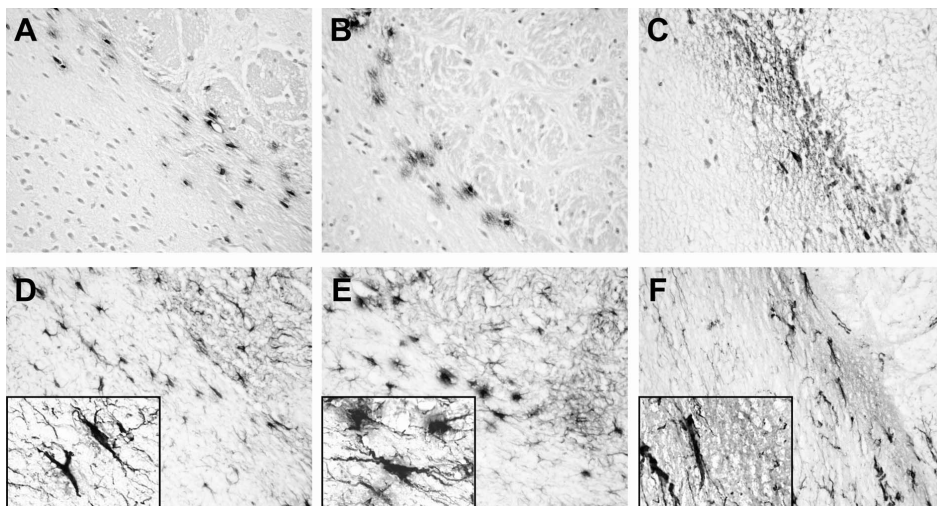
In Vitro Selectivity of gfa2 Enhanced Promoters in an Adenoviral Context

To obtain a better impression of the in vitro selectivity of the gfa2 and enhanced promoters in an adenoviral context, we infected all cell lines listed in material and methods with the adenoviral vectors and examined the β-galactosidase expression. X-gal staining showed robust β-galactosidase expression in all GFAP-positive cell lines, whereas only sporadic β-galactosidase staining was detected in the GFAP-negative cell lines. The only exception was the DU145 cell line that is derived from a rare prostate cancer brain metastasis.

To quantify the specificity of the adenoviral constructs for GFAP expressing cells, we calculated a selectivity index (SI). For each adenoviral construct, the SI is defined as the ratio of average β-galactosidase expression in the GFAP-positive cell lines over that in the GFAP-negative cell lines (including DU145). LacZ expression following AdCMVnLac was used to correct for differences in adenoviral infection efficiency among cell lines. The SI values (Table 1) indicate that both enhanced promoter constructs Adgfa2(ABD)$_3$nLac and Adgfa2(B)$_3$nLac as well as the regular Adgfa2nLac construct have significant selectivity for GFAP-positive cell lines. Thus, cell type selectivity of the gfa2 and enhanced promoters is preserved in an adenoviral context, at least in vitro. Moreover, the SI of Adgfa2(ABD)$_3$nLac and Adgfa2(B)$_3$nLac constructs was greater than that of the Adgfa2nLac construct while driving higher absolute β-galactosidase expression levels.

In Vivo Astrocyte Specificity of Adenoviral gfa2 Enhanced Promoter Constructs

To examine the selectivity of the adenoviral constructs in vivo, we injected the vectors into the brain of nude mice. Fig. 5 shows the β-galactosidase expression 3 days after injection of Adgfa2nLac, Adgfa2(B)$_3$nLac or AdCMVnLac. After injection with Adgfa2nLac (Fig. 5A, D) and Adgfa2(B)$_3$nLac (Fig. 5B, E), the blue staining is largely confined to GFAP expressing astrocytes. After injection of AdCMVnLac (Fig. 5C, F), additional staining of neurons is

Fig. 5 β-galactosidase expression in mouse brain following injection of adenoviral vectors. Adgfa2nLac (**A, D**), Adgfa2(B)$_3$nLac (**B, E**), or AdCMVnLac (**C, F**) was injected into the basal ganglia of nude mice (1x10^5 pfu). X-gal staining was performed 3 days after injection. Independent sections were either counterstained using nuclear fast red (red; **A, B, C**) or stained using polyclonal anti-GFAP (brown, **D-F**). After injection with both gfa2-based vectors. blue staining is observed in GFAP-positive astrocytes (**D, E**). Only after injection of AdCMVnLac, additional blue staining of neurons is observed (**F**). **A-F:** ×20; insets: ×100 amplification of a selected regions.
See Color Figures, p. 154.

observed. We conclude that the adenoviral gfa2 enhanced promoter constructs give high transgene expression levels in vivo while retaining their specificity for GFAP expressing cells.

Discussion

We constructed several enhanced gfa2-based promoters containing additional copies of either the B or ABD enhancer regions. Plasmids encoding the gfa2(B)$_3$ and gfa2(ABD)$_3$ promoters gave about 75-fold higher LacZ expression levels than the parental gfa2 promoter after transfection of U251 cells. Surprisingly, these promoters were not expressed at all in transgenic mice. A possible explanation for the repressed expression of the enhanced gfa2 promoters is that a significant long-term increase in the already robust activity of the gfa2 promoter is toxic [15]. In support of this hypothesis we have found that when U251 cells are stably transfected with pGfa2(ABD)$_3$nLac or the highly active pSVβGal positive control, the initial high levels of activity are lost with time in culture. Similar results with the CAT reporter in both mice and stably transfected cells suggest that the putative toxic effect is not reporter gene specific.

These results suggest that the enhanced gfa2 promoters will not be useful for long-term expression of transgenes, for example, for treatment of Alzheimer's disease[16] or Parkinson's

disease[17,18]. However, high level, short-term and glia-specific expression may be beneficial in the treatment of malignant gliomas. We therefore constructed adenoviral vectors containing the gfa2(B)$_3$ and gfa2(ABD)$_3$ promoters and compared these with control vectors encoding the basal gfa2 promoter or the strong universal CMV promoter. We report here that the adenoviral vectors encoding the enhanced gfa2 promoters were over 10 times more active than the adenovirus with the gfa2 basal promoter when transfected into GFAP-expressing glioma cells. In these cells, the mean reporter gene expression levels obtained with the Adgfa2(B)$_3$nLac and Adgfa2(ABD)$_3$nLac were 20-30% of the levels obtained with the AdCMVnLac control vector.

In an adenoviral context, the strength of the basal gfa2 promoter (2% of CMV) is comparable to the strength of other tissue-specific promoters available for adenoviral gene therapy, such as the VEGF-, CXCR4-, survivin-[19], and PSA-based promoters[20]. The gfa2 enhanced promoters on the other hand give rise to expression at the level of the strong viral CMV promoter in cell lines with high levels of GFAP. Such high expression levels have only recently been described for 'combined' promoters in adenoviral gene therapy of prostate cancer such as the PPT (93% of CMV) or PSES (30% of CMV) promoters[21,22]. Although many tissue-specific promoters lose their selectivity in an adenoviral context[23], both the adenoviral vector encoding the basal gfa2 promoter and the endoviral enhanced promoter constructs retained strong selectivity for GFAP-positive cells. We cloned the gfa2 and enhanced promoters in reverse orientation relative to wild-type E1 transcription, which might have contributed to the retained selectivity by preventing the influence of adenoviral enhancers in the adenoviral region containing the packaging signal.

Harkke et al.[24] reported loss of specificity of a similar gfa2 promoter construct cloned in reverse orientation into an E1-deleted adenoviral vector. However, this loss of specificity may be explained by the well-known rapid loss of GFAP expression of the cultured primary astrocytes that were used in this study. With a similar culture system, Smith-Arica et al.[25] found a perfect correlation between GFAP expression and reporter gene expression from a gfa2 promoter in an adenoviral vector, only when expression was tested on a cell-to-cell basis.

The strong and specific expression that we obtained with the enhanced gfa2 promoters in an adenoviral context makes these promoters ideal candidates for constructing adenoviral vectors specifically for glioma gene therapy. Recently, clinical trials have clearly demonstrated the safety and efficacy of adenoviral vectors for glioma gene therapy[26-31]. The newly developed enhanced gfa2 promoters can be used to improve the efficacy of glioma gene therapy by targeting high levels of expression of therapeutic genes to malignant glioma cells. In addition, strongly GFAP-positive, reactive astrocytes invade and surround malignant gliomas, which will add to local gene expression. Expression of therapeutic genes by these cells may increase the efficacy of glioma gene therapy, especially in regions where GFAP expression in the tumor cells themselves is reduced. An example would be enhancement

of the bystander effect that is critical for successful application of suicide genes such as HSV-tk[32] or increased delivery of conditionally replicating viruses. We are currently exploring the use of these enhanced promoters to specifically direct adenoviral replication to glial cells for the treatment of malignant gliomas.

Acknowledgments

References

1   Eng LF, Ghirnikar RS. GFAP and astrogliosis. *Brain Pathol 1994*; **4:** 229-237.

2   Doetsch F. The glial identity of neural stem cells. *Nat Neurosci 2003*; **6:** 1127-1134.

3   Ransom B, Behar T, Nedergaard M. New roles for astrocytes (stars at last). *Trends Neurosci 2003*; **26:** 520-522.

4   Su M, Hu H *et al.* Expression specificity of GFAP transgenes. *Neurochem Res 2004*; **29:** 2075-2093.

5   Besnard F, Brenner M *et al.* Multiple interacting sites regulate astrocyte-specific transcription of the human gene for glial fibrillary acidic protein. *J Biol Chem 1991*; **266:** 18877-18883.

6   Chen C, Okayama H. High-efficiency transformation of mammalian cells by plasmid DNA. *Mol Cell Biol 1987*; **7:** 2745-2752.

7   Chartier C, Degryse E *et al.* Efficient generation of recombinant adenovirus vectors by homologous recombination in Escherichia coli. *J Virol 1996*; **70:** 4805-4810.

8   Fallaux FJ, Kranenburg O *et al.* Characterization of 911: a new helper cell line for the titration and propagation of early region 1-deleted adenoviral vectors. *Hum Gene Ther 1996*; **7:** 215-222.

9   Graham FL, van der Eb AJ. A new technique for the assay of infectivity of human adenovirus 5 DNA. *Virology 1973*; **52:** 456-467.

10 Fallaux FJ, Bout A *et al.* New helper cells and matched early region 1-deleted adenovirus vectors prevent generation of replication-competent adenoviruses. *Hum Gene Ther 1998*; **9:** 1909-1917.

11 Michou AI, Santoro L *et al.* Adenovirus-mediated gene transfer: influence of transgene, mouse strain and type of immune response on persistence of transgene expression. *Gene Ther 1997*; **4:** 473-482.

12 Pietersen AM, van der Eb MM *et al.* Specific tumor-cell killing with adenovirus vectors containing the apoptin gene. *Gene Ther 1999*; **6:** 882-892.

13 Sanes JR, Rubenstein JL, Nicolas JF. Use of a recombinant retrovirus to study post-implantation cell lineage in mouse embryos. *Embo J 1986*; **5:** 3133-3142.

14 Brenner M, Kisseberth WC *et al.* GFAP promoter directs astrocyte-specific expression in transgenic mice. *J Neurosci 1994*; **14:** 1030-1037.

15 Smith JD, Sikes J, Levin JA. Human apolipoprotein E allele-specific brain expressing transgenic mice. *Neurobiol Aging 1998*; **19:** 407-413.

16 Feng X, Eide FF, Jiang H, Reder AT. Adeno-associated viral vector-mediated ApoE expression in Alzheimer's disease mice: low CNS immune response, long-term expression, and astrocyte specificity. *Front Biosci 2004*; **9:** 1540-1546.

17 Cortez N, Trejo F, Vergara P, Segovia J. Primary astrocytes retrovirally transduced with a tyrosine hydroxylase transgene driven by a glial-specific promoter elicit behavioral recovery in experimental parkinsonism. *J Neurosci Res 2000*; **59:** 39-46.

18 Do Thi NA, Saillour P *et al.* Delivery of GDNF by an E1,E3/E4 deleted adenoviral vector and driven by a GFAP promoter prevents dopaminergic neuron degeneration in a rat model of Parkinson's disease. *Gene Ther 2004*; **11:** 746-756.

19 Rein DT, Breidenbach M *et al.* Evaluation of tissue-specific promoters in carcinomas of the cervix uteri. *J Gene Med 2004*; **6:** 1281-1289.

20 Latham JP, Searle PF, Mautner V, James ND. Prostate-specific antigen promoter/enhancer driven gene therapy for prostate cancer: construction and testing of a tissue-specific adenovirus vector. *Cancer Res 2000*; **60:** 334-341.

21 Cheng WS, Kraaij R *et al.* A novel TARP-promoter-based adenovirus against hormone-dependent and hormone-refractory prostate cancer. *Mol Ther 2004*; **10:** 355-364.

22 Lee SJ, Kim HS *et al.* Novel prostate-specific promoter derived from PSA and PSMA enhancers. *Mol Ther 2002*; **6:** 415-421.

23 Shi CX, Hitt M, Ng P, Graham FL. Superior tissue-specific expression from tyrosinase and prostate-specific antigen promoters/enhancers in helper-dependent compared with first-generation adenoviral vectors. *Hum Gene Ther 2002*; **13:** 211-224.

24 Harkke S, Laine M, Jalanko A. Aspartylglucosaminidase (AGA) is efficiently produced and endocytosed by glial cells: implication for the therapy of a lysosomal storage disorder. *J Gene Med 2003*; **5:** 472-482.

25 Smith-Arica JR, Morelli AE *et al.* Cell-type-specific and regulatable transgenesis in the adult brain: adenovirus-encoded combined transcriptional targeting and inducible transgene expression. *Mol Ther 2000*; **2:** 579-587.

26 Smitt PS, Driesse M *et al.* Treatment of relapsed malignant glioma with an adenoviral vector containing the herpes simplex thymidine kinase gene followed by ganciclovir. *Mol Ther 2003*; **7:** 851-858.

27 Immonen A, Vapalahti M *et al.* AdvHSV-tk gene therapy with intravenous ganciclovir improves survival in human malignant glioma: a randomised, controlled study. *Mol Ther 2004*; **10:** 967-972.

28 Trask TW, Trask RP *et al.* Phase I study of adenoviral delivery of the HSV-tk gene and ganciclovir administration in patients with current malignant brain tumors. *Mol Ther 2000*; **1:** 195-203.

29 Sandmair AM, Loimas S *et al.* Thymidine kinase gene therapy for human malignant glioma, using replication-deficient retroviruses or adenoviruses. *Hum Gene Ther 2000*; **11:** 2197-2205.

30 Judy KD, Eck SL. The use of suicide gene therapy for the treatment of malignancies of the brain. In: Lattime EC, Stanton LG (eds). *Gene Therapy of Cancer*. Academic Press: San Diego, 2002.

31 Germano IM, Fable J, Gultekin SH, Silvers A. Adenovirus/herpes simplex-thymidine kinase/ganciclovir complex: preliminary results of a phase I trial in patients with recurrent malignant gliomas. *J Neurooncol 2003*; **65:** 279-289.

32 Puumalainen AM, Vapalahti M *et al.* Beta-galactosidase gene transfer to human malignant glioma in vivo using replication-deficient retroviruses and adenoviruses. *Hum Gene Ther 1998*; **9:** 1769-1774.

Targeting Malignant Gliomas with a Glial Fibrillary Acidic Protein (GFAP)-Selective Oncolytic Adenovirus

Maarten ter Horst[1], Eric Brouwer[1], Suzanne Verwijnen[2], Mark Rodijk[1], Marion de Jong[2], Rob Hoeben[3], Bertie de Leeuw[1], and Peter Sillevis Smitt[1]

Departments of [1]Neurology and [2]Nuclear Medicine, Erasmus University Medical Center, Rotterdam and [3]Department of Molecular Cell Biology, Leiden University Medical Center, Leiden, The Netherlands.
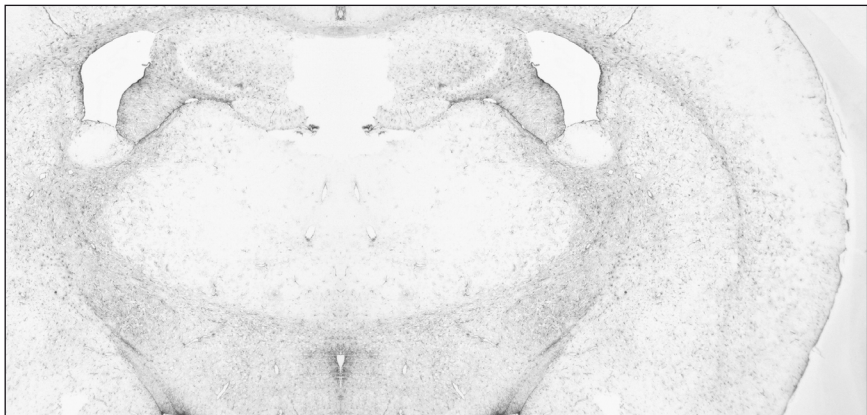
Abstract

Glial fibrillary acidic protein (GFAP) is an intermediate filament protein abundantly expressed in malignant gliomas. We have constructed a novel oncolytic adenovirus, Ad5-gfa2(B)3-E1 for treatment of these tumors. In this construct, the E1 region is under control of the tissue specific GFAP promoter (gfa2) with three additional copies of the glial specific 'B' enhancer. Infection of a GFAP positive cell line with Ad5-gfa2(B)3-E1 resulted in E1A and E1B expression at 75% and 30% of the levels obtained after wtAd5 infection. Q-PCR showed that Ad5-gfa2(B)3-E1 replicated 4.5 times more efficiently in the GFAP-positive than in the GFAP-negative cell lines. Cell viability assays showed efficient elimination of GFAP positive cells by Ad5-gfa2(B)3-E1, in some cell lines as efficiently as wtAd5, while the elimination was attenuated in GFAP negative cell lines.

When tested in human tumor xenografts in nude mice, Ad5-gfa2(B)3-E1 effectively suppressed the growth of GFAP-positive SNB-19 glial tumors but not of GFAP-negative A549 lung tumors. In Ad5-gfa2(B)3-E1, the E3 region was deleted to create space for future insertion of heterologous therapeutic genes. Experiments with dl7001, an E3 deleted variant of wtAd5, confirmed that the specificity of Ad5-gfa2(B)3-E1 replication was based on the promoter driving E1 and not on the E3 deletion. Strategies to further improve the efficacy of Ad5-gfa2(B)3-E1 for the treatment of malignant gliomas include the insertion of therapeutic genes in E3 or retargeting to receptors that are more abundantly expressed on primary glioma cells than CAR.

Introduction

Despite advances in neurosurgical techniques, radiation treatment and chemotherapy, the overall median survival of patients with a malignant glioma remains less than 1 year and fewer than 5% survive for 5 years or longer[1,2]. Based on the locally invasive, non-metastatic growth pattern of malignant gliomas and the poor prognosis of the patients, novel loco-regional treatment strategies such as gene therapy are under investigation for the treatment of these tumors[3].

Recently, a randomized clinical trial reported the successful adjuvant treatment of malignant glioma patients with a replication-defective adenoviral vector encoding HSV1-tk[4]. Despite their excellent safety record and preliminary evidence of efficacy, non-replicating viral vector systems are clearly limited by the requirement for effective tumor penetration and transduction of a large amount of tumor cells[5]. This led to the development of oncolytic viral vectors for the treatment of brain tumors, including herpes virus[6,7], reovirus[8] and condition-ally replicative adenoviral vectors (CRAds)[9-11].

CRAds effect greater transduction due to local replication and dispersion[12]. In addition, viral replication kills infected cells and causes local amplification of therapeutic effects[9-11]. To prevent damage to normal tissue, in particular the liver, CRAds are generally designed to replicate selectively in tumor cells. Such strategies include mutation-type CRAds and promoter-controlled-type CRAds. Deletions in the Rb-binding region of E1A (e.g. the delta24 adenovirus[13]) or in E1B (e.g. ONYX-015[14]) increased the tumor specificity of viral replication but in many cases also decreased the efficiency of viral replication[13,15]. In addition, the strin-gency of replication control in these CRAds is still under discussion[16,17]. Another approach is the use of tissue or tumor specific promoters (TTSP) to drive viral genes that are critical for replication, such as E1A, E1B or E4. Many well-characterized TTSP have been investigated in CRAds for cancer gene therapy to avoid damage to the host, especially the liver. Several CRAds controlled by tumor specific promoters have been examined in malignant glioma cells lines. These include the survivin[18], midkine (MK)[19], the cyclooxygenase-2 (COX-2)[20] and the hypoxia / hypoxia inducible factor (HIF) responsive promoter[21]. To our knowledge, no CRAd regulated by a strong and selective tissue specific promoter has been developed for specific treatment of gliomas.

Glial fibrillary acidic protein (GFAP) is an intermediate filament that is highly and selectively expressed in glial cells at both the mRNA and protein level[22]. In addition, immunohistochem-istry studies have confirmed high expression levels of GFAP protein in malignant gliomas, although the intensity of the staining can be very heterogeneous[23]. The GFAP promoter (gfa2) has previously been shown to retain its specificity when used to drive transgene expression in an adenoviral context [24,25]. Within the 2.2 kb gfa2 promoter segment, three important enhancer regions have been identified within, named A, B and D[26]. We previ-ously demonstrated that fusion of three B-enhancer regions with the gfa2 promoter resulted

in strong and highly specific marker gene expression in a replication-defective adenoviral vector[22]. We have now constructed a new oncolytic adenovirus with E1A regulated by the gfa2(B)3 promoter / enhancer (Ad5-gfa2(B)3-E1). To optimize glial specificity, we inserted the promoter-E1 sequence in the inverse orientation compared to wild-type (wt) E1 transcription. Here we show that replication and oncolytic efficacy of Ad5-gfa2(B)3-E1 is comparable to wtAd5 in GFAP-expressing cells while being attenuated in GFAP-negative cells. Treatment of subcutaneous, GFAP-positive SNB-19 tumors in nude mice with Ad5-gfa2(B)3-E1 resulted in significant slowing of tumor growth, although less than wtAd5, while no such effect was observed in GFAP-negative A549 subcutaneous tumors. Finally, we show that the attenuation of the oncolytic efficacy of Ad5gfa2(B)3-E1 *in vivo*, compared to wtAd5, probably results from the deletion of E3 in the former.

Materials and Methods

Cell lines

Cell lines were selected based on GFAP expression as determined by Western blotting and immunohistochemistry[22] and are summarized in Table 1.

U87MG and MRC-5 cells were cultured according to the ATCC's protocol in Eagle's Minimum Essential Medium (EMEM) (Invitrogen, Paisley, UK) with 0.1 mM non-essential amino acids, 2 mM L-glutamine, 1 mM sodium pyruvate, and 1500 mg/l sodium bicarbonate, 10% heat inactivated (30 min 56°C) fetal bovine serum (FBS) (Invitrogen), 100 I.U./ml penicillin and 100 µg/ml streptomycin (Invitrogen). A549, NCI-H1299, SK-BR3, CAMA-1, U251, SNB-19, GOS-3 and 10.278 were cultured in DMEM (Invitrogen) containing 4500mg/L glucose, L-glutamine and pyruvate with 10% FBS (Invitrogen), 100 I.U./ ml penicillin and 100

Table 1 Cell lines and GFAP expression

Cell line	Origin	GFAP	Source
U251	Glioblastoma multiforme	+	P Körnblith, NIH
SNB-19	Glioblastoma multiforme	+	DSMZ
GOS-3	Anaplastic oligo-astrocytoma	+	DSMZ
10.278	Glioblastoma multiforme	+	Erasmus MC
U87MG	Glioblastoma multiforme	+/-	ATCC
A549	Non-small cell lung carcinoma	-	ATCC
NCI-H1299	Non-small cell lung carcinoma	-	ATCC
SK-BR3	Breast adenocarcinoma	-	ATCC
CAMA-1	Breast adenocarcinoma	-	ATCC
MRC-5	Human normal fibroblast	-	ATCC

GFAP expression of cell lines was determined by Western blotting and immunohistochemistry[22].
DSMZ, Deutsche Sammlung von Mikroorganismen und Zellkulturen GmbH; ATCC, the American Type Culture Collection.

μg/ml streptomycin (Invitrogen) and passaged 1:20 (37°C; 5% CO2). The E1-transformed embryonal retina cell line PER.C6 was cultured on the same medium with extra glucose (3g/l) and passaged 1:5[27].

Adenoviral vector construction

The design of the adenoviral constructs is presented in Fig. 1.

Ad5-gfa2(B)3-nLacZ. We previously constructed an adenovirus serotype 5 based, E1-deleted and partially E3-deleted vector encoding the β-galactosidase marker gene (nLacZ) driven by the gfa2(B)3 promoter[22]. We have also demonstrated that the glia specificity of the gfa2(B)3 promoter was retained in this construct[22].

Ad5-gfa2(B)3-E1. The conditionally replicating adenovirus Ad5-gfa2(B)3-E1 was obtained by replacing the nLacZ sequence from the pShuttle plasmid corresponding to the Ad5-gfa2(B)3-nLacZ virus with the adenoviral E1 region (nucleotides (nt) 554 to 4119). Using site directed mutagenesis a SalI site was created in pAd5XhoIC, containing the adenoviral E1 region (nt 1 to5793) just in front of the start ATG of the E1A gene (position 552)(giving rise to plasmid pAd5XhoIC-Sal). Subsequently, the SalI-HindIII fragment of the nLacZ gene was cut out of the gfa2(B)3-Shuttle plasmid and replaced by the SalI-HindIII fragment from pAd5XhoIC-Sal, comprising the complete open reading frame from E1A and part of the E1B 55K open reading frame (pShuttle-gfa2(B)3-E1A). Subsequently a HindIII-partial SmaI fragment containing the rest of E1B plus pIX and the pIX polyA sequence was cut out of pAdXhoIC-Sal and ligated into plasmid pShuttle-gfa2B3-E1A cut with HindIII-EcoRV (pShuttle-gfa2(B)3-E1).
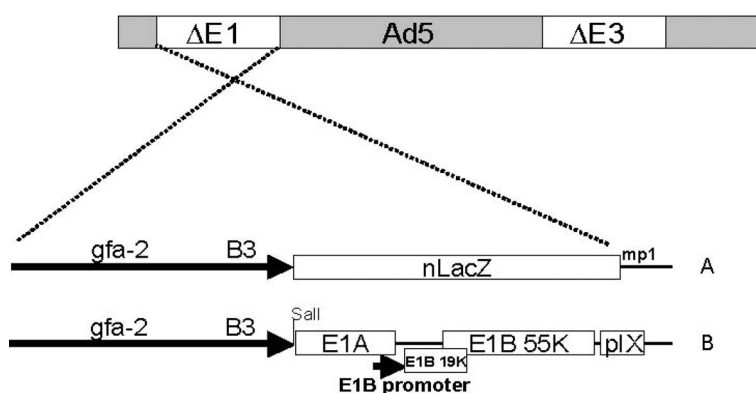
Fig. 1 Schematic of the adenoviral vectors used in this study. (A) The replication defective Ad5-gfa2(B)3-nLac contained the gfa2(B)3 'super' promoter to drive nLacZ. (B) Ad5-gfa2(B)3-E1 is replication competent and the gfa2(B)3 'super' promoter was fused to the adenovirus E1A region. Both the promoter-nLac (A) and promoter-E1 (B) sequences were inserted in the inverse orientation compared to wild-type E1 transcription.

The resulting Shuttle plasmid was digested with PmeI and transfected into E. coli BJ5183 containing the AdEasyI plasmid and colonies were selected on kanamycin-resistance plates. Genuine recombinants were selected, digested with PacI and transfected into 911 cells[28] using the calcium-phosphate technique[29]. Two independent plaques were picked and propagated on PERC6 cells[27] and checked for integrity of the DNA using HindIII and PstI digestion.

Wild-type Adenovirus type 5 (wtAd5) was kindly provided by Dr. R. Vogels (Crucell Holland BV, Leiden, Netherlands). Dl7001, an E3 deleted variant of wtAd5, was obtained from W.S. Wold (St. Louis University school of medicine, St Louis, MO)[30].

Vector production

All vectors were propagated to high titers on PER.C6 cells, CsCl gradient purified, dialysed and stored at -80°C in sucrose buffer (140 mM NaCl, 5 mM Na_2HPO_4, 1.5mM KH_2PO_4, 20 mM $MgCl_2$ and 5% sucrose). All batches were screened for replication competent adenovirus (RCA) and were negative for wtE1A promoter containing virus[31]. Titrations were performed on 911 cells and are presented as plaque forming units (pfu) per ml[28]. The titers ranged from 8.9×10^8 to 1.8×10^9 pfu/ml.

E1A and E1B expression

Cells (SK-BR3 and U251 cells) were seeded at a density of 2×10^5 cells/dish in a 24 well plate (Corning corporate, Corning, NY). The next day, the cells were infected with wtAd5 or Ad5-gfa2(B)3-E1 at 10 pfu/cell. After 2 h, the medium was removed and fresh medium was added. After 12 h of incubation the cells were washed with phosphate-buffered saline (PBS) (0.5 mM $MgCl_2$) and lysed in 300 µl of a mixture of 150 mM NaCl, 50 mM Tris pH 7.5, 0.1 % sodium dodecyl sulfate (SDS), 0.5 % sodium deoxycholate and 1% NP40. Lysates were sonicated, and protein concentrations were determined using the BCA Protein Assay Kit (Pierce, Rockford, IL). Equal amounts (13 µg) of protein were separated on an acrylamide gel (11%). Gels were processed as described above. Immunoblots were then incubated with mouse monoclonal anti-adenovirus type 5 E1A clone M58 (1:500, BD PharMingen, Franklin Lakes, NY), mouse monoclonal anti-E1B A_1C6, recognizing the 55 kDa E1B protein (1:3, kindly provided by R. Hoeben, Leiden, the Netherlands) for 30 min or mouse monoclonal anti-actin clone C4 (1:400, MP Biomedicals, Aurora, OH) for 120 min, followed by alkaline phosphatase conjugated rabbit anti-mouse secondary antibody (1:500, 30 min. RT, DAKO). The color reaction was developed with the Biorad AP Conjugate Substrate kit (Hercules, CA). To determine the E1A and E1B expression levels of GFAP positive cells, the immunoblots were scanned. Subsequently, the intensity levels of the E1A and E1B bands were determined by NIH-image (National Institute of Health, Bethesda, MD) and expressed as percentage of the levels obtained following wtAd5 infection.

Real-time quantitative PCR

Cells were cultured in 24-well plates at a density of 1x10^{5} cells/well, incubated overnight (37ºC) and infected with viral vectors after refreshing the medium. To study a single round of replication (Fig. 3), cells were infected at a concentration of 10 pfu/cell and harvested 48 hours after infection. To allow multiple rounds of replication and lateral dispersion (Fig. 6), cells were infected at a concentration of 0.1 pfu/cell and harvested after one week. After extensive washing of the cells, total DNA was isolated using Dneasy Tissue Kit (Qiagen, Valencia, CA); 20 µl proteinase and 200 µl Buffer AL were added and incubated at 70°C for 10 min followed by addition of 200 µl ethanol. The mixture was spun with a Dneasy (Quiagen) mini spin column and the DNA eluated with 3x70 µl buffer AE.

The ABI Prism 7700 sequence detection system (Applied Biosystems, Foster City, CA) was used for detecting real-time quantitative PCR products. The primers and probes for detecting adenovirus type 5 genome were previously described[32]: primer AdClipF (5'-GCG ACG GAT GTG GCA AAA GT-3'), primer AdClipR (5'-CCT AAA ACC GCG CGA AAA-3') and probe AdClipP (5'-CAC CGG CGC ACA CCA AAA ACG-3'; 5' labeled with 6-carboxylfluo-rescein and 3' labeled with tramethylrhodamine). The 25 µl PCR reaction mixture contained Taqman universal PCR Master Mix (Applied Biosystems), 300 nM each forward and reverse primer, 100 nM of the fluorogenic probe and 10ng of DNA. The initial denaturation step (2 min at 95°C) was followed by 40 cycles of 15 s at 95°C and 1 min at 60°C.

To quantify cellular DNA, primers located on an intron of Chromosome 11 were used. The forward primer C11-PBGD-F (5'-TGA GGC GGA TGC AGA TAC-3') and reverse primer C11-PBGD-R (5'-CCC ACC CAC GGT AGT AAT TC-3') have been applied in a SYBR-based assay, with the following protocol: PCR reactions were performed in a final volume of 25 µl containing 10 ng DNA, 300 nM forward and reverse primer and 12.5 µl SYBR-green PCR-master-mixture (Applied Biosystems). After 10 min denaturation and activation of the Taq-DNA-polymerase, PCR products were amplified in 35 cycles of 15 s at 95°C, annealed for 30 s at 62°C, ramped for 10 s to 72°C, extended for 20 s at 72°C, ramped for 10 s to 79°C and for 20s at 79°C. SYBR green fluorescent signals of the products were acquired after each cycle at 72°C. A reference dye, ROX was included in all assays to normalize data for non-PCR related signal variation. Calibration curves of Ct values were generated for the DNA extracted from purified wtAd5 and PBS infected cells and validated using linear regression analysis. The calibration curve was used to calculate the number of cells (Ch11 Q-PCR data) and the number of virus particles (Ad5 Q-PCR data). The quotient of these numbers equals the number of virus particles per cell (vp/cell). Less than 0.1 vp/cell indicated "no replication". We calculated the efficacy of replication (EOR) of Ad5-gfa2(B)3-E1 in each cell line by dividing Ad5gfa2(B)3-E1 vp/cell by wtAd5 vp/cell (Fig 3, 6) or Ad5gfa2(B)3-E1 vp/cell by dl7001 vp/cell (Fig 6), or dl7001 vp/cell by wtAd5 vp/cell (Fig 6). In this way, differences in adenoviral infectivity and other aspects of the adenoviral life-cycle can be normalized across cell lines[33].

In vitro cytotoxicity assay

Cells (SNB-19, U251, GOS-3, A549, NCI-H1299, SK-BR3) were cultured in 24-well plates at a density of 1×10^5 cells/well and infected the next day with Ad5-gfa2(B)3-nLacZ, Ad5-gfa2(B)3-E1 or wtAd5 at a dose of 0.1, 1, 10 or 100 pfu/cell. After 2 h medium was removed and fresh medium was added. After two days the cells were washed with PBS and 100 μl XTT (Sigma, St Louis, MO) in DMEM w/o phenol red and serum was added. After 2-6 h incubation at 37°C, the optical density (OD) 450 nm was measured. The relative survival was calculated to equalize for the different mitochondrial activity in cell lines and was expressed as a ratio of non-infected control and plotted versus vector dose. All experiments were performed in triplicate.

Subcutaneous tumor xenograft model in nude mice

All experimental protocols were approved by the Institutional Animal Care and Use Committee, in compliance with the Guide for the Care and Use of Laboratory Animals. Female nu/nu BALB/C mice (Charles River, Les Oncins, France), 5-6 weeks of age were purchased. Mice were hosted 3–4/cage and allowed access to food and water *ad libitum*. After 1 week, 1×10^7 SNB-19 or A549 cells were inoculated subcutaneously into both flanks in 250 μl of Hank's balanced salt solution (HBSS) (Invitrogen). The tumor growth was assessed by measuring bidimensional diameters three times a week with calipers. The tumor volume was determined by using the simplified formula of a rotational ellipse (length x width^2 x 0.5)[34]. When the tumor reached a volume of 100–150 mm^3, animals were randomly assigned into groups. A single dose of 4×10^7 plaque forming units (pfu) wtAd5 resp Ad5-gfa2(B)3-E1 or PBS was administered intratumorally in a total volume of 50 μl. The animals were killed by cervical dislocation when their tumors reached a volume of >2000 mm^3 or caused unethical animal harm. Each treatment group consisted of a minimum of four animals (eight tumors).

Statistical analysis

Data were analyzed using GraphPad Prism version 4.0 software (GraphPad Software, Inc., San Diego, CA, 2002). All tests (T-tests) and were carried out two-sided and $P < 0.05$ was considered statistically significant.

Results

E1A and E1B expression after infection with Ad5-gfa2(B)3-E1

The efficacy and selectivity of the gfa2(B)3 promoter in the context of a conditionally replicative adenoviral vector (CRAd) was first tested by examining E1A and E1B expression following infection with Ad5-gfa2(B)3-E1 (Fig. 2). The results were compared to those of the unattenuated virus, wtAd5. Infection with wtAd5 resulted in strong E1A and E1B expression
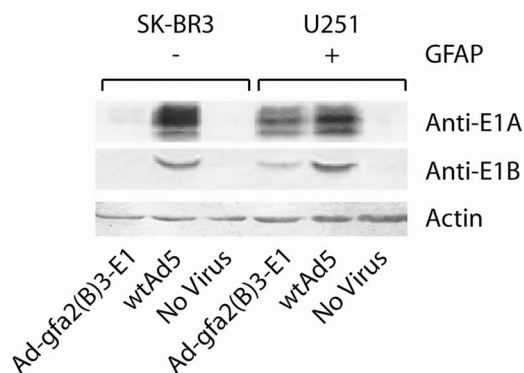
Fig. 2 Western blot analysis of the E1A and E1B-55kDa proteins. SK-BR3 (GFAP negative) and U251 (GFAP positive) cells were infected with Ad5-gfa2(B)3-E1 or wtAd5 at an MOI of 10 or no virus was added. Twelve hours later, cells were harvested, lysed and E1A and E1B proteins was determined by Western blotting. Actin was used as loading control.

after 12 h in both cell lines tested. Infection of the GFAP-positive glial cell line U251 with Ad5-gfa2(B)3-E1 resulted in E1A and E1B expression at 75% and 30% of the levels obtained after wtAd5 infection. After infection of the GFAP-negative cell line SK-BR3 with Ad5-gfa2(B)3-E1, E1A and E1B expression levels were nearly undetectable on Western blot. In the CRAd construct, the gfa2(B)3 promoter was functional, selective and able to drive high level E1A and E1B expression.

Replication of Ad5-gfa2(B)3-E1

To further establish the selectivity of Ad5-gfa2(B)3-E1 replication in GFAP expressing cells, we infected three GFAP-positive and three GFAP-negative cell lines with Ad5-gfa2(B)3-E1 or with wtAd5. Cells were infected at multiplicity of infection (MOI) 10 pfu/cell, resulting in direct infection of >95% of cells (not shown). The number of viral particles produced 48 h after infection was determined by real-time PCR. Infection with the replication-defective control vector Ad5-gfa2(B)3-nLacZ revealed no viral replication (< 0.1 vp/cell), while infection with wtAd5 produced 25,000-90,000 vp/cell 48 h after infection in all six cell lines tested.

In GFAP-positive cells, the vp/cell ratios were significantly higher following infection with Ad5-gfa2(B)3-E1 than in the GFAP-negative cells ($p<0.05$). Following infection with wtAd5, no significant differences were observed between GFAP-positive and GFAP-negative cells. We then calculated the efficacy of replication (EOR) of Ad5-gfa2(B)3-E1 in each cell line, relative to wtAd5, by dividing the Ad5-gfa2(B)3-E1 vp/cell by the vp/cell of wtAd5 (Fig. 3). After infection with Ad5-gfa2(B)3-E1 the mean EOR in the three GFAP-positive cell lines was 0.58 while it was 0.13 in the GFAP-negative cell lines ($p<0.05$). These data indicate that Ad5-gfa2(B)3-E1 replicated 4.5 times more efficiently in the GFAP-positive than in the GFAP-negative cell lines.
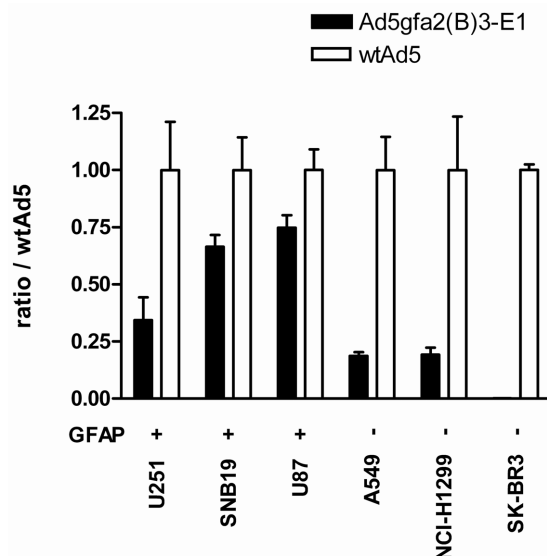
Fig. 3 Viral replication of Ad5-gfa2(B)3-E1. 1×10^5 cells were plated on 24-well plates. After 24h, the cells were infected at a MOI of 10 with Ad5-gfa2(B)3-E1 or wtAd5. After another 48h, DNA was isolated and the level of cellular and adenovirus DNA in samples was determined by Q-PCR. The efficacy of replication is calculated as the ratio of the vp/cell obtained by Ad5-gfa2(B)3-E1 and the vp/cell obtained by wtAd5.

Oncolysis induced by Ad5-gfa2(B)3-E1 in vitro

To test the efficacy and selectivity of Ad5-gfa2(B)3-E1 induced oncolysis, we performed a cell viability assay (XTT). We tested five glial cell lines with varying GFAP-expression levels and three control cell lines that were non-glial and GFAP-negative. This cell panel was infected with wtAd5, Ad5-gfa2(B)3-nLacZ or Ad5-gfa2(B)3-E1 at MOIs ranging from 0.1 to 100 pfu/cell. Forty-eight hours after infection the remaining viable cells were determined. As shown in Fig. 4, Ad5-gfa2(B)3-E1 eliminated GFAP positive cells (SNB-19, U251, U87MG, 10.278 and GOS-3) efficiently, and in some cell lines as efficiently as wtAd5. This indicated that Ad5-gfa2(B)3-E1 had retained oncolytic potency as compared to wtAd5. No clear correlation between oncolytic potency and GFAP expression level was observed. Importantly, the oncolytic effect of Ad5-gfa2(B)3-E1 was attenuated in the GFAP-negative cell lines (A549, NCI-H1299, SK-BR3), although these cells were highly susceptible to adenovirus infection as demonstrated by the effect of wtAd5. At MOI 10 and 100, the proportion of surviving cells in GFAP negative lines was significantly lower following wtAd5 infection than after infection with Ad5-gfa2(B)3-E1 ($p<0.05$). Infection with the replication-defective control virus Ad5-gfa2(B)3-nLacZ did not result in cell death.
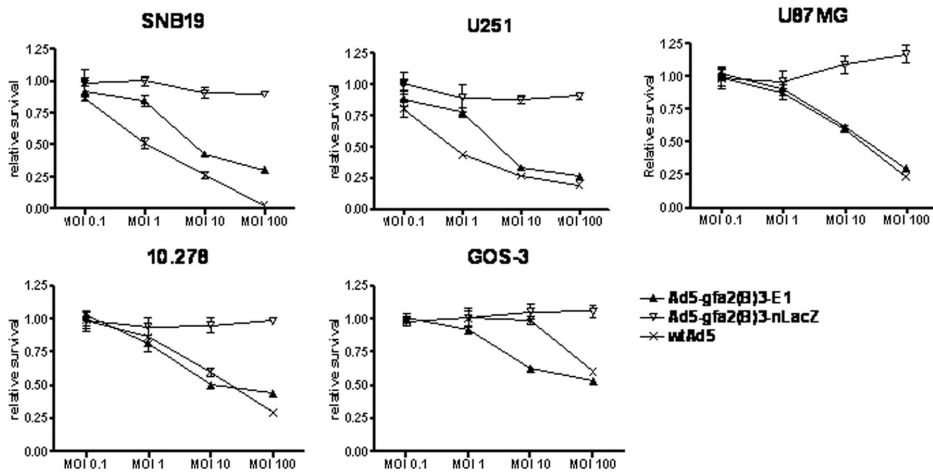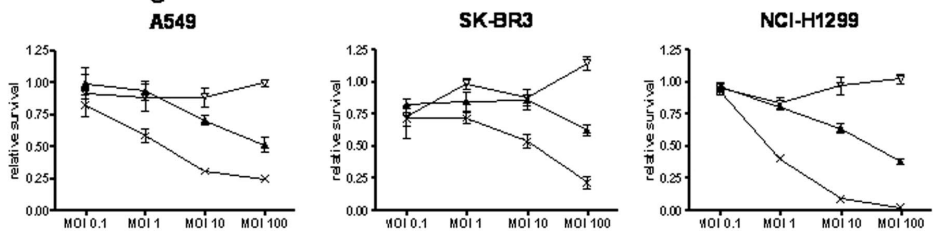
Fig. 4 Oncolytic effect of Ad5-gfa2(B)3-E1 in vitro. Cells were plated on 24-well plates and 24 h later infected with Ad5-gfa2(B)3-nLacZ, Ad5-gfa2(B)3-E1 or wtAd5 at different MOIs. Two days after infection, the number of surviving cells was assessed by the ability to reduce XTT. The average values of triplicate determinations are presented as proportion of the value obtained for uninfected controls. Error bars indicate SD.

Oncolysis induced by Ad5-gfa2(B)3-E1 in vivo

The previous experiments demonstrated that Ad5-gfa2(B)3-E1 was efficient and specific in eliminating GFAP-positive cancer cells *in vitro* and suggested that it could be used to eradicate GFAP-positive tumors *in vivo*. To test this hypothesis, we generated SNB-19 (GFAP-positive) and A549 (GFAP-negative) subcutaneous xenografts in nude mice. When the tumors had reached a volume of 100-150 mm^3, animals were treated by a single intratumoral injection of 4x10^7 pfu of wtAd5, Ad5-gfa2(B)3-E1 or PBS. In SNB19 xenografts, Ad5-gfa2(B)3-E1 injection reduced the tumor growth compared to the PBS injected animals. From day 14 onwards, there was a statistically significant difference in tumor volume compared to PBS (p<0.05). However, injection of wtAd5 into the SNB19 xenografts resulted in an even stronger oncolytic effect on tumor growth than Ad5-gfa2(B)3-E1 injection, which reached statistical significance at day 10 (p<0.05).
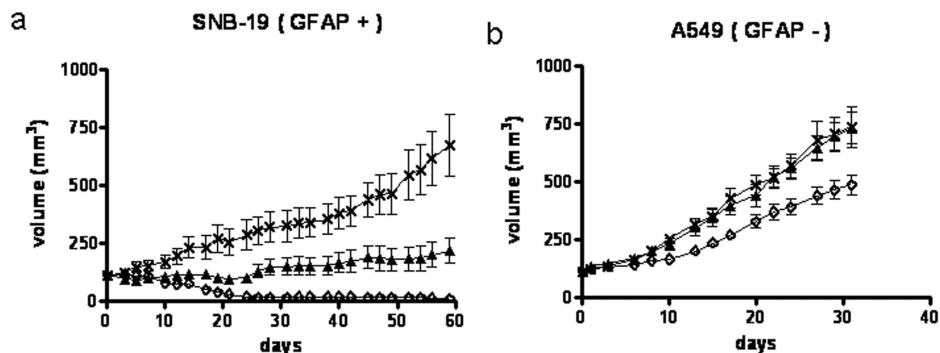
Fig. 5 Antitumor activity in subcutaneous xenografts. Tumor xenografts were established by injecting 1×10^7 SNB-19 (GFAP positive; A) or A549 (GFAP negative; B) cells suspended in 250 µl of HBSS in both flanks of nude mice. When tumor volumes reached about 100-150 mm^3, animals were treated with a single injection of 4×10^7 pfu wtAd5 or Ad5-gfa2(B)3-E1 or PBS in a total volume of 50 µl. Each treatment group consisted of 8-12 tumors. Ad5-gfa2(B)3-E1 injection resulted in a significant ($p < 0.05$) oncolytic effect in GFAP-positive SNB-19 xenografts (A) but not in GFAP-negative A549 xenografts (B). —✕— PBS —▲— Ad5-gfa2(B)3-E1 —◇— wtAd5. Error bars indicate SEM.

In contrast, the growth curve of A549 xenografts injected with Ad5-gfa2(B)3-E1 did not differ from the PBS injected controls ($p > 0.47$ at all time points). Injection of wtAd5 resulted in significantly reduced growth of the A549 xenografts compared to the controls ($p < 0.05$, 31 days after injection) (Fig. 5).

Deletion of E3 attenuates the oncolytic potency of Ad5-gfa2(B)3-E1

The attenuation of the oncolytic efficacy of Ad5-gfa2(B)3-E1 *in vivo* compared to wtAd5 in a GFAP positive tumor could either be caused by the insertion of the gfa2(B)3 promoter or by the deletion of E3 in the CRAd. To further assess the effect of the E3 deletion, we compared the replicative potential of Ad5-gfa2(B)3-E1 with dl7001, an E3 deleted variant of wtAd5, and with wtAd5, the gold-standard for efficacy. To allow several rounds of cell lysis and infection, as occurs *in vivo*, we infected cells with Ad5gfa2(B)3-E1, dl7001 and wtAd5 at MOI 0.1 (pfu/cell) and performed Q-PCR 1 week after infection. The EOR of Ad5gfa2(B)3-E1 relative to dl7001 was 2.4 in GFAP positive cell lines and 0.1 in GFAP negative cell lines ($p < 0.0005$). However, infection with both Ad5gfa2(B)3-E1 and dl7001 resulted in a lower yield of viral particles compared to wtAd5 (Fig. 6). Therefore, the attenuation of the oncolytic efficacy of Ad5gfa2(B)3-E1 relative to wtAd5 in GFAP-positive tumors *in vivo* may have been caused by the E3 deletion.
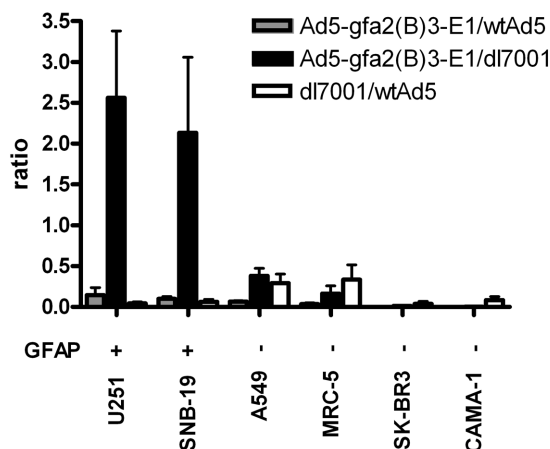
Fig. 6 E3 deletion and oncolytic efficacy in vitro. Cells (1×10^5) were plated on 24-well plates. After 24h, the cells were infected at a MOI of 0.1 with Ad5-gfa2(B)3-E1, wtAd5 or dl7001, an E3 deleted variant of wtAd5. After one week, allowing several rounds of replication and lateral dispersion, DNA was isolated and the level of cellular and adenovirus DNA in samples was determined by Q-PCR. The EOR of Ad5-gfa2(B)3-E1 in each cell line, relative to wtAd5 or dl7001 is presented. Error bars indicate SEM

Discussion

In this study, we describe a novel tissue-specific CRAd, named Ad5-gfa2(B)3-E1, for the treatment of malignant glioma. To obtain selectivity, we placed the E1A gene under the control of the GFAP promoter coupled to three 'B' enhancers and placed the promoter-E1 sequence in the inverse orientation compared to wild-type E1 transcription. Previously, we have demonstrated that the gfa2(B)3 promoter is very effective and selective when driving the β-galactosidase gene in a non-replicating adenoviral context[22]. The strength of the gfa2(B)3 promoter in the CRAd construct was confirmed by Western blot showing high E1A and E1B expression levels in GFAP-positive cells at 75% and 30% of the levels obtained following wtAd5 infection. In GFAP-positive cell lines, the high level of E1 protein expression correlated with effective replication as indicated by Q-PCR and oncolytic efficacy relative to wtAd5, 48 h after infection. In contrast, the oncolytic effect on GFAP-negative cells was attenuated compared to wtAd5, indicating selectivity.

In vivo injection of Ad5-gfa2(B)3-E1 into GFAP-positive SNB-19 xenografts resulted in significant slowing of tumor growth compared to injection of PBS. However, injection of wtAd5, the 'gold standard', resulted in an even stronger oncolytic effect, that was significant from day 10. An important difference between Ad5-gfa2(B)3-E1 and wtAd5 is deletion of the E3 region in the former[35] resulting in loss of adenovirus death protein (ADP)[36]. We chose for deletion of E3 to create space for future insertion of heterologous therapeutic genes, such as the HSV1-tk or cytosine deaminase (CD) suicide genes, that enhances the oncolytic efficacy

of replicating adenoviral vectors and may provide a 'fail-safe' when unexpected toxicity occurs [9]. However, ADP is required at late stages of infection for efficient cell lysis and release of adenovirus from infected cells and subsequent lateral spread. Another E3-lacking oncolytic adenovirus (H101) was recently tested in a Phase III randomized controlled trial in head and neck cancer. Intratumoral injection of H101 combined with chemotherapy reportedly resulted in a 79% response rate versus 40% in patients treated with chemotherapy alone (p<0.001)[37,38]. These and other clinical trials will provide more information on the efficacy of oncolytic viruses. Recent reports suggest that innate immune responses severely limit the duration of viral gene expression and replication. The resulting limitation of viral oncolysis may be partially reversed by immunosuppressive agents including cyclophosphamide[39,40].

An important safety issue is the selectivity of replication of CRAds. Following intratumoral injection of non-replicating Ad-tk into the woundbed of resected brain tumors, we could not culture Ad-tk from blood, urine, stool or nasal swabs[41]. These findings indicate that, following intratumoral injections into the brain, systemic spread of the vector occurs only at a low level or is efficiently cleared by the immune system[41]. However, we did observe replication of Ad5-gfa2(B)3-E1 and oncolytic efficacy after infection of GFAP-negative tumor cell lines (Figs. 3 and 4). Replication in these cell lines may be related to their malignant background, because following injection of Ad-gfa2(B)3-LacZ into GFAP-negative cell lines sporadic β-galactosidase expressing cells were detected. In contrast, injection of Ad-gfa2(B)3-LacZ into the brains of nude mice resulted in β-galactosidase staining in GFAP positive cells only[22].

Another safety concern is the replicative potential of Ad5gfa2(B)3-E1 in non-malignant GFAP-positive astrocytes surrounding the tumor. Toxicity may be attenuated however by the non-dividing state of normal astrocytes because adenoviruses replicate more efficiently in rapidly dividing cells[42]. In addition, the high GFAP-expression levels in the reactive astrocytes that infiltrate the tumor may result in high level expression of therapeutic transgenes following infection with Ad5gfa2(B)3-E1 and increased oncolytic efficacy[43-45].

Most CRAds for glioma treatment have been created by introduction of mutations in E1A or E1B resulting in tumor selective replication. A major drawback of such CRAds has been the attenuation of the replicative potential as compared to wtAd5[13,46]. For treatment of malignant glioma several tumor specific CRAds have been described, employing the survivin, MK, COX-2 or HIF promoter[18-21]. Because no quantitative end-points were used, a comparison with other CRAds remains difficult.

In conclusion, the gfa2(B)3 promoter, when used to control the expression of the adenovirus E1 gene, allows efficient and selective adenoviral replication and oncolysis both *in vitro* and *in vivo*. We are currently improving the oncolytic efficacy of the vector by inserting a therapeutic gene in E3. In addition, we will examine whether the specificity of the vector can be enhanced by retargeting to another receptor than CAR, such as CD46, in an orthotopic model[47].

Acknowledgments

References

1 Surawicz TS, Davis F *et al.* Brain tumor survival: results from the National Cancer Data Base. *J Neurooncol 1998*; **40:** 151-160.

2 McLendon RE, Halperin EC. Is the long-term survival of patients with intracranial glioblastoma multiforme overstated? *Cancer 2003*; **98:** 1745-1748.

3 Pulkkanen KJ, Yla-Herttuala S. Gene therapy for malignant glioma: current clinical status. *Mol Ther 2005*; **12:** 585-598.

4 Immonen A, Vapalahti M *et al.* AdvHSV-tk gene therapy with intravenous ganciclovir improves survival in human malignant glioma: a randomised, controlled study. *Mol Ther 2004*; **10:** 967-972.

5 Lam JT, Kanerva A *et al.* Inter-patient variation in efficacy of five oncolytic adenovirus candidates for ovarian cancer therapy. *J Gene Med 2004*; **6:** 1333-1342.

6 Harrow S, Papanastassiou V *et al.* HSV1716 injection into the brain adjacent to tumour following surgical resection of high-grade glioma: safety data and long-term survival. *Gene Ther 2004*; **11:** 1648-1658.

7 Markert JM, Medlock MD *et al.* Conditionally replicating herpes simplex virus mutant, G207 for the treatment of malignant glioma: results of a phase I trial. *Gene Ther 2000*; **7:** 867-874.

8 Wilcox ME, Yang W *et al.* Reovirus as an oncolytic agent against experimental human malignant gliomas. *J Natl Cancer Inst 2001*; **93:** 903-912.

9 Nanda D, Vogels R *et al.* Treatment of malignant gliomas with a replicating adenoviral vector expressing Herpes simplex virus-thymidine kinase. *Cancer Res 2001*; **61:** 8743-8750.

10 Nemunaitis J, Ganly I *et al.* Selective replication and oncolysis in p53 mutant tumors with ONYX-015, an E1B-55kD gene-deleted adenovirus, in patients with advanced head and neck cancer: a phase II trial. *Cancer Res 2000*; **60:** 6359-6366.

11 Grill J, Lamfers ML *et al.* The organotypic multicellular spheroid is a relevant three-dimensional model to study adenovirus replication and penetration in human tumors in vitro. *Mol Ther 2002*; **6:** 609-614.

12 Alemany R, Balague C, Curiel DT. Replicative adenoviruses for cancer therapy. *Nat Biotechnol 2000*; **18:** 723-727.

13 Fueyo J, Alemany R *et al.* Preclinical characterization of the antiglioma activity of a tropism-enhanced adenovirus targeted to the retinoblastoma pathway. *J Natl Cancer Inst 2003*; **95:** 652-660.

14 Bischoff JR, Kirn DH *et al.* An adenovirus mutant that replicates selectively in p53-deficient human tumor cells. *Science 1996*; **274:** 373-376.

15 Kruyt FA, Curiel DT. Toward a new generation of conditionally replicating adenoviruses: pairing tumor selectivity with maximal oncolysis. *Hum Gene Ther 2002*; **13:** 485-495.

16 Edwards SJ, Dix BR *et al.* Evidence that replication of the antitumor adenovirus ONYX-015 is not controlled by the p53 and p14(ARF) tumor suppressor genes. *J Virol 2002*; **76:** 12483-12490.

17 Heise C, Hermiston T *et al.* An adenovirus E1A mutant that demonstrates potent and selective systemic anti-tumoral efficacy. *Nat Med 2000*; **6:** 1134-1139.

18 Van Houdt WJ, Haviv YS *et al.* The human survivin promoter: a novel transcriptional targeting strategy for treatment of glioma. *J Neurosurg 2006*; **104:** 583-592.

19 Kohno S, Nakagawa K *et al.* Midkine promoter-based conditionally replicative adenovirus for malignant glioma therapy. *Oncol Rep 2004*; **12:** 73-78.

20 Ahmed A, Thompson J *et al.* A conditionally replicating adenovirus targeted to tumor cells through activated RAS/P-MAPK-selective mRNA stabilization. *Nat Biotechnol 2003*; **21:** 771-777.

21 Post DE, Van Meir EG. A novel hypoxia-inducible factor (HIF) activated oncolytic adenovirus for cancer therapy. *Oncogene 2003*; **22:** 2065-2072.

22 de Leeuw B, Su M *et al.* Increased glia-specific transgene expression with glial fibrillary acidic protein promoters containing multiple enhancer elements. *J Neurosci Res 2006*; **83:** 744-753.

23 Cosgrove M, Fitzgibbons PL *et al.* Intermediate filament expression in astrocytic neoplasms. *Am J Surg Pathol 1989*; **13:** 141-145.

24 Vandier D, Rixe O *et al.* Inhibition of glioma cells in vitro and in vivo using a recombinant adenoviral vector containing an astrocyte-specific promoter. *Cancer Gene Ther 2000*; **7:** 1120-1126.

25 Morelli AE, Larregina AT *et al.* Neuronal and glial cell type-specific promoters within adenovirus recombinants restrict the expression of the apoptosis-inducing molecule Fas ligand to predetermined brain cell types, and abolish peripheral liver toxicity. *J Gen Virol 1999*; **80:** 571-583.

26 Besnard F, Brenner M *et al.* Multiple interacting sites regulate astrocyte-specific transcription of the human gene for glial fibrillary acidic protein. *J Biol Chem 1991*; **266:** 18877-18883.

27 Fallaux FJ, Bout A *et al.* New helper cells and matched early region 1-deleted adenovirus vectors prevent generation of replication-competent adenoviruses. *Hum Gene Ther 1998*; **9:** 1909-1917.

28 Fallaux FJ, Kranenburg O *et al.* Characterization of 911: a new helper cell line for the titration and propagation of early region 1-deleted adenoviral vectors. *Hum Gene Ther 1996*; **7:** 215-222.

29 Graham FL, van der Eb AJ. Transformation of rat cells by DNA of human adenovirus 5. *Virology 1973*; **54:** 536-539.

30 Ranheim TS, Shisler J *et al.* Characterization of mutants within the gene for the adenovirus E3 14.7-kilodalton protein which prevents cytolysis by tumor necrosis factor. *J Virol 1993*; **67:** 2159-2167.

31 Pietersen AM, van der Eb MM *et al.* Specific tumor-cell killing with adenovirus vectors containing the apoptin gene. *Gene Ther 1999*; **6:** 882-892.

32 Ma L, Bluyssen HA *et al.* Rapid determination of adenoviral vector titers by quantitative real-time PCR. *J Virol Methods 2001*; **93:** 181-188.

33 Jakubczak JL, Ryan P *et al.* An oncolytic adenovirus selective for retinoblastoma tumor suppressor protein pathway-defective tumors: dependence on E1A, the E2F-1 promoter, and viral replication for selectivity and efficacy. *Cancer Res 2003*; **63:** 1490-1499.

34 Dethlefsen LA, Prewitt JM, Mendelsohn ML. Analysis of tumor growth curves. *J Natl Cancer Inst 1968*; **40:** 389-405.

35 He TC, Zhou S *et al.* A simplified system for generating recombinant adenoviruses. *Proc Natl Acad Sci U S A 1998*; **95:** 2509-2514.

36 Tollefson AE, Ryerse JS *et al.* The E3-11.6-kDa adenovirus death protein (ADP) is required for efficient cell death: characterization of cells infected with adp mutants. *Virology 1996*; **220:** 152-162.

37 Garber K. China approves world's first oncolytic virus therapy for cancer treatment. *J Natl Cancer Inst 2006*; **98:** 298-300.

38 Crompton AM, Kirn DH. From ONYX-015 to armed vaccinia viruses: the education and evolution of oncolytic virus development. *Curr Cancer Drug Targets 2007*; **7:** 133-139.

39 Fulci G, Breymann L *et al.* Cyclophosphamide enhances glioma virotherapy by inhibiting innate immune responses. *Proc Natl Acad Sci U S A 2006*; **103:** 12873-12878.

40 Lamfers ML, Fulci G *et al.* Cyclophosphamide increases transgene expression mediated by an oncolytic adenovirus in glioma-bearing mice monitored by bioluminescence imaging. *Mol Ther 2006*; **14:** 779-788.

41 Smitt PS, Driesse M *et al.* Treatment of relapsed malignant glioma with an adenoviral vector containing the herpes simplex thymidine kinase gene followed by ganciclovir. *Mol Ther 2003*; **7:** 851-858.

42 Park MT, Lee MS *et al.* Influence of culture passages on growth kinetics and adenovirus vector production for gene therapy in monolayer and suspension cultures of HEK 293 cells. *Appl Microbiol Biotechnol 2004*; **65:** 553-558.

43 Antunes L, Angioi-Duprez KS *et al.* Analysis of tissue chimerism in nude mouse brain and abdominal xenograft models of human glioblastoma multiforme: what does it tell us about the models and about glioblastoma biology and therapy? *J Histochem Cytochem 2000*; **48:** 847-858.

44 Puumalainen AM, Vapalahti M *et al.* Beta-galactosidase gene transfer to human malignant glioma in vivo using replication-deficient retroviruses and adenoviruses. *Hum Gene Ther 1998*; **9:** 1769-1774.

45 Schiffer D, Giordana MT, Mauro A, Migheli A. Reactive astrocytes in the morphologic composition of peripheral areas of gliomas. *Tumori 1988*; **74:** 411-420.

46 Harada JN, Berk AJ. p53-Independent and -dependent requirements for E1B-55K in adenovirus type 5 replication. *J Virol 1999*; **73:** 5333-5344.

47 Brouwer E, Havenga MJ *et al.* Human adenovirus type 35 vector for gene therapy of brain cancer: improved transduction and bypass of pre-existing anti-vector immunity in cancer patients. *Cancer Gene Ther 2007*; **14:** 211-219.

PART 3

Delivery of adenovirus
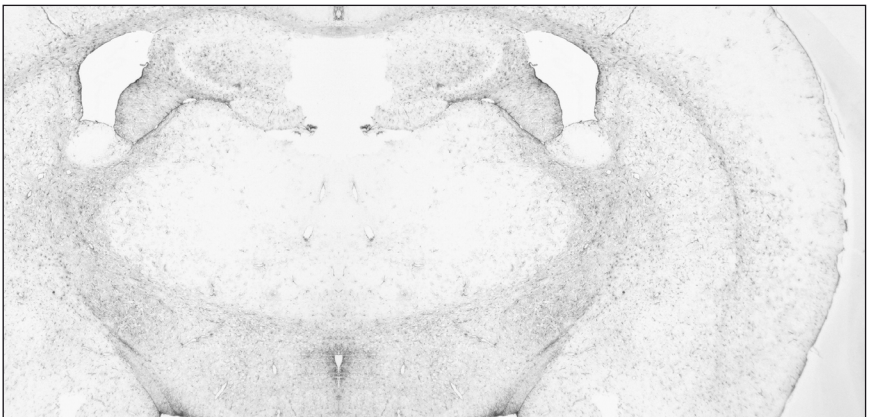
CHAPTER 3

Locoregional Delivery of Adenoviral Vectors

Maarten ter Horst[1], Suzanne Verwijnen[2], Eric Brouwer[1], Rob Hoeben[3], Marion de Jong[2], Bertie de Leeuw[1], and Peter Sillevis Smitt[1]

[1]Department of Neurology, Erasmus University Medical Center, Rotterdam;
[2]Department of Nuclear Medicine, Erasmus University Medical Center, Rotterdam;
[3]Department of Molecular Cell Biology, Leiden University Medical Center, Leiden, The Netherlands.
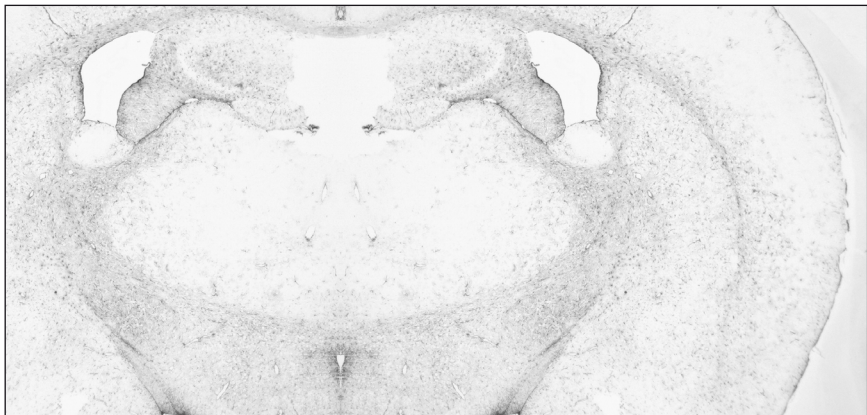
Abstract

The overall median survival of patients with a malignant glioma is <1 y. Because malignant gliomas rarely metastasize outside the skull, locoregional treatment strategies, such as gene therapy, are under investigation. Recently, convection-enhanced delivery (CED) has been presented as a method to improve delivery of large molecules. The goal of this study was to evaluate wether CED improves intratumoral delivery of adenoviral vectors and compare it with single injection (SI) and multiple injection (4x,MI).

Methods: A replication-deficient adenoviral vector encoding the herpes simplex virus thymidine kinase (HSV-tk) and the human somatostatin receptor subtype 2 (sst_2) was administered into nude mice bearing subcutaneous U87MG xenografts. Tumors were injected with 1.5×10^9 plaque-forming units of Ad5.tk.sstr by CED, SI, or MI. Three days later, $[^{99m}Tc\text{-}N_4^{0\text{-}1}, Asp^0, Tyr^3]$octreotate ($^{99m}Tc$-Demotate 2) was injected intravenously to monitor the virus-induced sst_2 expression. γ-Camera imaging was performed for in vivo imaging, and the tumor uptake of ^{99m}Tc-Demotate 2 was determined by γ-counter. Furthermore, the tumor was sectioned and ex vivo autoradiography was performed. After decay of radioactivity, adjacent sections were submitted to in vitro autoradiography with ^{125}I-DOTA-Tyr^3-octreotate, which was used to calculate the transduced areas.

Results: Transfected xenograft tissues showed high sst_2 expression and were clearly visualized with a γ-camera. Accumulation of radioactivity was 2-fold higher in the tumors that were injected with MI compared with CED and SI (P = 0.01). CED and SI resulted in equal uptake of radioactivity in the tumors. The measured areas of transduction in ex vivo and in vitro autoradiographs showed a high concordance (r^2 = 0.89, P<0.0001). The maximum area of transfection was significantly larger after MI than after CED (P<0.05) or SI (P= 0.05). Also, the measured volume of distribution was twice as high after administration of Ad5.tk.sstr by MI (56.6 mm^3) compared with SI (25.3 mm3) or CED (26.4 mm3).

Conclusion: CED does not increase adenoviral vector distribution in a glioma xenograft model compared to SI. Therefore, in the clinic MI is probably the most effective delivery method for the large adenoviral particle (70 nm) in malignant gliomas.

Introduction

The overall prognosis of patients with malignant gliomas is dismal, with a median survival of <1 y[1]. Despite progress in neurosurgery, chemotherapy, and radiotherapy, the survival of these patients has not changed during the last several decades. Because of the poor prognosis of malignant gliomas, new treatment modalities are being developed. As malignant gliomas rarely metastasize outside the skull, some modalities focus on locoregional treatment strategies. Examples include local application of cytotoxic-drugs impregnated wafers, local application of targeted toxins and intratumoral injection of viral vectors for gene therapy or virotherapy[2-4].

Adenoviral vectors are among the most promising gene delivery vehicles currently available for glioma therapy, because they can be produced at large quantities in high titer batches and because relatively large segments of foreign DNA carrying therapeutic genes can be incorporated. Recently, a small randomized study clearly demonstrated the efficacy of an Adenovirus serotype 5 (Ad5) carrying the herpes simplex virus thymidine kinase gene (HSV1-tk) in combination with ganciclovir (GCV) in malignant glioma[5]. Ad5-tk treatment significantly increased the mean survival from 39 to 71 weeks (p<0.01), indicating some efficacy of the treatment.

In spite of these promising results, 2 major hurdles have been identified that limit the efficacy of Ad5 based gene therapy in malignant gliomas. First, the Coxsackie Adenovirus Receptor (CAR) is poorly expressed on primary glioma cells, resulting in low transduction efficiency compared with established cell lines[6]. Various strategies have been developed to successfully retarget Ad vectors to other receptors that are expressed at higher levels on malignant glioma cells, such as integrins or CD46[7,8]. Another major obstacle is the limited tissue penetration of the virus after injection into glioma tissue. A carefully conducted clinical study demonstrated that the distribution of the vector into brain tissue is limited to an average 5 mm from the needle tract[9]. One approach to improve tissue penetration is the development of conditionally replicative adenoviruses (CRAds)[10,11]. The release of CRAd progeny by infected tumor cells provides a potential to amplify the oncolytic effect by lateral spread through solid tumors.

Another way to improve tissue penetration of the virus is the exploration of new delivery methods. Recently, convection enhanced delivery (CED) was developed as a means to improve delivery of macromolecules throughout the brain[12-14]. CED is based on continuous infusion of drugs via intracranial catheters, enabling convective distribution of high drug concentrations over large volumes of the target tissue[15]. CED has been successfully applied in clinical glioma trials to administer large molecules, including immunotoxins[4,16]. CED has also been used to deliver viral vectors, including adenovirus, to the brain. In experimental models, delivery of viral vectors by CED resulted in improved transduction of the brain[17-21].

In clinical gene therapy trials, the adenoviral vectors were administered into the gliomas by either a single injection, through a catheter or by multiple wound bed injection following reresection[2,5,9]. The goal of this study was to evaluate wether CED improves intratumoral delivery of an adenoviral vector in a mouse xenograft glioma model. We compared the volume of tumor that was transduced by the adenoviral vector after CED with the volumes obtained by single injection (SI) and multiple injection (4x; MI) of the same amount of virus.

To monitor the distribution of the adenoviral vector, we used the human somatostatin receptor subtype 2 (sst_2) gene in combination with the radiolabeled tracer [^{99m}Tc-N$_4$$^{0-1}$,Asp^0,Tyr^3]octreotate (^{99m}Tc-Demotate 2), which has high selectivity and high affinity for the sst_2 receptor[22]. We found that radioactive uptake and volume of distribution after CED were comparable to SI. After MI, the transduced tumor volume and the maximum area of transduction were 2-3 fold increased compared with both SI and CED.

Materials and Methods

Cell Culture

The U87MG human glioblastoma multiforme (GBM) cell line was obtained from the American Type Culturing Collection; the U251 human GBM cell line from P Körnblith (National Institutes of Health, Bethesda, MD), and the rat pancreatic tumor cell line CA20948 was available at our institution[23]. U87MG cells were cultured in MEM (Invitrogen) with 0.1 mM non-essential amino acids, 2 mM L-glutamine, 1 mM sodium pyruvate, 1500 mg/l sodium bicarbonate, 10% heat inactivated (30 min 56°C) FBS (Invitrogen), 100 I.U./mL penicillin and 100 µg/mL streptomycin (Invitrogen). U251 was cultured in DMEM (Invitrogen) containing 4500mg/L glucose, 580 mg/L L-glutamine and 110 mg/L pyruvate with 10% FBS (Invitrogen), 100 I.U./mL penicillin and 100 µg/mL streptomycin (Invitrogen). CA20948 was cultured in the DMEM medium as described above with 0.1 mg/L fungizone supplemented. Medium was changed twice a week. Cells were cultured at 37ºC in a 5% CO_2 atmosphere.

Adenoviral Vectors Ad5.tk.sstr and Ad5.CMV.nLacZ

Construction of Ad5.tk.sstr and Ad5.CMV.nLacZ has been described before[24,25]. Briefly, Ad5.tk.sstr is a replication-incompetent adenoviral vector that contains the sst_2 and the herpes simplex virus thymidine kinase (tk) genes in the deleted E1 region. Both genes are regulated by separate immediate early cytomegalovirus (CMV) promoters. The E1-deleted Ad5.CMV.nLacZ vector contains the β-galactosidase (nLacZ) driven by a CMV promoter. Both vectors were propagated to high titers on PER.C6 cells, CsCl gradient purified, dialyzed, and stored at -80°C in sucrose buffer (140 mM NaCl, 5 mM Na_2HPO_4, 1.5mM KH_2PO_4, 20 mM $MgCl_2$ and 5% sucrose). All batches were screened for replication competent adenovirus (RCA)[26] and met the criterion of <1 plaque-forming unit (pfu) of wtE1A promoter containing virus per

10^7 pfu. Titration's were performed on 911 cells and are presented as pfu/mL [27]. The titers ranged from $6x10^{10}$ to $3x10^{11}$ pfu/mL.

Radiolabeling of Peptides

[^{99m}Tc-N$_4^{0-1}$, Asp^0, Tyr^3]octreotate (^{99m}Tc-Demotate 2) was provided by Dr. T. Maina, Institute of Radioisotopes, Athens, Greece and prepared as described earlier[22]. Briefly, 20 µg Demotate 2 (10^{-3} M), in 50 µl 0.5 M phosphate buffer (pH 10.5), and 5 µl 0.1 M Na$_3$-citrate and 410 µl ^{99m}TcO$_4$ (Ultratechnekow, Tyco Healthcare, Petten, The Netherlands) were mixed, and the reaction was started by the addition of 20 µg SnCl$_2$ (2 mg SnCl$_2$ per ml ethanol, freshly made) at room temperature. After 15 min, another 20 µg SnCl$_2$ in ethanol were added and mixed. After 30 min, 8 µl of 1M HCl and 50 µl ethanol were added and the solution was sterilized by filtration through a Millex 0.22 µm GV filter (Millipore). The radiochemical purity was tested by HPLC and was >90 %. The mean specific activity of ^{99m}Tc-Demotate 2 was 40-200 MBq/µg.

DOTA-Tyr^3-octreotate was labeled with ^{125}I as described earlier[28]. The mean radiochemical purity was >90 %. The mean specific activity of DOTA-^{125}I-Tyr^3-octreotate was 0.2 MBq/mmol. Octreotide was supplied by Novartis. All chemicals used are purchased from Aldrich.

Adenoviral Stability

During CED, the adenoviral vector is exposed to room temperature for up to 3 h and to transport through Teflon (DuPont) tubing. To examine the effect of room temperature on adenoviral stability, we sampled aliquots of Ad5.CMV.nLacZ placed on the bench at room temperature every 30 min. To study the effect of passage through tubing, Ad5.CMV.nLacZ from the same batch was pushed (1µl/min) through the same tubing used for CED experiments over a 3-h period and aliquots were sampled every thirty minutes. Infectivity of the aliquots was examined by infecting U251 cells and measuring β-galactosidase activity. U251 cells were plated into 24 well plates at a density of $2x10^5$ cells/well in 1 ml DMEM containing 10% FBS and incubated overnight at 37°C. After changing the medium, the aliquots containing Ad5.CMV.nLacZ were added in triplicate at a concentration of 100 pfu/cell. The medium was changed two hours after starting the infection. After 48 hours of incubation at 37°C the medium was removed, the cells were washed with PBS and assayed for β-galactosidase activity by the Galacto-Light Plus^{TM} system (Applied Biosystems) using a Packard Top Count NXT luminometer (PerkinElmer Life sciences, Meriden, CT). The same experiments were repeated after the addition of BSA (New England Biolabs, Ipswich, MA) at a concentration of 0.1 mg/ml.

Animal Experiments

All experimental protocols were approved by the Institutional Animal Care and Use Committee, in compliance with the Guide for the Care and Use of Laboratory Animals. Male

NMRI nu/nu mice (Charles River, Les Oncins, France), 5-6 wk of age were purchased. Mice were maintained at 3 or 4 per cage and allowed access to food and water ad libitum. After 1 wk, 1×10^7 U87MG or CA20948 cells were inoculated subcutaneously into both flanks in 250 µl of HBSS (Invitrogen). The tumor growth was assessed 3 times a week by measuring bidimensional diameters with calipers. The tumor volume was determined by using the simplified formula of a rotational ellipse (length x width^2 x 0.5)[29]. Anesthesia was induced with isoflurane in oxygen and nitrous oxygen. Body temperature was maintained at 37°C using a heat pad. When the tumors reached a volume of approximately 250 mm^3, animals were injected with a total dose of 1.5×10^9 pfu of Ad5.tk.sstr or PBS into the tumor. We compared 3 delivery strategies: SI, (4x; MI) and CED. In SI experiments, the total viral dose was administered in 22 µl with 1 injection. In the MI experiments, the total viral dose was diluted in 50 µl and was administered by 4 separate injections into 4 different tumor quadrants. In CED, the viral dose was diluted in 180 µl and was infused at 1µl/min for 180 min. The continuous infusion was preformed with a constant flow pump (Harvard Apparatus). A 27-gauge hypodermic needle was connected to an air tight 250-µl Hamilton syringe with 30 cm of Teflon tubing. For SI and MI, we used a 50µl Hamilton syringe fitted with a 27-gauge needle. As a positive control we used mice bearing sst$_2$-positive rat pancreatic CA20948 xenografts. Seventy-two hours after administration of the vector, 0.5 µg ^{99m}Tc-Demotate 2 was injected into the dorsal vein of the penis in a total volume of 200 µl. γ-Camera images were acquired for 10 min, 3.5 hr after ^{99m}Tc-Demotate 2 injection, using a Rota II γ -camera system (Siemens) equipped with a low energy collimator. The animals were sacrificed 4 hr after ^{99m}Tc-Demotate 2 injection. The tumors were taken out and weighed. After determining the radioactivity in a LKB-1282-Compugammasystem (Perkin Elmer) γ-counter, the tumors were frozen in Tissue-Tek (Sakura). For each adenovirus injected tumor the total background activity was calculated on the based of the means of the PBS-injected U87MG tumors (percentage injected-dose per gram of tissue[%ID/g]). After subtracting the background activity, the adenoviral vector-induced radioactivity was expressed as percentage of injected dose (%ID) per tumor.

Autoradiography

The presence of radioactivity in tissue sections was detected by ex vivo and in vitro autoradiography. Tumors were embedded in Tissue-Tek and processed for cryosectioning. Tissue sections (10 µm) were obtained at 0.3-mm intervals throughout the tumor and mounted on SuperFrost plus slides (Menzel). For ex vivo autoradiography, sections were exposed to a phosphor screens (Packard Instruments, Meriden, CT) for 2 d. The screens were analyzed using Cyclone phosphor imager (Packard Instruments) and a computer-assisted OptiQuant 03.00 image processing system (Packard Instruments). In vitro autoradiography was performed on the tumors sections after decay of ^{99m}Tc-Demotate 2. Tissue sections (10µm) were mounted on glass slides and stored at -20ºC for at least 1 day to improve adhesion of

the tissue to the slide. The sections were preincubated for 10 minutes at 4ºC, using buffer A, containing 167 mM Tris-HCl pH 7.7, 5 mM $MgCl_2$ and 0.25% BSA. The sections were then incubated for 60 minutes in the same buffer, in the presence of 10^{-10}M ^{125}I-DOTA-Tyr^3-octreotate, 1% BSA and 40 µg/ml Bacitracin. The sections were then washed twice for 5 min in buffer A and once in buffer A without BSA. After a short wash with distilled water, the sections were dried and exposed to phosphor image screens for 1 d. Non-specific binding was determined in an adjacent section in the presence of 10^{-6} M octreotide. Sections of rat brain and CA20948 tumor served as positive controls.

Volume of Adenoviral Vector Distribution

We used the in vitro autoradiography slides to calculate the volume of tumor transduced by the adenoviral vector. On the sections, we defined the boundaries of radioactivity by setting a threshold of 5 times background activity. We then used Scion Image software (Scion) to calculate the area of radioactivity. Then, we plotted the areas of all adjacent slides and determined the area under the curve expressing the volume of distribution using GraphPad Prism version 4.0 software (GraphPad Software, Inc.).

Statistical Analysis

Data were analyzed using GraphPad Prism. All tests (T-test, ANOVA) were 2-sided and $P<0.05$ was considered statistically significant.

Results

Adenoviral Stability During CED

Delivery by CED exposes the adenoviral vector to 3 h of room temperature and to passage through the tubing. To determine the effect of these factors on adenoviral stability, we simulated a 3-h CED experiment on the bench top. After exposure to three hours of room temperature, the infectivity of the vector dropped from 2.3 x 10^6 relative light units (RLU) to 1.3 x 10^6 RLU without passage through the tubing and to 1.4 x 10^6 RLU after additional exposure to the tubing (Fig. 1). The decline of infectivity over time was significant in both instances ($P<0.01$), but was mainly due to a drop in the first 30 minutes. Clearly, passage through the tubing did not negatively affect the infectivity of the vector. We then examined the effect of addition of BSA on stability. After 3 h on the bench top at room temperature, the infectivity remained stable at 2.0 x 10^6 RLU. After a 3-h exposure followed by passage through the tubing, the infectivity of the vector dropped from 2.0 x 10^6 to 1.5 x 10^6 RLU ($P=0.09$). Because addition of BSA did not significantly increase vector stability during simulation of CED on the bench top, in vivo experiments were carried out without BSA.
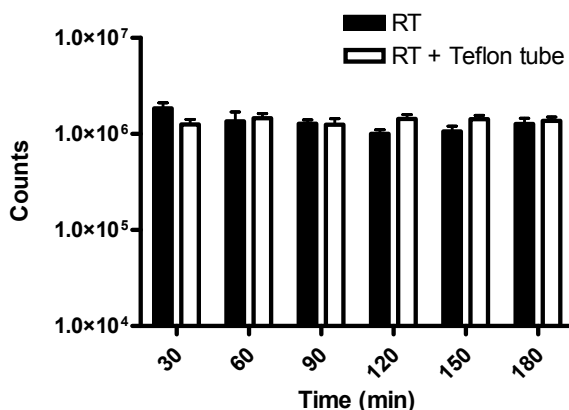
Fig. 1 Adenoviral vector stability at room temperature after passage through Teflon tubing. Aliquots of Ad5.CMV.nLacZ, stored at room temperature (RT), were sampled every 30 min over a 3-h period. In parallel, aliquots from the same batch were collected after transport through Teflon tubing (1µl/min). U251 cells were incubated with the aliquots (100 pfu/cell), and β-galactosidase activity was measured 2 d later. The β-galactosidase activity decreased over time, but was not affected by transport through tubing. Error bars represent SD.

### γ-*Camera Images After CED, SI and MI of Ad5.tk.sstr*

Animals carrying established bilateral subcutaneous U87MG tumors were injected with 1.5×10^9 pfu Ad5.tk.sstr or PBS. Three different delivery strategies were used: SI, (4x; MI), and CED. Three days after the injection of the viral vector, the radioactive tracer ^{99m}Tc-Demotate 2 was injected intravenously and the animals were imaged. All Ad5.tk.sstr injected tumors were readily visualized with radioactive ^{99m}Tc-Demotate 2 with the γ-camera (Fig. 2). In addition, a stronger signal was visible in tumors injected with MI than in tumors treated with SI or CED. These findings indicate the feasibility of in vivo imaging using the Ad5.tk.sstr/^{99m}Tc-Demotate 2 system.

Radioactivity Accumulation in the Tumor

After imaging, the animals were sacrificed and the radioactivity in the tumors was measured (Table 1). The accumulation of radioactivity (%ID) was significantly higher in the tumors that

Table 1. Virus induced tumor uptake of ^{99m}Tc-Demotate 2 in Xenografts-Bearing mice after Ad5.tk.sstr administration either by CED, SI or MI. Three days after infection, each mouse was injected i.v. with 0.5 µg ^{99m}Tc-Demotate 2 (20-100 MBq) and euthanized 4 h later (14-15 tumors per group). Uptake is expressed as %ID of infected tumor tissue. Accumulation of radioactivity was significantly higher in the tumors that were injected with MI as compared to CED and SI (ANOVA, P< 0.05).

Injection	%ID	SEM
CED	0.34	0.08
SI	0.37	0.08
MI	0.82	0.17
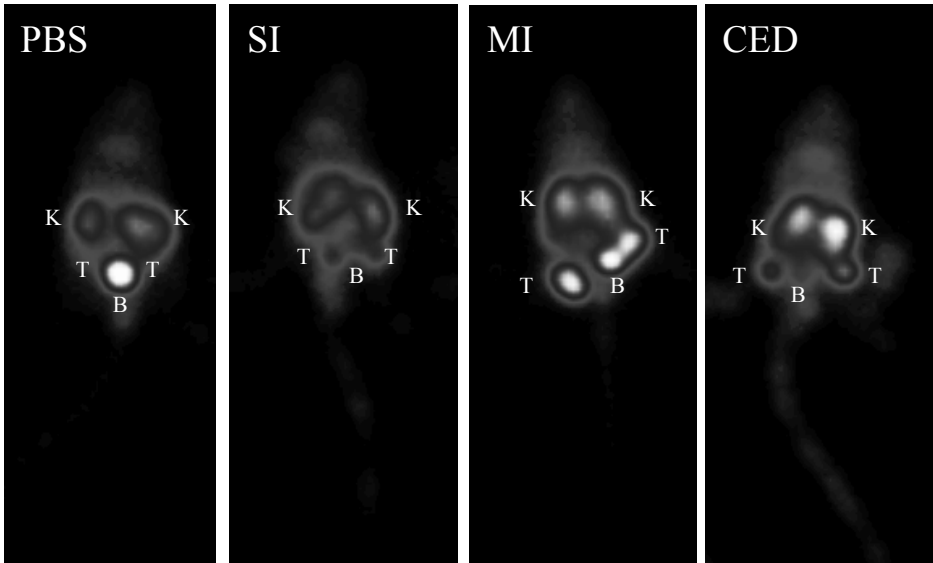
**Fig. 2** γ-Camera images of NMRI *nu/nu* mice. Mice bearing U87MG xenografts 3.5 h after intravenous administration of 0.5 µg ^{99m}Tc-Demotate 2 (100 MBq). Three days before imaging, tumors had been injected with PBS (left) or 1.5×10^9 pfu Ad5.tk.sstr administered either with CED, SI, or (4x; MI). Both tumors in each animal received the same treatment. Images are representative and demonstrate that MI results in better tracer uptake than CED and SI. B = bladder; K = kidney; T = tumor.
See Color Figures, p. 155.

were injected with MI as compared to CED and SI (p = 0.01) confirming the γ-camera results. CED and SI resulted in equal uptake of radioactivity in the tumors.

Autoradiography and Quantitation of Vector Distribution

After sectioning, U87MG xenografts were submitted to autoradiography (Fig. 3). Ex vivo autoradiographs visualized transduced areas of the tumors (Fig. 3A and 3E). The representative autoradiographs clearly showed a larger area of radioactivity in the section of the tumor treated with MI (Fig. 3E) than that treated with SI (Fig. 3A). After decay of ^{99m}Tc-Demotate 2, in vitro autoradiographic studies were performed with ^{125}I-DOTA-Tyr^3-octreotate and showed areas of transduction similar to the ex vivo autoradiographs (Fig. 3B and 3F). Adding excess unlabeled octreotide completely blocked uptake of radioactivity, indicating the specificity of the observed binding of ^{125}I-DOTA-Tyr^3-octreotate to the transduced sst$_2$ receptor (Figs. 3C and 3G). The area of transduction was calculated for each section using Scion Image. The area of transduction calculated on the in vitro autoradiographs correlated significantly with the area calculated on the ex vivo autoradiograph of the same section ($r^2 = 0.89$, p<0.0001). Because the in vitro autoradiographs can be obtained from a large number of sections at the same time, we used this method to determine the maximum area and volume of transduction for all tumors. First, we determined for each tumor the maximum area of transduction on
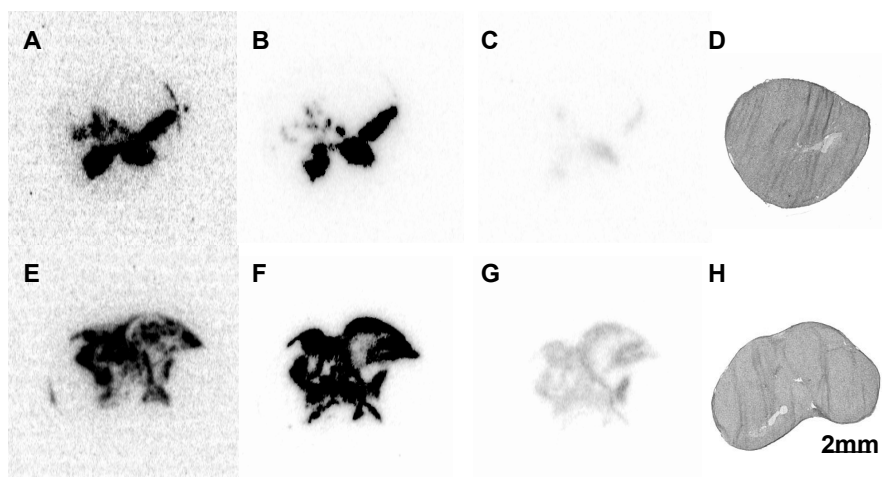
Fig. 3 Autoradiographs of Ad5.tk.sstr injected U87MG xenografts by single injection (A-D) or by multiple injection (E-H). Ex vivo autoradiographs were performed 4 h after injection of ^{99m}Tc-Demotate 2 (A and E). In vitro autoradiographs were performed on adjacent slides with ^{125}I-DOTA-Tyr^3-octreotate (B and F). Binding was displaced by excess unlabeled octreotide (C and G). Adjacent tumor sections were visualized with hematoxilin-eosin staining (D and H). Representative sections demonstrate that the area of viral distribution is larger in sections from tumors injected with MI compared with SI. See Color Figures, p. 156.
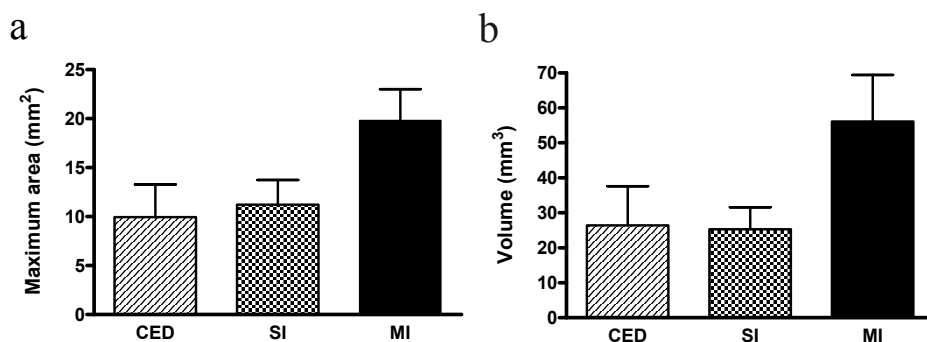
Fig. 4 Quantitation of vector distribution. Area of vector distribution was calculated using serial in vitro autoradiography sections incubated with ^{125}I-DOTA-Tyr^3-octreotate. (A) In each tumor the section with the largest area was selected. The maximum area of vector distribution depends significantly on the method of vector delivery (MI vs. CED P<0.05, MI vs. SI P=0.05, CED vs. SI P= 0.8). (B) To calculate the volume of vector distribution, all radioactive areas of consecutive sections were plotted and the area under the curve was calculated. Data are the mean ± SEM, eight tumors in each group.

a single section for each delivery method (Fig. 4A). The maximum area of transduction was significantly larger following MI than after CED (p<0.05) or SI (p= 0.05). Then, we plotted the areas of all the adjacent slides and calculated the area under the curve representing the volume of distribution. Fig. 4B presents the volumes of distribution obtained with the 3 different delivery techniques. The volume of distribution was twice as high following administration of Ad5.tk.sstr by MI (56.6 mm^3) compared to SI (25.3 mm^3) or CED (26.4 mm^3).

Discussion

The local pattern of recurrence and absence of metastasis outside the CNS make malignant gliomas suitable candidates for locoregional treatment strategies, including gene therapy. Convection enhanced delivery (CED) was recently developed to increase the volume of distribution of large molecules through the brain[12-14,21]. In this study, we applied CED in an attempt to improve the local delivery of adenoviral vectors. We compared CED with SI and (4x; MI) of a replication-deficient adenoviral vector in a subcutaneous mouse xenograft tumor model. To monitor the distribution of the virus, we inserted the gene encoding the human sst_2. Expression of sst_2 was visualized in vivo by intravenous injection of ^{99m}Tc-Demotate 2 followed by γ-camera imaging and the accumulation of radioactivity was quantitated with a γ-counter. The volume and maximum area of transduction of the tumor was taken as a measure of in vivo vector distribution and was measured using in vitro autoradiography. Before comparing CED with MI and SI, we investigated the adenoviral stability and recovery from the CED infusion device. Sanftner et al.[21] showed up to 90% absorption of an adeno-associated virus, determined by quantitative polymerase chain reaction, to the device depending on the tubing used. These authors observed excellent vector recovery when using fused silica and silicon tubing. In our adenoviral test setting, the Teflon tubing did not affect adenoviral infectivity, indicating good vector recovery. However, exposure of the vector for 3 h at room temperature resulted in a 43% decline of infectivity. The decline in infectivity by exposure to room temperature was most prominent in the first 30 minutes and was not prevented by addition of BSA.

Direct comparison of CED with SI and MI demonstrated that both accumulation of radioactivity and the largest area of transduction on a single section were significantly larger following MI than after CED or SI. Also, the volume of transduction was increased 2-fold. However, CED did not increase the maximum area or the volume of tumor transduction as compared to SI. Lack of distribution enhancement by CED compared to SI could be attributed to the flow, time and volume settings of CED; to the size of the adenoviral particle; or the interaction between the adenovirus and the tissue.

For optimal CED of drugs, several relevant variables have been identified, including catheter size, flow rate, molecular weight of the drug and tissue characteristics[30,31]. Backflow of the infused drugs is depending on catheter size and flow rate[30] which should not exceed 1 μl/min[19]. We used the recommended maximum flow rate and did not observe backflow. Furthermore, increased molecular weight and particle size decrease delivery[12,14,32,33].

Betz et al.[18] applied CED to deliver a replication defective-adenoviral vector (70-100 nm)[34] to rat brain and studied various infusion parameters. Variations in flow rate, concentration and infectious titer resulted in a volume of adenoviral transduction ranging from 4-27 mm^3 for 0.3-9 x 10^9 virus particles. MacKay et al.[32] performed CED experiments using different sized liposome's (40- 200 nm in diameter) and reported a reduction in brain penetration with

increase in size. Kroll et al.[35] reported that increasing the dose of Monocrystalline Iron Oxide Nanocompounds (MION), a viral sized agent, rather than convection might result in the best volume of transduction. On the other hand, Brust et al.[19] showed that infusion of 1 µl/min over a longer period of time (2.5 h) is more effective than infusion of smaller volumes with the same dose of adenovirus. Although we used the same infusion rate and a volume of 180 µl, we found comparable levels of radioactive accumulation between SI and CED indicating that in our setting the increase of injected volume did not result in an improved volume of distribution.

We used the sst_2 marker gene to visualize adenoviral vector distribution in vivo and ex vivo. Recently, Maina et al.[22,36] described new somatostatin analogues, ^{99m}Tc-Demotate 1 and ^{99m}Tc-Demotate 2 for the visualization of the somatostatin receptor in endocrine tumors. At present, ^{111}In-OctreoScan is the standard substrate for diagnostic imaging and staging of sst_2 expressing tumors. However, somatostatin analogues based on ^{99m}Tc are promising alternatives because of optimal nuclear characteristics, low cost and easy availability via commercial 99Mo/99mTc generators[22]. In this study, we found high ^{99m}Tc-Demotate 2 uptake in infected U87MG xenografts by in vivo γ-camera imaging and ex vivo autoradiography. The high and significant correlation between the ex vivo and in vitro autoradiographs indicate that the intravenously injected ^{99m}Tc-Demotate 2 efficiently permeates the entire tumor.

Our results showed no significant difference in adenoviral vector distribution between CED and SI but, conversely, showed an increase in radioactive uptake and volume of distribution in MI. For that reason, in the clinic, MI is probably the most effective delivery method for the large adenoviral particle (70 nm) in malignant gliomas. Several clinical studies have demonstrated that administration of adenoviral vectors through multiple injections into the brain is probably safe, although silent hemorrhages and transient neurological deficits have been described[2,9]. Our study shows that even small experimental tumors are not entirely transduced after MI. Additional strategies such as radionuclide therapy with, for example ^{177}Lu- and ^{90}Y-labelled somatostatin analogues[37] or the HSV-tk / ganciclovir "bystander effect"[38,39] or using (conditional) adenoviral replication[10,11] will be required to obtain eradication of experimental tumors or clinically relevant tumor responses.

Conclusion

Our study showed that CED did not increase adenoviral vector distribution in a glioma xenograft model compared to SI. Therefore, in the clinic, MI is probably the most effective method to deliver the large adenoviral particle into (brain) tumors. Furthermore, ^{99m}Tc-Demotate 2 seems a good candidate to image and quantitate the distribution and expression level of the sst_2 marker.

Acknowledgement

References

1 Behin A, Hoang-Xuan K, Carpentier AF, Delattre JY. Primary brain tumours in adults. *Lancet 2003*; **361:** 323-331.

2 Smitt PS, Driesse M *et al.* Treatment of relapsed malignant glioma with an adenoviral vector containing the herpes simplex thymidine kinase gene followed by ganciclovir. *Mol Ther 2003*; **7:** 851-858.

3 Westphal M, Hilt DC *et al.* A phase 3 trial of local chemotherapy with biodegradable carmustine (BCNU) wafers (Gliadel wafers) in patients with primary malignant glioma. *Neuro-oncol 2003*; **5:** 79-88.

4 Laske DW, Youle RJ, Oldfield EH. Tumor regression with regional distribution of the targeted toxin TF-CRM107 in patients with malignant brain tumors. *Nat Med 1997*; **3:** 1362-1368.

5 Immonen A, Vapalahti M *et al.* AdvHSV-tk gene therapy with intravenous ganciclovir improves survival in human malignant glioma: a randomised, controlled study. *Mol Ther 2004*; **10:** 967-972.

6 Miller CR, Buchsbaum DJ *et al.* Differential susceptibility of primary and established human glioma cells to adenovirus infection: targeting via the epidermal growth factor receptor achieves fiber receptor-independent gene transfer. *Cancer Res 1998*; **58:** 5738-5748.

7 Fueyo J, Alemany R *et al.* Preclinical characterization of the antiglioma activity of a tropism-enhanced adenovirus targeted to the retinoblastoma pathway. *J Natl Cancer Inst 2003*; **95:** 652-660.

8 Brouwer E, Ophorst O *et al.* Improved adenoviral vectors for gene therapy of malignant glioma: 95th Annual Meeting of the American Association for Cancer Research; Orlando, 2004, pp. P1182.

9 Lang FF, Bruner JM *et al.* Phase I trial of adenovirus-mediated p53 gene therapy for recurrent glioma: biological and clinical results. *J Clin Oncol 2003*; **21:** 2508-2518.

10 Kirn DH, McCormick F. Replicating viruses as selective cancer therapeutics. *Mol Med Today 1996*; **2:** 519-527.

11 Russell SJ. Replicating vectors for cancer therapy: a question of strategy. *Semin Cancer Biol 1994*; **5:** 437-443.

12 Bobo RH, Laske DW *et al.* Convection-enhanced delivery of macromolecules in the brain. *Proc Natl Acad Sci U S A 1994*; **91:** 2076-2080.

13 Vogelbaum MA. Convection enhanced delivery for the treatment of malignant gliomas: symposium review. *J Neurooncol 2005*; **73:** 57-69.

14 Lieberman DM, Laske DW *et al.* Convection-enhanced distribution of large molecules in gray matter during interstitial drug infusion. *J Neurosurg 1995*; **82:** 1021-1029.

15 Mardor Y, Rahav O *et al.* Convection-enhanced drug delivery: increased efficacy and magnetic resonance image monitoring. *Cancer Res 2005*; **65:** 6858-6863.

16 Husain SR, Puri RK. Interleukin-13 receptor-directed cytotoxin for malignant glioma therapy: from bench to bedside. *J Neurooncol 2003*; **65:** 37-48.

17 Bankiewicz KS, Eberling JL *et al.* Convection-enhanced delivery of AAV vector in parkinsonian monkeys; in vivo detection of gene expression and restoration of dopaminergic function using pro-drug approach. *Exp Neurol 2000*; **164:** 2-14.

18 Betz AL, Shakui P, Davidson BL. Gene transfer to rodent brain with recombinant adenoviral vectors: effects of infusion parameters, infectious titer, and virus concentration on transduction volume. *Exp Neurol 1998*; **150:** 136-142.

19 Brust D, Feden J *et al.* Radiosensitization of rat glioma with bromodeoxycytidine and adenovirus expressing herpes simplex virus-thymidine kinase delivered by slow, rate-controlled positive pressure infusion. *Cancer Gene Ther 2000*; **7:** 778-788.

20 Nguyen TT, Pannu YS *et al.* Convective distribution of macromolecules in the primate brain demonstrated using computerized tomography and magnetic resonance imaging. *J Neurosurg 2003*; **98:** 584-590.

21 Sanftner LM, Sommer JM *et al.* AAV2-mediated gene delivery to monkey putamen: evaluation of an infusion device and delivery parameters. *Exp Neurol 2005*; **194:** 476-483.

22 Maina T, Nock BA *et al.* [^{99m}Tc]Demotate 2 in the detection of sst$_2$-positive tumors: A preclinical comparison with [^{111}In]DOTA-Tate. *Eur J Nucl Med 2006*; **33:** 831-840.

23 Reubi JC, Horisberger U *et al.* Absence of somatostatin receptors in human exocrine pancreatic adenocarcinomas. *Gastroenterology 1988*; **95:** 760-763.

24 Hemminki A, Belousova N *et al.* An adenovirus with enhanced infectivity mediates molecular chemotherapy of ovarian cancer cells and allows imaging of gene expression. *Mol Ther 2001*; **4:** 223-231.

25 Michou AI, Santoro L *et al.* Adenovirus-mediated gene transfer: influence of transgene, mouse strain and type of immune response on persistence of transgene expression. *Gene Ther 1997*; **4:** 473-482.

26 Pietersen AM, van der Eb MM *et al.* Specific tumor-cell killing with adenovirus vectors containing the apoptin gene. *Gene Ther 1999*; **6:** 882-892.

27 Fallaux FJ, Bout A *et al.* New helper cells and matched early region 1-deleted adenovirus vectors prevent generation of replication-competent adenoviruses. *Hum Gene Ther 1998*; **9:** 1909-1917.

28 Bakker WH, Krenning EP *et al.* In vivo use of a radioiodinated somatostatin analogue: dynamics, metabolism, and binding to somatostatin receptor-positive tumors in man. *J Nucl Med 1991*; **32:** 1184-1189.

29 Dethlefsen LA, Prewitt JM, Mendelsohn ML. Analysis of tumor growth curves. *J Natl Cancer Inst 1968*; **40:** 389-405.

30 Chen MY, Lonser RR *et al.* Variables affecting convection-enhanced delivery to the striatum: a systematic examination of rate of infusion, cannula size, infusate concentration, and tissue-cannula sealing time. *J Neurosurg 1999*; **90:** 315-320.

31 Chen ZJ, Broaddus WC *et al.* Intraparenchymal drug delivery via positive-pressure infusion: experimental and modeling studies of poroelasticity in brain phantom gels. *IEEE Trans Biomed Eng 2002*; **49:** 85-96.

32 MacKay JA, Deen DF, Szoka FC, Jr. Distribution in brain of liposomes after convection enhanced delivery; modulation by particle charge, particle diameter, and presence of steric coating. *Brain Res 2005*; **1035:** 139-153.

33 Mamot C, Nguyen JB *et al.* Extensive distribution of liposomes in rodent brains and brain tumors following convection-enhanced delivery. *J Neurooncol 2004*; **68:** 1-9.

34 Fields BN, Knipe DM *et al. Virology*. Lippincott Williams & Wilkins: Philadelphia, PA, 1996.

35 Kroll RA, Pagel MA *et al.* Increasing volume of distribution to the brain with interstitial infusion: dose, rather than convection, might be the most important factor. *Neurosurgery 1996*; **38:** 746-752; discussion 752-744.

36 Maina T, Nock B *et al.* [99mTc]Demotate, a new 99mTc-based [Tyr3]octreotate analogue for the detection of somatostatin receptor-positive tumours: synthesis and preclinical results. *Eur J Nucl Med Mol Imaging 2002*; **29:** 742-753.

37 de Jong M, Kwekkeboom D, Valkema R, Krenning EP. Radiolabelled peptides for tumour therapy: current status and future directions. Plenary lecture at the EANM 2002. *Eur J Nucl Med Mol Imaging 2003*; **30:** 463-469.

38 Rubsam LZ, Boucher PD *et al.* Cytotoxicity and accumulation of ganciclovir triphosphate in bystander cells cocultured with herpes simplex virus type 1 thymidine kinase-expressing human glioblastoma cells. *Cancer Res 1999*; **59:** 669-675.

39 Vincent AJ, Esandi MC *et al.* Preclinical testing of recombinant adenoviral herpes simplex virus thymidine kinase gene therapy for central nervous system malignancies. *Neurosurgery 1997*; **41:** 442-451.

PART 4

Imaging of adenovirus
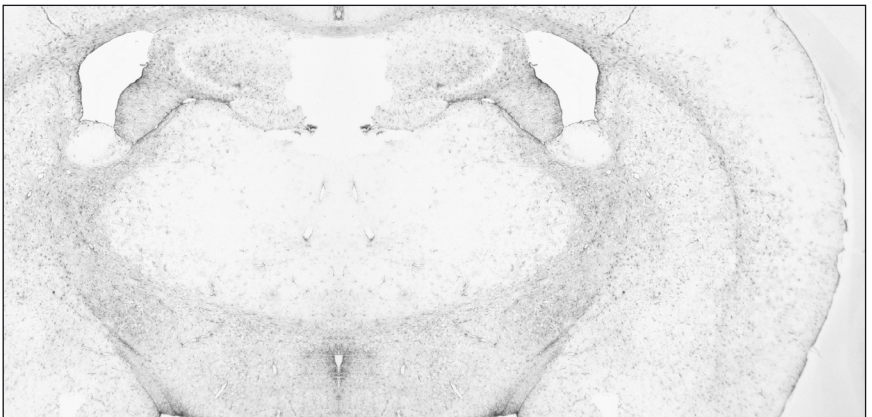
CHAPTER 4.1

[123I]FIRU, a tracer for the 'molecular imaging' of HSV1-tk suicide gene transfer

Maarten ter Horst[1,4], Dharmin Nanda[1,2], Kevin Morin[6], Suzanne Verwijnen[3], Max Kros[5], Flavio Forrer[3], Marion de Jong[3], Edward Knaus[6], Leonard Wiebe[6], and Peter Sillevis Smitt[1]

From the Departments of [1]Neuro-oncology, [2]Neurosurgery, [3]Nuclear Medicine, [4]Anesthesiology and [5]Pathology, Erasmus University Medical Center, Rotterdam, The Netherlands; the [6]Faculty of Pharmacy and Pharmaceutical Sciences, University of Alberta, Edmonton, Canada
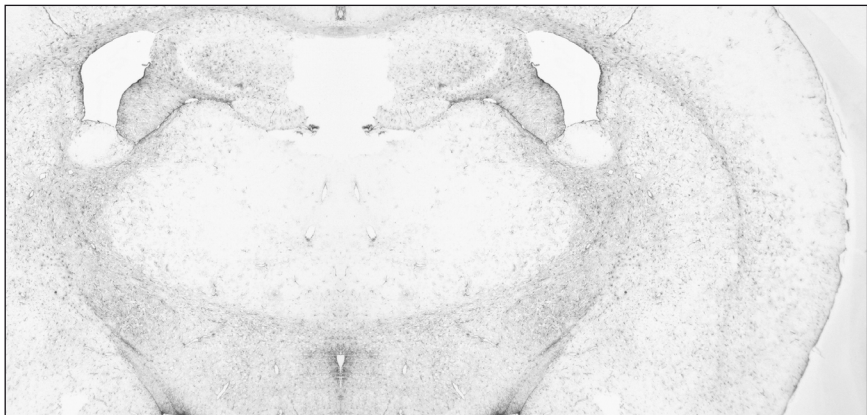
Abstract

Several radiopharmaceuticals have been proposed for *in vivo* imaging of the Herpes simplex virus-1 thymidine kinase (HSV1-tk) gene expression. We compared the *in vitro* toxicity of FIRU to the related compounds GCV (ganciclovir), FIAU and IVFRU. Furthermore, *in vivo* images using small animal SPECT, biodistribution, early kinetics and toxicity of FIRU were examined. **Methods:** The cytotoxicity of the compounds was determined in cell lines constitutively expressing the HSV1-tk gene and non-expressing maternal cell lines, using the MTT assay. Small animal SPECT images, biodistribution and early kinetics of [^{123}I]FIRU were examined in nude mice carrying 9L and 9L-tk subcutaneous tumors. The *in vivo* toxicity of FIRU was tested in mice and rats. **Results:** *In vitro t*oxicity studies demonstrated lower toxicity of FIRU as compared to FIAU in both non-HSV1-TK expressing cells (IC$_{50}$ ratio 3.8–500) and in HSV1-TK expressing cells (IC$_{50}$ ratio 1.7-2 x 10^7). SPECT images using [^{123}I]FIRU were able to visualize HSV-tk expression in mouse xenografts *in vivo*. Biodistribution and early kinetics studies of [^{123}I]FIRU in tumor bearing mice showed initial phase and terminal phase half-lives of respectively 0.8 h and 1.3 h (blood); 0.1 h and 4 h (muscle); and 0.5 h and 6.7 h (9L tumor). In 9L-tk+ tumors, [^{123}I]FIRU accumulated for about one hour, followed by a slower decrease of activity with a half-life of 11.3 h. Mice and rats receiving up to 200 times the projected clinical dose showed no toxicity.

Conclusions: The favorable toxicity and imaging profile make radiolabeled FIRU a promising agent for imaging of HSV1-tk gene transfer in clinical studies.

Introduction

Interest in non-invasive imaging and quantification of therapeutic transgene production is growing with increasing clinical applications of gene therapy[1-3]. The most commonly used methods for 'molecular imaging' of gene transfer are based on radionuclide's followed by PET or SPECT scanning[4]. Radionuclide imaging of transgene expression makes use of marker genes such as the cell surface gene of the human somatostatin receptor type 2 (sst_2)[5,6], genes encoding transporter proteins including the sodium/iodide symporter[7], or genes encoding enzymes that selectively metabolize the radionuclide tracer resulting in intracellular sequestration such as the herpes simplex virus type 1 thymidine kinase (HSV1-tk) gene[8-13].

The HSV1-tk gene is the most frequently used therapeutic gene in cancer gene therapy[14-16]. Various radiotracers based on uracil nucleosides and acycloguanosine derivatives that are selective substrates for this virus encoded enzyme have been proposed for the non-invasive imaging of HSV1-tk gene expression. The most commonly used radio-iodinated substrate for monitoring HSV1-tk gene expression is 1-(2-fluoro-2-deoxy-β-D-arabinofuranosyl)-5-iodouracil (FIAU; fialuridine)[17]. Another nucleoside with high sensitivity for HSV-TK is 1-(2-fluoro-2-deoxy-β-D-arabinofuranosyl)-thymine (FMAU). Because of their severe mitochondrial toxicity in normal cells and fatal toxicity to neurons and liver in clinical studies[18-23], FMAU and FIAU are not suitable for antiviral therapeutic applications but can be used as tracer molecules. Interestingly, the toxicity of FIAU reflects its phosphorylation by mammalian nucleoside kinases and subsequent incorporation into mammalian DNA[21,24,25]. Thus, radioiodinated FIAU uptake reflects not only activation by the viral kinase (HSV1-TK), but also uptake by mammalian cells not expressing HSV1-TK. This limits its selectivity, and may influence sensitivity, depending on the relative activity of the viral and mammalian enzymes.

Other nucleosides with high specificity for HSV1-TK include 1-(2-fluoro-2-deoxy-β-D-ribofuranosyl)-5-(*E*)-(2-iodovinyl)-uracil (IVFRU), 1-(2-fluoro-2-deoxy-β-D-ribofuranosyl)-5-iodouracil (FIRU)[11] and 9-(4-fluoro-3-hydroxy-methyl-butyl)guanine (FHGB)[26]. In a comparative study, uptake of FIRU in HSV1-tk expressing cells was similar to uptake of FIAU and IVFRU. Importantly, incorporation of FIRU into nucleic acids was only about one-tenth the incorporation of FIAU[23]. Biodistribution studies with [123I]FIRU have demonstrated a maximum uptake of 22 % of the injected dose per gram tissue in mice carrying HSV1-tk expressing tumor xenografts, and favorable imaging characteristics of [123I]FIRU following adenoviral HSV1-tk adenoviral gene transfer in a xenograft tumor model has been demonstrated[12]. The relative performance of several radioiodinated nucleosides in HSV1-tk-expressing cells depends to some degree on the cell type and the design of the gene cassette[23].

In the present study, we describe a Sep-Pak column-based method for purification of radioiodine labeled FIRU that can be easily applied to manufacturing of clinical grade batches. We subsequently present small animal SPECT images using [123I]FIRU as a reporter probe

to visualize HSV-tk expression in mouse xenografts *in vivo*. Finally, we examined the early kinetics of iodine labeled FIRU and its toxicity profile *in vitro* and *in vivo*.

Materials and Methods

Compounds

Ganciclovir (Cymevene; GCV) was purchased from Roche (Mijdrecht, Netherlands). IVFRU, FIAU and FIRU were synthesized using literature methods[27]. The structure formulae of the 4 compounds are depicted in Fig. 1. Carrier-added (radio)iodination was achieved by electrophilic iodination/destannylation of 1-(2-fluoro-2-deoxy-β-D-ribofuranosyl)-5-tributylstannyluracil (FTBSRU), the FIRU precursor, as previously described[12,28]. For recovery and purification of [123I]FIRU, the labeling mixture was passed through an activated Sep-Pak column; iodide was first eluted with H_2O, followed by elution of [123I]FIRU in 50 % aqueous ethanol and recovery of unreacted FTBSRU precursor in 96 % ethanol. For the *in vitro* and *in vivo* toxicity experiments, 'cold' FIRU was synthesized by a similar procedure, but omitting [123I]NaI from the reaction mixture.
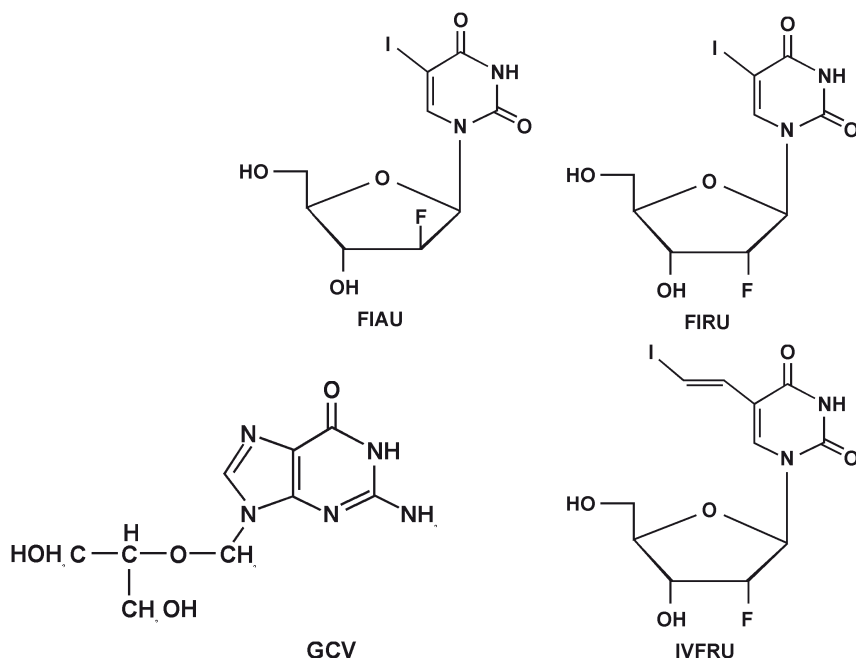
Fig. 1 Structural formula of ganciclovir (GCV: Mw 255), FIRU (Mw 372), FIAU (Mw 372) and IVFRU (Mw 398). Note that the only difference between FIAU and FIRU is the 2'-fluoro-arabino ("up") substitution in FIAU versus the 2'-fluoro-ribo ("down") substitution in FIRU.

HPLC analysis of [^{123}I]FIRU

An aliquot of eluted [^{123}I]FIRU was diluted with HPLC-solvent, and an aliquot of this solution was injected into the HPLC-system (Waters-Instruments (Etten-Leur, The Netherlands) using a Partisil 10 column (ODS 4.6 mm x 250 mm; Whatman, Maidstone, England). UV-absorbance was measured at 254 nm. The outlet of the UV detector was connected to a well-type NaI crystal (Canberra Packard Benelux sa, Zellik, Belgium). Isocratic elution (1 mL/min) was carried out using acetonitrile/milliQ-water 10/90 vol %.

Cell culture

Murine fibrosarcoma KBALB, human osteosarcoma R-970-5 (a TK- mutant of R-970-5) and human 143B cell lines were purchased from American Type Culture Collection (ATCC, Manassas, VA). The rat 9L gliosarcoma brain tumor cell line was a gift from Dr. K.M. Hebeda (Dept. Experimental Neurosurgery, Free University Hospital Amsterdam, The Netherlands). The EMT-6 mouse mammary tumor cell line was obtained from the Cross Cancer Institute (Edmonton, Canada). The KBALB-STK cell line, which expresses HSV1-tk, was obtained from Dr. Scott Freeman (Tulane University Medical Center, New Orleans, USA.)[29]. The 143B and 9L cell lines were stably transfected using an HSV1-tk-carrying retrovirus construct, followed by G418 selection (250 µg – 1 mg/mL) (Life Technologies, Breda, The Netherlands). The corresponding HSV-tk positive cell lines were further selected for GCV sensitivity and were named 143B-LTK and 9L-tk+ respectively[30,31]. Cell lines were maintained in Dulbecco's modified Eagles medium (DMEM; Life Technologies) supplemented with 10 % fetal bovine serum (FBS; Life Technologies), penicillin (100 U/mL) and streptomycin (100 µg/mL). Only EMT-6 cells were routinely maintained in Waymouth medium, and 143B cells were maintained in DMEM containing 5-bromo-2'-deoxyuridine (15 µg/mL). KBALB-STK, 143B-LTK and 9L-tk+ cells were maintained in medium that had 250 µg - 1 mg/mL G-418 (Life Technologies) added in addition to FBS and antibiotics. Cells were cultured at 37°C in a 5 % CO2 atmosphere.

MTT Cytotoxicity Assay Method

Exponentially growing cells were trypsinized, centrifuged and suspended in growth medium and readjusted to $8x10^3$ cells/mL. The cells were seeded into 96-well plates at $8x10^2$ cells/well and incubated at 37 ºC, 5 % CO_2 for 24 h. The compounds were dissolved in DMEM medium and incubated with the cells in 96-well plates at a volume of 100 µL to produce a final concentration of design. Control wells were filled with 100 µL of DMEM medium. The plates were incubated for 72 h at 37 ºC in a humidified atmosphere containing 95 % air and 5 % CO_2. At the end of incubation, 3-(4,5-dimethyl-2-thiazolyl)-2,5-diphenyl-2*H*-tetrazolium bromide (MTT, Sigma, Zwijndrecht, The Netherlands) was added, and the plates were incubated at 37 ⁰C for 4 h. Dimethylsulfoxide was added to dissolve the formazan crystals, and the plate wells were then read at 540 nm on a scanning multi-well spectrophotometer.

Animal experiments

The Institutional Animal Care and Use Committee, in compliance with the Guide for the care and Use of Laboratory Animals, approved all experimental protocols. For the biodistribution studies, five- to six-week old female NIH-bg-nu-xid mice were purchased[32] from Harlan Sprague Dawley Inc., Oxon, England. For the animal SPECT experiments two, five- to six-week old male nu/nu NMRI mice (Charles River, Les Oncins, France) were purchased. Mice were hosted 3-4 per cage and allowed access to food and water ad libitum. After one week, 9L or 9L-tk$^+$ cells (10^7 cells in 500 µL HBSS; Life Technologies) were inoculated subcutaneously into both flanks. Tumor growth was monitored by measuring bidimensional diameters three times a week with calipers, and tumor volume was determined by applying the simplified formula of a rotational ellipse (l x w^2 x 0.5)[33]. The experiments were performed when the 9L and the 9L-tk $^+$ tumors had reached a volume of approximately 1000 mm^3. For the biodistribution experiments, [^{123}I]FIRU (3 MBq) was injected intravenously into the tail vein. Biodistribution of [^{123}I]FIRU was determined 15 min, and 1, 2, 4 and 24 h post injection (p.i.). Four mice were examined at each time point. Tumor, brain, thyroid gland, heart, lungs, stomach, kidney, spleen, skin, muscle, femur and blood were collected, the weight was measured and radioactivity was determined in the gamma counter. The radioactivity is expressed as percentage of the injected dose / gram organ (%ID/g).

For the SPECT experiment [^{123}I]FIRU (40 MBq) was injected intravenously into the penis vein and the animals were scanned 4 hr later.

SPECT and Software

SPECT imaging was performed with the four-headed multiplexing multi-pinhole small animal SPECT (Bioscan Inc., Washington D.C.). Each head is outfitted with an application specific tungsten collimator. For this study we imaged with the 9-pinhole-mouse apertures that are comprised of a total of 36 1.3 mm diameter pinholes imaging a cylindrical field of view that is 32 mm in diameter by 14 mm in length. These mouse apertures provide a reconstruction resolution below 1.0 mm at 159 keV with an average sensitivity of 1100 cps/MBq across the field of view (FOV). The axial FOV is extended using a step-and-shoot helical scan to perform a total body scan of the animal (total distance 85 mm). The energy-peak for the camera was set at 159 keV. The window width was ± 10%. An acquisition time of 20 sec. per projection was chosen. Acquisition time was 20 min. per animal. After the acquisition the data were reconstructed iteratively with the HiSPECT© software (Bioscan Inc., Washington DC), a dedicated ordered subset-expectation maximization (OSEM) software package for multiplexing multi-pinhole reconstruction. The SPECT is calibrated with a phantom such that voxel values in the reconstruction provide a proper estimate of the activity level without further calculation.

In vivo toxicity testing

Twenty-four male Wistar rats (weight approximately 50 g) and 24 male BALB-c mice (5-6 weeks old) were purchased from Harlan Sprague Dawley Inc., Oxon, England. Non-radioactive precursor was iodinated with non-radioactive ICl, followed by Sep-Pak purification, as described for [123I]FIRU. For the animal experiments, the ethanol fraction was air dried and dissolved in PBS. The FIRU was subsequently administered by tail vein injection into the animals, based on the projected dose to be administered to human subjects (100 µg of radiolabelled FIRU; nominally 1.4 µg/kg). Rats and mice were divided in 3 groups of 8 animals receiving 0, 20 or 200 times the anticipated clinical dose. Animals were observed daily and euthanized by pentobarbital sodium injection seven days after FIRU administration. Blood was drawn by cardiac puncture for hematological (Hb, Ht, leukocytes and platelets) and chemical tests (sodium, potassium, creatinin, ASAT, ALAT, alkaline phosphatase, αGT, LDH and amylase). Liver, spleen, pancreas, heart, lungs, kidneys, esophagus, stomach, duodenum, bladder, lymph nodes, striated muscle, salivary glands and sciatic nerve were dissected out immediately and fixed in formalin. After paraffin embedding, sections were cut and stained with H&E and examined by a licensed pathologist (M.K.).

Statistical analysis

The hematological and chemistry parameters in the three dose groups of rats and mice were compared using ANOVA. When a significant difference between groups was detected, we used post-hoc Dunnett's Multiple Comparison Test to determine the groups that differed significantly. All P-values are two-sided and a significance level α = 0.05 was used. All statistical analyses were performed using GraphPad Prism version 4.0 software (GraphPad Software, Inc., San Diego, CA).

Results

Analytic HPLC chromatograms before (a) and after Sep-Pak purification (b) are shown in Fig. 2. In profile (a), unbound radioactivity, presumably as radioiodide, elutes at the column void volume (~1.5 min), and [123I]FIRU is detected at ~ 4 min. Profile (b) is a chromatogram of the 50 % ethanol Sep-Pak eluant, showing only a single radioactive peak at the FIRU elution time. No unreacted FTBSRU was evident in this fraction (by UV detection; data not shown). The radiochemical purity was >97 % with a labeling yield of 56 ±10 %; specific activity not less than 690 MBq/µmol. This specific activity is lower than achievable using a 'no carrier' oxidant such as hydrogen peroxide[34], but there is no evidence to suggest that this specific activity negatively influences uptake. In studies using radioactive IUdR and FIAU, it has been reported that uptake in the presence of respective carrier (10 µM) will reduce uptake of
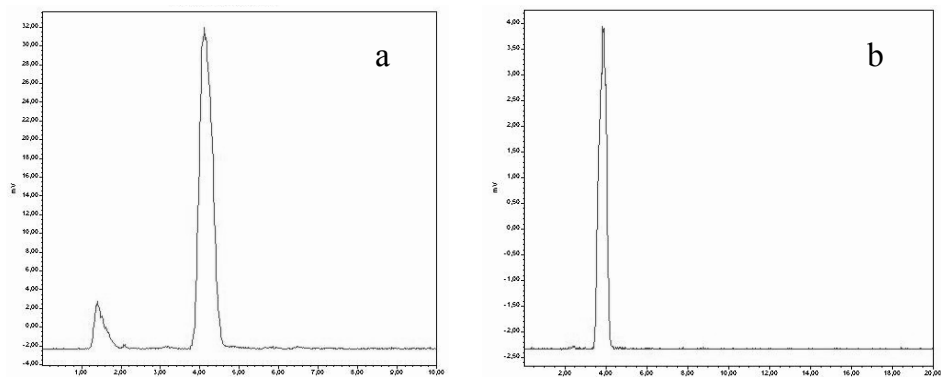
Fig. 2 HPLC analysis of [^{123}I]FIRU. Radiolabeled FIRU elutes from the HPLC column at 4 min. Panel a depicts the HPLC result of [^{123}I]FIRU before Sep-Pak purification. Panel b shows HPLC analysis of the 50 % ethanol fraction (v/v ethanol/H$_2$O) of the Sep-Pak column, which contains only [^{123}I]FIRU.

radioactivity by 3 - 10 fold over a 100 min incubation period[34]; consequently, in the present studies, in which FIRU concentrations are approximately 0.004 µM, little if any effect is to be anticipated.
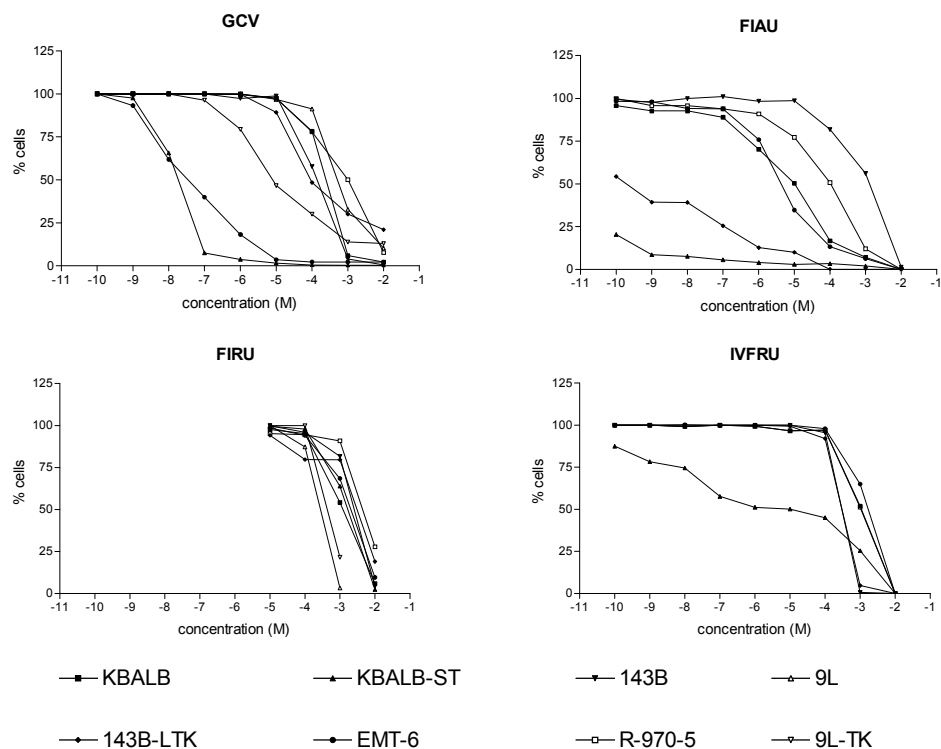
Fig. 3 *In vitro* toxicity of GCV, FIRU, FIAU and IVFRU. At increasing doses, all compounds become toxic in all cells. In the HSV1-TK expressing cells, FIRU is clearly less toxic than FIAU, GCV and FIAU.

In vitro toxicity of FIRU

Fig. 3 shows the cytotoxicity of increasing concentrations of ganciclovir, FIRU, FIAU and IVFRU in the cell lines tested. The relative inhibitory concentration of 50% (IC_{50}) of FIRU compared to FIAU and ganciclovir is shown in Table 1. When the compounds are phosphorylated (in HSV1-tk expressing cells), FIAU is 7 logs more toxic than FIRU. This finding most probably reflects the incorporation of phosphorylated FIAU into cellular DNA as opposed to FIRU[27]. However, in non-HSV1-tk expressing dividing cells, FIAU is also more toxic than FIRU (1-2 logs), presumably reflecting some phosphorylation of FIAU by endogenous TK[24,25].

Table 1. Summary of cytotoxicity (IC_{50}, M) of ganciclovir, FIRU and FIAU in non-HSV1-tk and in HSV1-tk expressing cells.

|	IC_{50} of GCV	IC_{50} of FIAU	IC_{50} of FIRU	Ratio IC_{50} FIRU:FIAU
Non-HSV1-TK expressing cells:				
KBALB	4.8×10^{-4} M	1.0×10^{-5} M	1.5×10^{-3} M	150
143B	1.0×10^{-4} M	2.0×10^{-3} M	7.5×10^{-3} M	3.8
R-970-5	1.2×10^{-3} M	1.0×10^{-4} M	7.0×10^{-3} M	70
EMT-6	2.0×10^{-4} M	6.5×10^{-6} M	3.0×10^{-3} M	500
HSV1-TK expressing cells:				
KBALB-STK	3.0×10^{-8} M	1.0×10^{-10} M	2.0×10^{-3} M	2×10^7
143B-LTK	6.5×10^{-8} M	3.0×10^{-10} M	5.0×10^{-3} M	1.7×10^7

In vivo imaging of [^{123}I]-FIRU distribution using small animal SPECT

Animals carrying established 9L tumors in the left flank and 9L-tk+ tumors in the right flank were intravenously injected with [^{123}I]-FIRU (40MBq). Four hours later, the animals were sacrificed and scanned (Fig. 4). The high-resolution SPECT images clearly visualize the uptake of the radiopharmaceutical in the 9L-tk+ tumor, while the 9L tumor remains at background level.

Biodistribution and early kinetics of [^{123}I]FIRU

The biodistribution of [^{123}I]FIRU in 9L-tk+ tumors, 9L tumors, muscle, thyroid, stomach, blood and brain at 15 min and 1, 2, 4 and 24 h p.i. (Fig. 5) is compatible with rapid renal clearance of the tracer from the body, resulting in increased muscle/muscle, blood/blood and brain/brain ratios over time. A maximum tissue uptake of 23 % ID/g tissue was reached in the 9L-tk+ tumors 4 h after [^{123}I]FIRU injection compared to muscle (<2 %), thyroid (2.2 %), stomach (6.2 %), blood (<2 %) and brain (<2 %). The accumulation of radioactivity in thyroid and stomach indicates, as reported previously[28], some partial de-iodination of [^{123}I] FIRU.

Blood, muscle and HSV1-tk negative tumors clearly showed bi-exponential elimination characteristics (Fig. 6). The half-lives for the initial phase were 0.8 h (blood), 0.1 h (muscle) and 0.5 h (9L tumor). The half-lives for the terminal phase were 1.3 h (blood), 4 h (muscle)
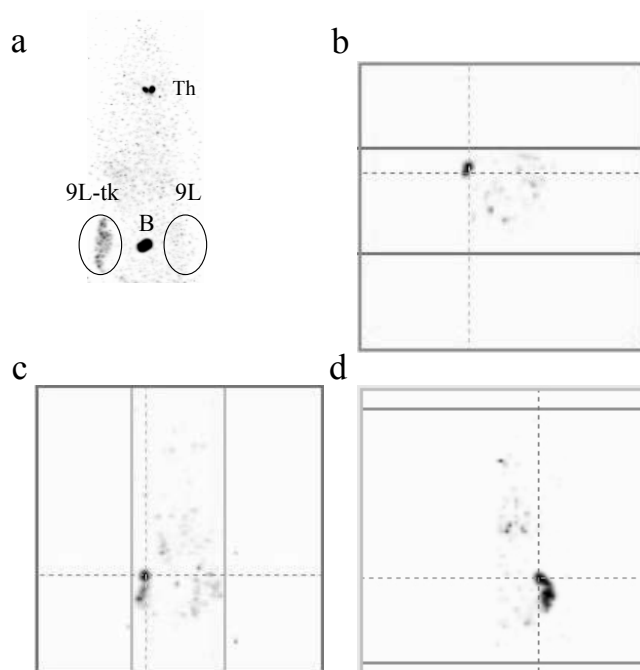
Fig. 4 Small animal SPECT image using [^{123}I]FIRU as reporter probe. 3D-reconstruction of the whole mouse acquired by multipinhole SPECT is shown in (a). The transaxial (b), coronal (c) and saggital (d) slices of the mouse clearly visualize the HSV-tk positive tumor (9L-tk+) in the left flank. The HSV-tk negative tumor (9L) in the right flank remained at back-ground level. Th thyroid; B bladder. See Color Figures, p. 157.
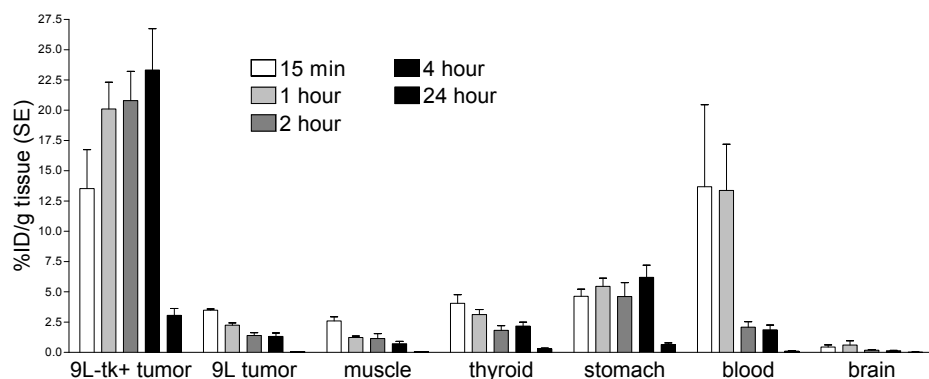
Fig. 5 Biodistribution of [^{123}I]FIRU. The percentage of the injected dose per gram of tissue (%ID/g tissue) is measured at 15 min and 1, 2, 4 and 24 h after injection. The maximum tumor uptake of 23 %ID/g tissue in HSV1-tk expressing tumors is reached four hours after injection.

and 6.7 h (wild-type 9L tumor). After an initial accumulation of about one hour of ^{123}I-FIRU in the HSV-tk positive 9L-tk+ tumors, the activity decreases more slowly with a half-life of 11.3 h (Fig 6).
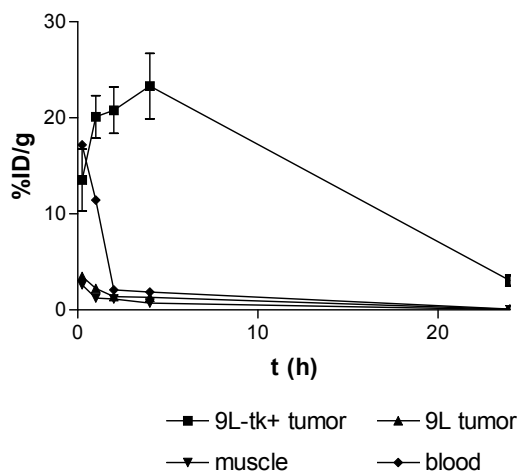
Fig. 6 Early biokinetics of [123I]FIRU. While the elimination of [123I]FIRU from blood, muscle and HSV1-tk negative tumor (9L) is clearly biphasic, the activity accumulates in HSV1-tk positive tumor (9L-tk+) followed by a much slower decrease of the incorporated activity.

In vivo toxicity of FIRU

None of the rats and mice showed clinical signs of disease. Hematological and biochemical parameters tested did not differ between animals receiving PBS, 20x or 200x the projected human dose of FIRU. Pathological examination of all organs did not demonstrate any abnormality indicative of toxicity.

Discussion

This paper describes a simple Sep-Pak based method for the purification of radio-iodinated FIRU allowing large scale, clinical grade production. The described carrier-mediated labeling method is simple, and purification over a Sep-Pak column is much more convenient than preparative HPLC, in particular for the production of clinical grade under GMP conditions.

Using the described labeling and purification strategy, [123I]FIRU was routinely produced with a radiochemical purity > 97 %, a labeling yield of ~ 56 % and a specific activity not less than 690 MBq/μmol.

The *in vitro* toxicity of FIRU, FIAU and related compounds was studied in a number of cell lines. In constitutively HSV1-tk expressing cell lines, the toxicity of FIRU was significantly lower than FIAU. This lack of toxicity of the phosphorylated FIRU compound is most likely due to the fact that FIRU is not incorporated into the DNA of the mammalian dividing cell[27], as opposed to FIAU[24,25]. In dividing cells that don't express HSV1-tk, FIRU was also less toxic than FIAU. This difference probably reflects a lower affinity of the endogenous TK enzyme for FIRU than for FIAU, but in neither case is uptake sufficient to warrant use as a cell

proliferation marker[35]. Uptake of FIAU was reported to be about 20-fold higher than that of IUdR in D-247 MG cells, leading those authors to conclude that [^{125}I]FIAU might have greater cytotoxicity for this cell line than [^{125}I]IUdR[34].

In the past decade significant progress has been made in using PET and SPECT imaging methods to detect the expression of specific genes, such as HSV1-tk, in living animals[36-38]. Recently, a multiplexing multi-pinhole small-animal SPECT system has been described with greatly improved sensitivity while achieving high resolutions[39,40]. Using this system, we could clearly demonstrate the uptake of FIRU in HSV-tk expressing xenografts (Fig. 4).

Choi et al[41] earlier showed microSPECT images of [^{123}I]FIAU uptake in HSV-tk expressing xenografts. These high-resolution SPECT images clearly demonstrated inhomogeneous tracer uptake in one of the xenografts, suggesting necrosis of the interior portion of the tumor. In our study we did not observe inhomogenous uptake nor did we see necrotic areas on pathological examination, probably due to limited tumor size. Progress in nuclear technology and fusion of multiple imaging modalities, such as SPECT and CT, will further enhance the sensitivity and accuracy of molecular imaging.

The biodistribution (Table 1) and biokinetics (Fig. 5) studies show selective accumulation of ^{123}I-FIRU in HSV1-tk+ tumors in the first hour after administration. Subsequently, the radioactivity incorporated in these tumors decreases with a much longer half-life than in the surrounding tissues. The optimal imaging time with [^{123}I]FIRU is 4 h post-injection[12,27].

Finally, in preparation of clinical studies, we performed toxicity studies with 'cold' FIRU in rats and mice. The injected amount of FIRU per animal was 1x, 20x or 200x fold (mg/kg) of the intended human dose for imaging (100 µg (0.27 µmol) / 70 kg). Because the mitochondrial toxicity associated with FIAU manifests mainly as hepatotoxicity, pancreatitis, neuropathy or myopathy, we focused on these organs and the hematopoietic system [21]. This multisystem mitochondrial toxicity is probably caused by the high rate at which FIAU is incorporated into mitochondrial DNA[42,43]. We could detect no clinical, laboratory or pathological signs of toxicity due to FIRU. In particular, all liver function tests and amylase levels were normal. Pathological examination of liver and pancreas and of the peripheral nervous system and muscle was completely normal.

We conclude that radiolabeled FIRU can be easily produced in clinical grade batches. In addition, the safety profile and clear imaging properties make FIRU a good candidate tracer for clinical imaging of HSV1-tk gene transfer.

Acknowledgments

References

1. Nanda D, Driesse MJ, Sillevis Smitt PA. Clinical trials of adenoviral-mediated suicide gene therapy of malignant gliomas. *Prog Brain Res 2001*; **132:** 699-710.

2. Min JJ, Gambhir SS. Gene therapy progress and prospects: noninvasive imaging of gene therapy in living subjects. *Gene Ther 2004*; **11:** 115-125.

3. Blasberg RG, Tjuvajev JG. Molecular-genetic imaging: current and future perspectives. *J Clin Invest 2003*; **111:** 1620-1629.

4. Ray P, Bauer E *et al.* Monitoring gene therapy with reporter gene imaging. *Semin Nucl Med 2001*; **31:** 312-320.

5. Zinn KR, Buchsbaum DJ *et al.* Noninvasive monitoring of gene transfer using a reporter receptor imaged with a high-affinity peptide radiolabeled with 99mTc or 188Re. *J Nucl Med 2000*; **41:** 887-895.

6. Ter Horst M, Verwijnen SM *et al.* Locoregional Delivery of Adenoviral Vectors. *J Nucl Med 2006*; **47:** 1483-1489.

7. Carlin S, Akabani G, Zalutsky MR. In vitro cytotoxicity of (211)at-astatide and (131)I-iodide to glioma tumor cells expressing the sodium/iodide symporter. *J Nucl Med 2003*; **44:** 1827-1838.

8. Tjuvajev JG, Finn R *et al.* Noninvasive imaging of herpes virus thymidine kinase gene transfer and expression: a potential method for monitoring clinical gene therapy. *Cancer Res 1996*; **56:** 4087-4095.

9. Haubner R, Avril N *et al.* In vivo imaging of herpes simplex virus type 1 thymidine kinase gene expression: early kinetics of radiolabelled FIAU. *Eur J Nucl Med 2000*; **27:** 283-291.

10. Gambhir SS, Barrio JR *et al.* Imaging of adenoviral-directed herpes simplex virus type 1 thymidine kinase reporter gene expression in mice with radiolabeled ganciclovir. *J Nucl Med 1998*; **39:** 2003-2011.

11. de Vries EF, van Waarde A *et al.* [(11)C]FMAU and [(18)F]FHPG as PET tracers for herpes simplex virus thymidine kinase enzyme activity and human cytomegalovirus infections. *Nucl Med Biol 2000*; **27:** 113-119.

12. Nanda D, de Jong M *et al.* Imaging expression of adenoviral HSV1-tk suicide gene transfer using the nucleoside analogue FIRU. *Eur J Nucl Med Mol Imaging 2002*; **29:** 939-947.

13. Verwijnen SM, Sillevis Smith PA *et al.* Molecular imaging and treatment of malignant gliomas following adenoviral transfer of the herpes simplex virus-thymidine kinase gene and the somatostatin receptor subtype 2 gene. *Cancer Biother Radiopharm 2004*; **19:** 111-120.

14. St Clair MH, Lambe CU, Furman PA. Inhibition by ganciclovir of cell growth and DNA synthesis of cells biochemically transformed with herpesvirus genetic information. *Antimicrob Agents Chemother 1987*; **31:** 844-849.

15. Moolten FL, Wells JM. Curability of tumors bearing herpes thymidine kinase genes transferred by retroviral vectors. *J Natl Cancer Inst 1990*; **82:** 297-300.

16. Pulkkanen KJ, Yla-Herttuala S. Gene therapy for malignant glioma: current clinical status. *Mol Ther 2005*; **12:** 585-598.

17. Tjuvajev JG, Stockhammer G *et al.* Imaging the expression of transfected genes in vivo. *Cancer Res 1995*; **55:** 6126-6132.

18. McLaren C, Chen MS *et al.* Drug resistance patterns of herpes simplex virus isolates from patients treated with acyclovir. *Antimicrob Agents Chemother 1985*; **28:** 740-744.

19. Pankiewicz KW, Nawrot B *et al.* Nucleosides. 146. 1-Methyl-5-(2-deoxy-2-fluoro-beta-D-arabinofuranosyl)uracil, the C-nucleoside isostere of the potent antiviral agent 1-(2-deoxy-2-fluoro-beta-D-arabinofuranosyl)thymine (FMAU). Studies directed toward the synthesis of 2'-deoxy-2'-substituted arabino nucleosides. 6. *J Med Chem 1987*; **30:** 2314-2316.

20 Abbruzzese JL, Schmidt S *et al.* Phase I trial of 1-(2'-deoxy-2'-fluoro-1-beta-D-arabinofuranosyl)-5-methyluracil (FMAU) terminated by severe neurologic toxicity. *Invest New Drugs 1989*; **7:** 195-201.

21 Cui L, Yoon S, Schinazi RF, Sommadossi JP. Cellular and molecular events leading to mitochondrial toxicity of 1-(2-deoxy-2-fluoro-1-beta-D-arabinofuranosyl)-5-iodouracil in human liver cells. *J Clin Invest 1995*; **95:** 555-563.

22 Wang J, Eriksson S. Phosphorylation of the anti-hepatitis B nucleoside analog 1-(2'-deoxy-2'-fluoro-1-beta-D-arabinofuranosyl)-5-iodouracil (FIAU) by human cytosolic and mitochondrial thymidine kinase and implications for cytotoxicity. *Antimicrob Agents Chemother 1996*; **40:** 1555-1557.

23 Morin KW, Duan W *et al.* Cytotoxicity and cellular uptake of pyrimidine nucleosides for imaging herpes simplex type-1 thymidine kinase (HSV-1 TK) expression in mammalian cells. *Nucl Med Biol 2004*; **31:** 623-630.

24 Klecker RW, Katki AG, Collins JM. Toxicity, metabolism, DNA incorporation with lack of repair, and lactate production for 1-(2'-fluoro-2'-deoxy-beta-D-arabinofuranosyl)-5-iodouracil in U-937 and MOLT-4 cells. *Mol Pharmacol 1994*; **46:** 1204-1209.

25 Grant AJ, Feinberg A *et al.* Incorporation of metabolites of 2'-fluoro-5-iodo-1-beta-D-arabinofuranosylcytosine into deoxyribonucleic acid of neoplastic and normal mammalian tissues. *Biochem Pharmacol 1982*; **31:** 1103-1108.

26 Green LA, Nguyen K *et al.* A tracer kinetic model for 18F-FHBG for quantitating herpes simplex virus type 1 thymidine kinase reporter gene expression in living animals using PET. *J Nucl Med 2004*; **45:** 1560-1570.

27 Wiebe LI, Knaus EE, Morin KW. Radiolabelled pyrimidine nucleosides to monitor the expression of HSV-1 thymidine kinase in gene therapy. *Nucleosides Nucleotides 1999*; **18:** 1065-1066.

28 Mercer JR, Xu LH, Knaus EE, Wiebe LI. Synthesis and tumor uptake of 5-82Br- and 5-131I-labeled 5-halo-1-(2-fluoro-2-deoxy-beta-D-ribofuranosyl)uracils. *J Med Chem 1989*; **32:** 1289-1294.

29 Ramesh R, Munshi A *et al.* Expression of costimulatory molecules: B7 and ICAM up-regulation after treatment with a suicide gene. *Cancer Gene Ther 1996*; **3:** 373-384.

30 Vincent AJ, Vogels R *et al.* Herpes simplex virus thymidine kinase gene therapy for rat malignant brain tumors. *Hum Gene Ther 1996*; **7:** 197-205.

31 Wang ZX, Duan W *et al.* Synthesis of 1-(2-deoxy-beta-D-ribofuranosyl)-2,4-difluoro-5-substituted-benzenes: "thymine for evalation as anticancer and antiviral agents. *Nucleosides Nucleotides 2001*; **20:** 41-58.

32 Kamel-Reid S, Dick JE. Engraftment of immune-deficient mice with human hematopoietic stem cells. *Science 1988*; **242:** 1706-1709.

33 Dethlefsen LA, Prewitt JM, Mendelsohn ML. Analysis of tumor growth curves. *J Natl Cancer Inst 1968*; **40:** 389-405.

34 Vaidyanathan G, Zalutsky MR. Preparation of 5-[131I]iodo- and 5-[211At]astato-1-(2-deoxy-2-fluoro-beta-D-arabinofuranosyl) uracil by a halodestannylation reaction. *Nucl Med Biol 1998*; **25:** 487-496.

35 Tjuvajev JG, Joshi R *et al.* Noninvasive imaging of HSV1-tk marker gene with FIAU for monitoring transfer and expression of other therapeutic genes by multi-gene delivery vectors. *J. Nucl med 1998*; **39:** 130P.

36 Shah K, Jacobs A, Breakefield XO, Weissleder R. Molecular imaging of gene therapy for cancer. *Gene Ther 2004*; **11:** 1175-1187.

37 Blasberg RG. Molecular imaging and cancer. *Mol Cancer Ther 2003*; **2:** 335-343.

38 Sharma V, Luker GD, Piwnica-Worms D. Molecular imaging of gene expression and protein function in vivo with PET and SPECT. *J Magn Reson Imaging 2002*; **16:** 336-351.

39 Schramm NU, Ebel G *et al.* High-resolution SPECT using multipinhole colliation. *IEEE Trans Nucl Sci 2003*; **50:** 315-320.

40   Lackas C, Schramm NU *et al.* T-SPECT: a novel imaging technique for small animal research. *IEEE Trans Nucl Sci 2005*; **52:** 181-187.

41   Choi SR, Zhuang ZP *et al.* SPECT imaging of herpes simplex virus type1 thymidine kinase gene expression by [(123)I]FIAU(1). *Acad Radiol 2005*; **12:** 798-805.

42   Lewis W, Griniuviene B *et al.* Depletion of mitochondrial DNA, destruction of mitochondria, and accumulation of lipid droplets result from fialuridine treatment in woodchucks (Marmota monax). *Lab Invest 1997*; **76:** 77-87.

43   Lewis W, Levine ES *et al.* Fialuridine and its metabolites inhibit DNA polymerase gamma at sites of multiple adjacent analog incorporation, decrease mtDNA abundance, and cause mitochondrial structural defects in cultured hepatoblasts. *Proc Natl Acad Sci U S A 1996*; **93:** 3592-3597.

CHAPTER 4.2

Molecular imaging following adenoviral gene transfer visualizes sst$_2$ and HSV1-tk expression

Suzanne Martine Verwijnen[1], Maarten ter Horst[2], Peter Sillevis Smitt[2], Rob Hoeben[3], Flavio Forrer[1], Cristina Müller[1], Wout A.P. Breeman[1], Eric Krenning[1], and Marion de Jong[1].

Departments of [1]Nuclear Medicine and [2]Neurology, Erasmus MC, Rotterdam, The Netherlands; Department of [3]Molecular Cell Biology, Leiden University Medical Center, Leiden, The Netherlands.
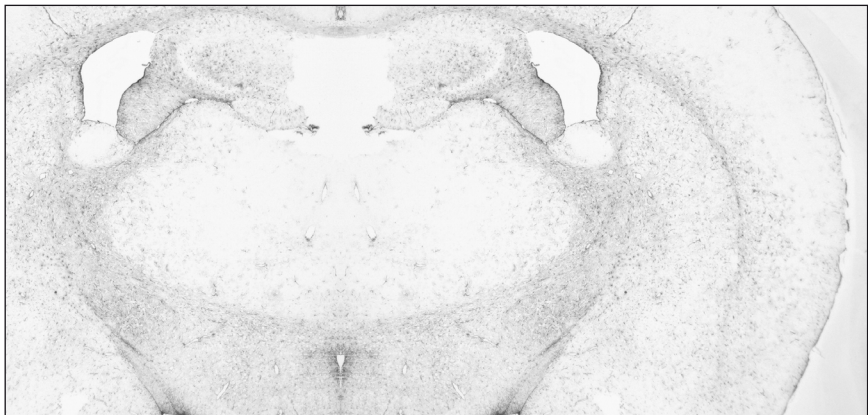
Abstract

Purpose: Gene therapy is an interesting approach to improve cancer treatment. Single photon emission computed tomography (SPECT) allows imaging of reporter gene expression non-invasively over time following gene transfer. The aim of this study was to use a novel integrated animal SPECT/CT to image and quantify human somatostatin receptor subtype 2 (sst_2) and to monitor Herpes Simplex Virus thymidine kinase (HSV-tk) expression following $Ad5.tk.sst_2$ gene transfer into tumor-bearing mice.

Methods: U87MG tumor-bearing mice were infected with $Ad5.tk.sst_2$ by intra-tumoral injection. Three days thereafter mice were injected with either $[^{99m}Tc-N_4^{0-1},Asp^0,Tyr^3]$octreotate or 1-(2'-deoxy-2'-fluoro-1'-β-D-ribofuranosyl)-5-$[^{123}I]$iodo-uracil to target sst_2 and HSV-tk, respectively and SPECT images were acquired. At several time points (3-7 days) post infection, sst_2 expression was imaged and quantified using SPECT/CT. Three days post infection, mice were euthanized for biodistribution studies and tumors were cryosectioned for *ex vivo* and *in vitro* autoradiography and immunohistochemistry to visualize the distribution pattern of sst_2 or HSV-tk expression.

Results: Using SPECT/CT, we could non-invasively image sst_2 and HSV-tk expression after $Ad5.tk.sst_2$ gene therapy. Up to a week after infection, sst_2 expression could be imaged and quantified. Autoradiography and immunohistochemistry showed non-homogeneous expression patterns of sst_2 and HSV-tk in infected tumors, probably visualizing the needle tracts of the viral injection.

Conclusions: This study demonstrates that sst_2 and HSV-tk genes can be used to image the location and duration of gene expression after intra-tumoral $Ad5.tk.sst_2$ gene transfer using SPECT/CT imaging. SPECT/CT is a useful tool for monitoring and quantification of receptor expression in vector-based gene transfer.

Introduction

Over the last years, the interest for and research in non-invasive imaging of small animals has grown extensively[1]. These imaging techniques include positron emission tomography (PET), single-photon emission computed tomography (SPECT), computed tomography (CT), magnetic resonance imaging and optical imaging. PET and SPECT enable visualization of e.g. biological processes in living animals. In the last decade, dedicated small animal imaging equipment with high resolution and high sensitivity has been developed[2-5]. These systems enable accurate quantification of radioactivity in particular organs, such as rat kidneys[6]. In the field of gene therapy, SPECT and PET imaging are helpful techniques to determine the location, duration and level of expression of the desired transgene[7], in preclinical as well as in clinical studies.

A good tumor candidate for gene therapy is glioblastoma multiforme (GBM). Patients suffering from GBM have a median survival rate of less than one year[8], showing the extreme aggressiveness of this tumor. The current standard treatment for GBM patients includes surgery, radiotherapy and chemotherapy. However, it is evident that these treatment modalities are not sufficiently effective, since the prognosis of these patients remains poor. Gene therapy is anticipated to be an attractive treatment option for GBM patients because of the localization of the tumor in the skull and the fact that distant metastases are uncommon. Clinical gene therapy trials for GBM have proven to be safe for patients and the environment, although the tumoricidal effects in these trials have been limited[9]. The lack of quantitative information on vector-mediated gene expression or functional protein activity was one of the weak points in these trials. Therefore, non-invasive imaging of transgene expression following treatment is of high interest.

In the present preclinical study, we investigated whether high-resolution animal SPECT/CT imaging would be suitable for monitoring transgene expression of human GBM tumors in mice. We used the Ad5.tk.sst$_2$ adenoviral vector[7,10,11], that carries two reporter genes encoding Herpes Simplex Virus type 1 thymidine kinase (HSV-tk) enzyme and human somatostatin receptor subtype 2 (sst$_2$). The HSV-tk gene is widely used in suicide gene therapy studies[12,13]. Expression of HSV-tk in the target tissue leads to the production of the enzyme thymidine kinase (tk), which phosphorylates, for example, the prodrug ganciclovir (GCV). Phosphorylated forms of GCV are incorporated into the cellular DNA, followed by inhibition of DNA synthesis and thus leading to tumor cell death[14]. Monitoring of HSV-tk gene expression can be achieved using various radiolabeled nucleoside analogs, including ^{123}I or ^{124}I labeled 1-(2'-deoxy-2'-fluoro-1'-β-D-arabinofuranosyl)-5-iodo-uracil (FIAU)[15,16], 1-(2'-deoxy-2'-fluoro-1'-β-D-arabinofurasyl)-5-methyl-uracil (FMAU)[17], (E)-5-(2-iodovinyl)-2'-fluoro-2'-deoxyuridine (IVFRU)[18], 1-(2'-deoxy-2'-fluoro-1'-β-D-ribofuranosyl)-5-iodo-uracil (FIRU)[19] or ^{18}F-labeled 9-(4-fluoro-3-hydroxy-methyl-butyl)guanine (FHBG)[20]. These compounds are

specifically phosphorylated by HSV-tk in the same way as GCV and consequently trapped in the cell interior.

The second transgene in the $Ad5.tk.sst_2$ vector is the sst_2-encoding gene. Since the discovery of the frequent overexpression of somatostatin receptors (sst) on diverse tumor types, radiolabeled somatostatin analogs that bind to sst on tumors have been developed for imaging and therapeutic application. Examples of sst targeting peptides currently being used in the clinic include [DTPA]octreotid [21], [DOTA,Tyr^3]octreotide[22], DOTA-lanreotide[23] and [DOTA^0,Tyr^3]octreotate[24]. Sst imaging and therapy are mostly being performed in patients with neuroendocrine tumors, because of the high expression level of receptors on these tumors. Other sst-positive tumors can be visualized and treated as well, provided that the accumulation of the radiolabeled sst analog in the tumor is high enough[25]. The above mentioned peptides can be used for peptide receptor radionuclide therapy (PRRT) when they are labeled with therapeutic radionuclides that emit β-particles such as ^{177}Lu or ^{90}Y, that have a higher energy and a longer particle range compared to γ-emitters used for imaging.

Previously we reported on the high expression of both sst_2 and HSV-tk after viral infection of human glioma cell lines *in vitro*[7]. In the present study we aimed to non-invasively image gene expression, i.e. both sst_2 and HSV-tk, using [^{99m}Tc-N$_4$$^{0-1}$,Asp^0,Tyr^3]octreotate ([^{99m}Tc] Demotate 2)[26] and [^{123}I]FIRU[19], respectively, *in vivo*. We used human U87MG glioma tumor cells in this study that originally express neither sst_2 nor HSV-tk. Following intra-tumoral viral infection of U87MG tumor-bearing mice, we performed *in vivo* imaging, quantification and longitudinal expression studies using a novel animal SPECT/CT platform with high resolution and sensitivity and *in vitro* and *ex vivo* autoradiography. In addition, we determined the pattern of gene expression in order to investigate whether or not both genes were expressed simultaneously after viral infection.

Materials and methods

Cell Culture

The U87MG human glioblastoma/astrocytoma tumor cell line was purchased from the American Type Culture Collection (Manassas, Virginia). The CA20948 rat pancreatic tumor cell line was originally induced by azaserine[27,28]. The 9L and 9L-tk rat gliosarcoma tumor cell lines were kindly provided by Dr. K.M. Hebeda (Dept. of Experimental Neurosurgery, Free University Hospital Amsterdam, The Netherlands). 9L-tk was stably transfected with the HSV-tk gene under G418 selection[29]. CA20948 and 9L-tk tumor cells were used as positive controls for sst_2 and HSV-tk gene expression, respectively, while 9L was used as a negative control for HSV-tk gene expression.

CA20948 cells were cultured in Dulbecco's modified Eagle's medium (DMEM, Gibco, Breda, The Netherlands) supplemented with 2 mM glutamate (Gibco), 1 mM sodium pyruvate

(Gibco) and 0.1 mg/l fungizone (Gibco). 9L and 9L-tk were both grown in DMEM, the latter supplemented with 0.25 mg/ml G418 (Gibco). U87MG were grown in modified Eagle's medium (MEM, Gibco) supplemented with 0.1 mM non-essential amino acids (Gibco), 2 mM L-glutamine (Gibco) and 1 mM sodium pyruvate. All media were also supplemented with 10% heat-inactivated fetal bovine serum (Gibco) and 50 IU/ml penicillin/streptomycin (Gibco). All cells were cultured in a humidified atmosphere at 37ºC containing 5% CO_2.

Radiolabeling with ^{99m}Tc

Demotate 2 stock solution (a kind gift from Dr. Nock and Dr. Maina, Demokritos, Athens, Greece) was prepared by dissolving 300 nmol lyophilized material in 300 μl milliQ and stored in small aliquots at –20°C. The labeling was slightly modified as described earlier[26]. In short, saline solution containing [^{99m}Tc]Na-TcO^{4-} (2.5-4 GBq ^{99m}Tc/ml) was eluted from a commercial ^{99}Mo/^{99m}Tc generator (Ultratechnekow, Tyco Healthcare, Petten, The Netherlands). Two μl of the stock solution was mixed with 50 μl 0.5 mol/l Na_2HPO_4 (pH 11.5–12), 5 μl 0.1 mol/l trisodiumcitrate solution, 420 μl eluate (range 900–1500 MBq ^{99m}TcO^{4-}) and 10 μL of freshly prepared $SnCl_2$ solution (2 mg/ml $SnCl_2$/ethanol, Sigma, Zwijndrecht, The Netherlands). After a 15 minute (min) incubation at room temperature (RT), the pH was adjusted to 7-8 by addition of 10 μl 1 mol/l HCl, and finally 50 μl ethanol was added.

Radiolabeling with ^{111}In

^{111}InCl$_3$ was purchased from Tyco Healthcare (Petten, The Netherlands). [DOTA^0,Tyr^3]octreotate was labeled with ^{111}In as previously reported[30]. In order to prevent oxidation and radiolysis quenchers such as ascorbate (Bufa BV, Uitgeest, The Netherlands), ethanol and gentisic acid (Tyco Health Care, Petten, The Netherlands) were added prior to radiolabeling[31]. After cooling the samples, 10 μl 4 mM DTPA was added.

Commercially available [DTPA^0]octreotide (OctreoScan) kits were obtained from Tyco Health Care and radiolabeled as previously described[7]. The radiochemical purity was tested using instant thin layer chromatography and was determined to be >95%.

HPLC

Chromatographic analysis of [^{99m}Tc]Demotate 2 and [^{111}In-DOTA^0,Tyr^3]octreotate was performed on a Waters Breeze HPLC system (Waters, Etten-Leur, The Netherlands) based on a 1525 binary HPLC pump also connected to a Unispec MCA γ-detector (Canberra, Zellik, Belgium). A Symmetry C$_{18}$ 4.6 • 250 mm 5 μm HPLC column (Waters) was used as stationary phase, whereas the eluent system consisted of 0.1% TFA in H_2O (solvent A) and methanol (solvent B) applying the following gradient protocol: 0-2 min 100% A (flow rate 1 ml/min), 2-3 min 55% B, 3-30 min 65% B (flow rate 0.5 ml/min), 30-38 min 100% B (flow rate 1 ml/min), 38-40 min 100% B (flow rate 1 ml/min), 40-46 min 100% A (flow rate 1 ml/min).

Radiolabeling with ^{123}I

^{123}I-NaI was purchased from Cygne (Eindhoven, The Netherlands). FIRU was labeled with ^{123}I as previously published[18]. After the labeling procedure, ethanol in the solution was vaporized by air flow for ten minutes.

Amplification of the viral vector Ad5.tk.sst$_2$

The Ad5.tk.sst$_2$ is a replication incompetent adenoviral vector that contains the sst$_2$ and the HSV1-tk genes[10]. A separate early CMV promoter regulates both genes. Large scale amplification of Ad5.tk.sst$_2$ was carried out on PER.C6 cells as previously described[32] and the virus was titrated by plaque assay on 911 cells, yielding a mean of 3×10^{10} plaque forming units/ml (PFU/ml).

Tumor-bearing animals

The animal experimental protocol was approved by the Institutional Animal Care and Use Committee, and was in compliance with the Guide for the Care and Use of Laboratory Animals. Four to six week-old male NMRI nude/nude mice were purchased from Charles River Laboratories (Sulzfeld, Germany). One week after arrival, the animals were inoculated subcutaneously with CA20948, 9L, 9L-tk or U87MG tumor cells on the left and right flank or on the shoulder, under isoflurane/oxygen anaesthesia (Pharmachemie, Haarlem, The Netherlands). Suspensions of about 10^7 cells in 200 µl Hanks' Balanced Salt Solution (HBSS, Gibco) was prepared.

In vivo viral infection

Three days prior to the *in vivo* experiments, the mice were anaesthetized with inhalation anaesthesia (isoflurane/oxygen, Pharmachemie) and the U87MG tumors (with a volume of 150-300 mm^3) were injected in 4-5 different directions with 50 µl viral solution, containing 1.5×10^9 PFU Ad5.tk.sst$_2$. CA20948, 9L, 9L-tk and additional U87MG tumors were simultaneously injected with saline.

Tracer injection

On the day of the SPECT/CT scan, the animals (n=3 per group) were injected into the penis vein with 200 µl of radiolabeled tracer (either 100 MBq/1 µg [^{99m}Tc]Demotate 2 or 40 MBq/0.6 µg [^{123}I]FIRU) under inhalation anaesthesia. Due to the non-homogeneous expression, we expected a suboptimal SPECT image and decided to inject a high amount of radioactivity in order to visualize the expression of these genes. Biodistribution studies were performed on animals injected with 10 MBq/0.5µg [^{99m}Tc]Demotate 2 and 3 MBq/0.1 µg [^{123}I]FIRU. Both biodistribution studies and SPECT/CT scans were performed at 4 hours post injection (p.i.) of the tracer.

SPECT and CT imaging studies

SPECT and CT imaging were performed with a four-headed multiplexing multi-pinhole NanoSPECT/CT camera (Bioscan Inc., Washington D.C., USA). SPECT was acquired as described previously[6]. Briefly, animals were anaesthetized with a mixture of ketalin and xylazine and were imaged with mouse apertures that comprise a total of 36 1.4-mm-diameter pinholes. The energy-peak of the camera was set at 140 keV for ^{99m}Tc and 159 keV for ^{123}I. An acquisition time of 40 seconds/projection was chosen, resulting in an total acquisition time of 20 min per animal, imaging the whole body. CT scans were performed with the integrated CT-scanner. The tube voltage was set at 45 kVp. An exposure time of 1 second/projection was chosen, imaging with 180 projections/rotation, lasting 6 min for a whole body CT. The SPECT acquisitions were reconstructed iteratively with the HiSPECT software (Bioscan Inc.) and quantification was performed using the MIPtool program (Mediso Ltd., Budapest, Hungary).

Longitudinal study

In an additional study we examined sst_2 expression in Ad5.tk.sst_2 infected U87MG tumors over time. Three animals bearing two U87MG tumors were injected with $2x10^9$ PFU Ad5. tk.sst_2 in one tumors and with saline in the other. Three days after infection, a SPECT/CT scan was made 4 hours after injection of 100 MBq/1 µg [^{99m}Tc]Demotate 2. At days 4 and 6, the animals were injected with 50 MBq/0.5 µg and 100 MBq/1 µg [^{111}In-DTPA^0]octreotide, respectively, and scanned at 4 hours post tracer injection. Quantification of the scans was performed as described above.

Biodistribution and ex vivo autoradiography

Four hours p.i. of the radiolabeled tracer, the animals were sacrificed and blood, tissue samples and tumors were collected and counted in a gamma counter (LKB-1282-Compugammasystem, Perkin Elmer, Groningen, The Netherlands). The tumors were frozen immediately after counting, embedded in TissueTek (Sakura, Zoeterwoude, The Netherlands) and processed for cryosectioning. Ten µm tissue sections were mounted on SuperFrostPlus glass slides (Menzel, Braunschweig, Germany) and exposed overnight to phosphor imaging screens (Perkin Elmer, Boston, USA) in X-ray cassettes (Kodak, Vianen, The Netherlands) for *ex vivo* autoradiography. Three adjacent sections were stored at -20°C and used only after radioactive decay for *in vitro* autoradiography and immunohistochemistry (see below). The exposed phosphor screens were analyzed using a Cyclone phosphor imager and a computer-assisted OptiQuant image processing system (version 03.00, Perkin Elmer).

In vitro autoradiography

In vitro autoradiography was performed as previously described[33] in order to investigate viral gene expression in the infected U87MG tumors. CA20948 and 9L-tk tumors were used

as a positive control for sst_2 and HSV-tk gene expression, respectively. Sections of Ad5.tk.sst_2-infected and saline injected U87MG tumors, CA20948, 9L-tk tumors and rat brain (that also served as a positive control for sst_2-specific binding) were incubated 10^{-10} M [^{111}In-DOTA^0-Tyr^3]octreotate. Blocking experiments were performed with adjacent sections by incubation with 10^{-10} M [^{111}In-DOTA^0,Tyr^3]octreotate with 10^{-6} M octreotide (Novartis, Basel, Switzerland) in the same buffer. After incubation the sections were washed, dried and exposed to phosphor screens overnight. The screens were analyzed as explained above.

Immunohistochemistry

Immunohistochemistry was performed as previously reported[34]. The primary antibody Rabbit-anti-HSV-thymidine kinase (with the courtesy of Dr. W. Summers, Yale University, New Haven, Connecticut) was used in a dilution of 2% and incubated for one hour at RT. After washing, horseradish peroxidase-conjugated secondary antibody swine-anti-rabbit-Ig (DAKOcytomation, Glostrup, Denmark) was incubated in optimal dilution (4%) for 1 hour at RT. Visualization of the specific signal was achieved with H_2O_2 activated diaminobenzidine (DAB) substrate (DAKOcytomation). Nuclei were counterstained using haematoxylin (Fluka Chemika, Buchs, Switzerland).

Statistical analysis

Data are expressed as mean ± SEM. Results were statistically analyzed using two-way ANOVA. Differences were considered statistically significant when P was <0.05. When this was the case, a Bonferroni post-test was performed to compare all groups. All statistical analysis was performed with GraphPad Prism 4.0 program.

Results

Labeling of [^{99m}Tc]Demotate 2, [^{111}In-DOTA^0,Tyr^3]octreotate and [^{123}I]FIRU

Labeling of [^{99m}Tc]Demotate 2 could be performed up to a specific activity (SA) of 250 MBq ^{99m}Tc per nmol [^{99m}Tc]Demotate 2 and a radiochemical purity (RCP) of >80% (range 80-87%, n=6), with no significant reduction of ^{99m}Tc-incorporation or reduction in RCP (HPLC results are not shown). Increase in amount or multiple additions of SnCl$_2$ or prolongation of the reaction time did not result in an increase of ^{99m}Tc-incorporation or RCP.
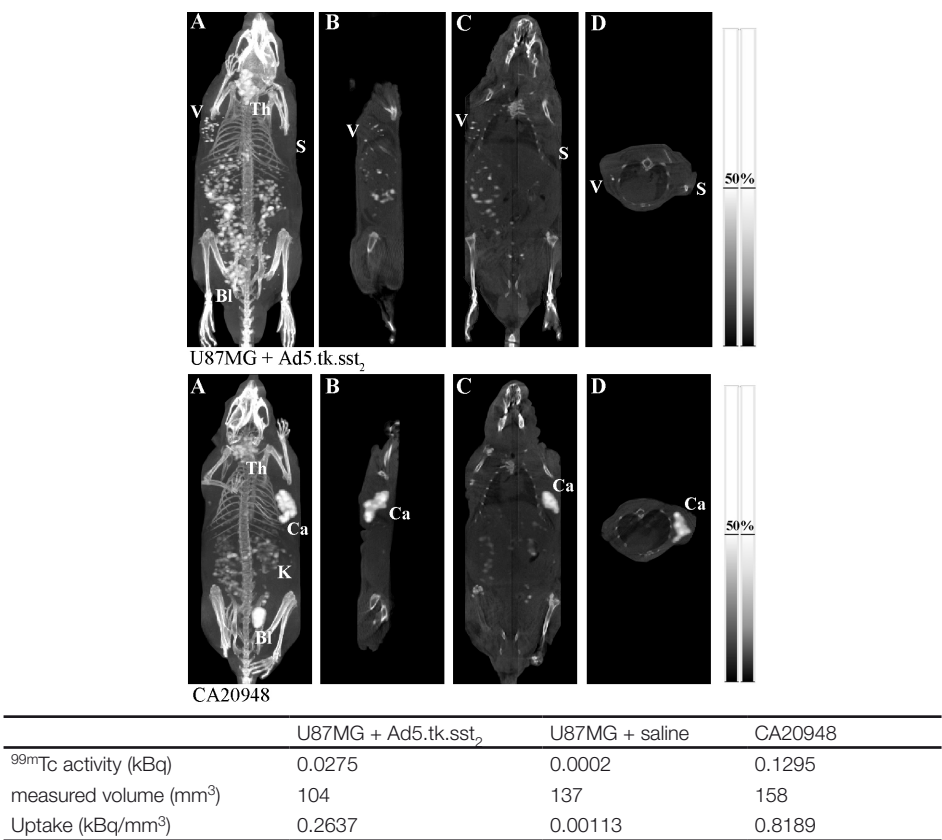
The incorporation of ^{111}In was >95%. The mean SA of [^{111}In-DOTA^0,Tyr^3]octreotate was 144 MBq/nmol and the mean SA of [^{111}In-DTPA^0]octreotide was 139 MBq/nmol.

The mean labeling yield of [^{123}I]FIRU was 38% (0.89 MBq/nmol). No purification steps were necessary, due to high radiochemical purity of >97%[35].

Animal SPECT/CT imaging studies

Fig. 1 shows two examples of SPECT/CT images of animals injected with [^{99m}Tc]Demotate 2. Visually, the saline-injected U87MG tumor showed no [^{99m}Tc]Demotate 2 uptake, while accumulation of the radiopharmaceutical was found in Ad5.tk.sst$_2$-infected U87MG tumors. The quantification results showed 200 times more radioactivity in the Ad5.tk.sst$_2$ infected tumor than in the saline injected tumor. Furthermore, the radiolabeled tracer was not homogeneously distributed throughout the Ad5.tk.sst$_2$-infected tumor probably because the virus did not spread within the tumor tissue. The CA20948 sst$_2$-positive tumor, used as a positive control, showed a higher and more homogeneous uptake compared to the viral

	U87MG + Ad5.tk.sst$_2$	U87MG + saline	CA20948
^{99m}Tc activity (kBq)	0.0275	0.0002	0.1295
measured volume (mm^3)	104	137	158
Uptake (kBq/mm^3)	0.2637	0.00113	0.8189

Fig. 1 Animal SPECT/CT scans. The upper panel shows a mouse bearing one Ad5.tk.sst$_2$ infected U87MG tumor and one saline-injected U87MG tumor. The lower panel shows a sst$_2$-positive CA20948 tumour-bearing mouse. Both where scanned 4 hours p.i. of 100 MBq (1 μg) [^{99m}Tc]Demotate 2. Maximum intensity projection images (A), sagittal (B), coronal (C) and transversal (D) slices are shown at the height of the tumor. Images are representative examples of n=3 animals per group. Grey scale = CT image, Color scale = SPECT image, slice thickness=0.30 mm. (Th=thyroid, Bl=bladder, K=kidney, V=viral-infected U87MG tumor, S=saline-injected U87MG tumor, Ca=CA20948 tumor). The table shows quantification results of these images. See Color Figures, p. 158.
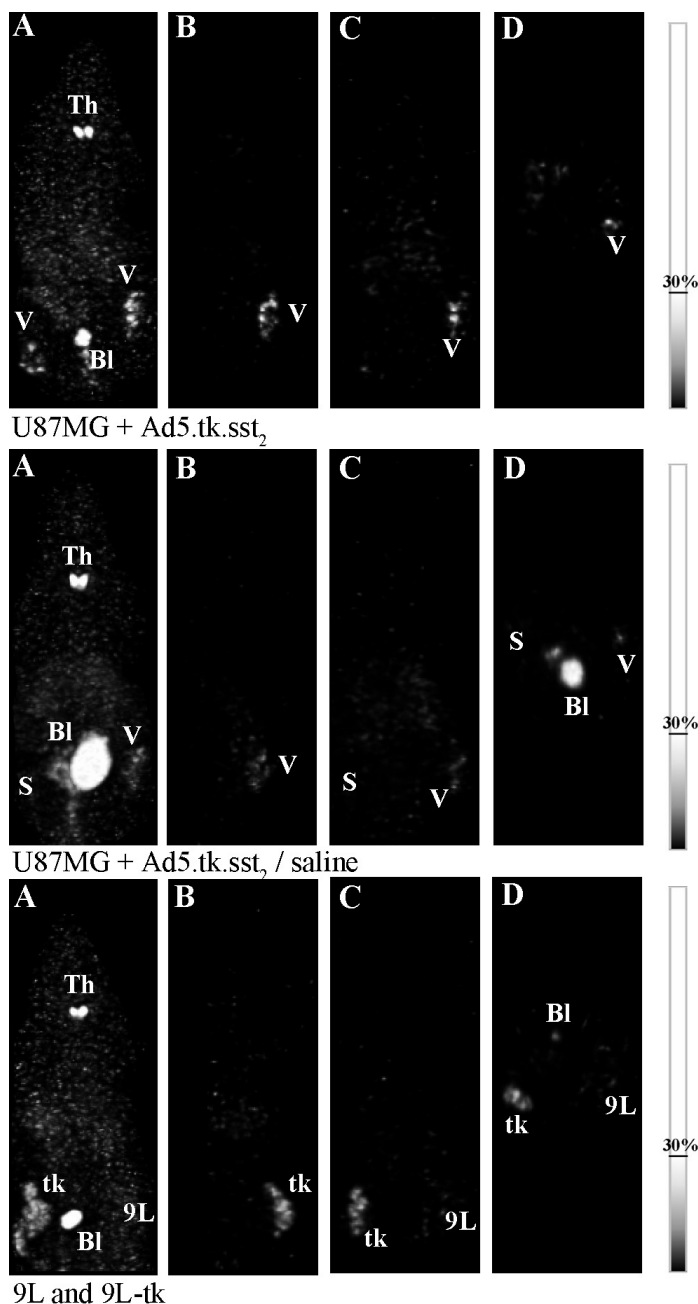
U87MG + Ad5.tk.sst$_2$

U87MG + Ad5.tk.sst$_2$ / saline

9L and 9L-tk

Fig. 2 Animal SPECT scans of Ad5.tk.sst$_2$ infected or saline injected U87MG and 9L-tk/9L tumor bearing mice injected with 40 MBq/0.6 μg [^{123}I]FIRU, 4 hours p.i. of the radiolabelled tracer. Whole body images (A), coronal (B), sagittal (C) and transversal (D) slices are shown at the height of the tumor, slice thickness=0.30 mm. Images are examples of n=3 animals per group. (Th=thyroid, Bl=bladder, V=viral-infected U87MG tumor, S=saline injected U87MG tumor, tk=9L-tk tumor, 9L=9L tumor). See Color Figures, p. 159.
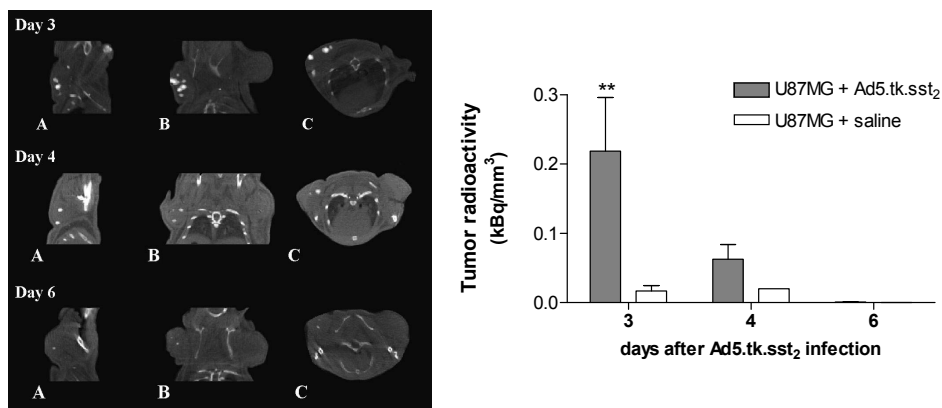
Fig. 3 Longitudinal study in a mouse bearing one Ad5.tk.sst$_2$ infected and one saline injected U87MG tumor. On day 3, 4 and 6 after infection the mouse was injected with either 100 MBq/1 µg [^{99m}Tc] Demotate 2 (on day 3) or [^{111}In-DTPA^0]octreotide (on days 4 and 6); SPECT and CT images were made. SPECT images are shown at the height of the tumor, slice thickness=0.30 mm. The graph shows the quantification results of at least n=2 animals. (sagittal (A), coronal (B) and transversal (C) slices are shown). Data is expressed as mean ± SEM kBq/mm^3. ** P<0.01. See Color Figures, p. 160.

infected tumor. In addition, these SPECT/CT images showed accumulation of radioactivity in the thyroid, bowel, liver, kidneys and bladder.

Uptake of [^{123}I]FIRU was found in Ad5.tk.sst$_2$-infected tumors, as shown in Fig. 2. No CT acquisition was made of these animals. 9L-tk tumors, serving as a positive control for HSV-tk expression, showed high radioactivity while the radioactivity in saline injected U87MG and 9L tumors, that do not express viral tk, was not above background. Thyroid, bladder and to a lesser extent liver also showed some accumulation of radioactivity in these animals.

Longitudinal study

The results of longitudinal imaging of Ad5.tk.sst$_2$-induced sst$_2$ expression in U87MG tumors are shown in Fig. 3. The images are depicted with the same settings of the color scale and show that the tumoral radioactivity after injection of sst$_2$ analogs decreased over time. Quantification of these images showed that, even though tracer radioactivity decreased, it remained detectable until at least seven days after infection. All SPECT images showed higher radioactivity accumulation in the virally infected tumors than in the saline injected tumors.

Biodistribution

The results of the biodistribution study are summarized in Fig. 4. The mean of four ([^{99m}Tc] Demotate 2) or two ([^{123}I]FIRU) independent experiments was calculated, resulting in at least 5 animals per tracer group. The organ distribution (Fig. 4A) shows a significant higher uptake of [^{99m}Tc]Demotate 2 in liver of viral infected animals than in the saline treated animals. In Ad5.tk.sst$_2$-infected U87MG tumors, we found almost 2% ID/g tumor in animals injected
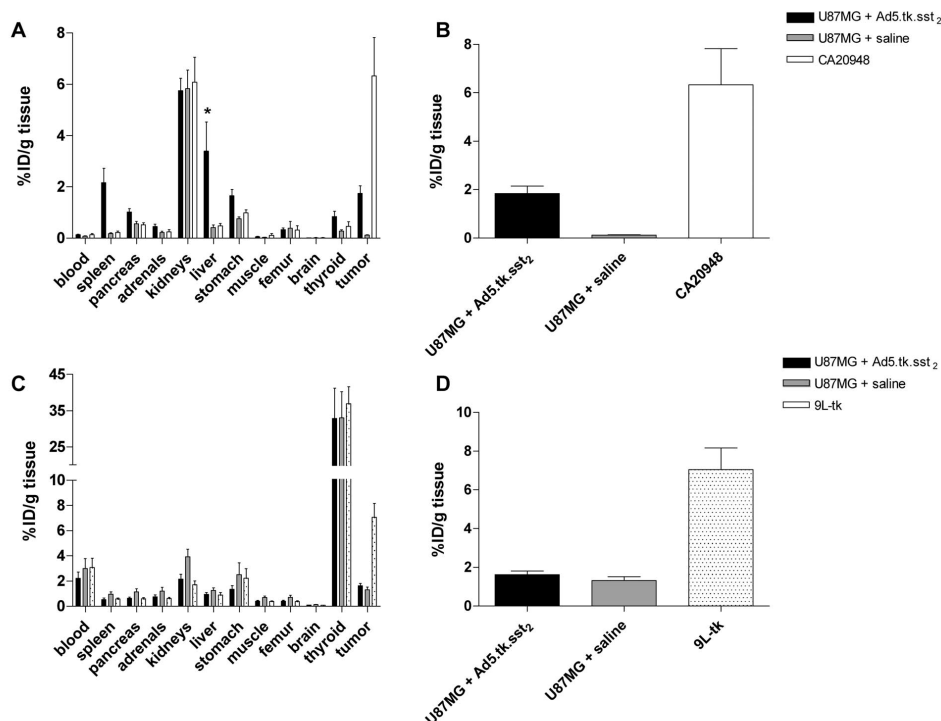
Fig. 4 (A) Biodistribution of [^{99m}Tc]Demotate 2 at 4 hours p.i. (B) Tumour uptake in Ad5.tk.sst$_2$ (n=35) and saline injected U87MG (n=12) bearing mice 4 hours after i.v. injection of 10 MBq/0.5 µg [^{99m}Tc]Demotate 2. CA20948 tumor was used as a sst$_2$-positive control (n=14). (C) Biodistribution of [^{123}I]FIRU at 4 hours p.i. (D) Tumour uptake in Ad5.tk.sst$_2$ (n=10) and saline injected U87MG (n=14) bearing mice 4 hours after i.v. injection of 3 MBq/0.1 µg [^{123}I]FIRU. 9L-tk tumor was used as a HSV-tk-positive control (n=10). U87MG tumors were infected 72 hours prior to the biodistribution with 1.5 x 10^9 PFU Ad5.tk.sst$_2$. All data are expressed as mean + SEM %IA/g tissue. Fig. A and C show results of at least n=5. * P<0.05.

with [^{99m}Tc]Demotate 2 at 4 hr p.i., while the saline-injected U87MG tumors showed only 0.1% uptake at this time point (Fig. 4B). These findings indicate that the uptake of [^{99m}Tc]Demotate 2 in Ad5.tk.sst$_2$-infected U87MG tumors was mediated via sst$_2$ expressed on Ad5.tk.sst$_2$-infected tumor cells.

The biodistribution of [^{123}I]FIRU, however, showed no specific differences between infected and non-infected animals (Fig. 4C). Especially, we could not find a significantly higher uptake in Ad5.tk.sst$_2$ infected tumors compared to that in the saline-injected controls (Fig. 4D). The uptake of [^{123}I]FIRU in HSV-tk-expressing cells was comparable to that of [^{99m}Tc]Demotate 2 in sst$_2$-expressing tumors (1.625 vs 1.744 %IA/g tissue, respectively).

Ex vivo and in vitro autoradiography

Fig. 5 shows examples of *ex vivo* autoradiographs of frozen tumor sections at 4 hours after injection of [^{99m}Tc]Demotate 2 (A) or [^{123}I]FIRU (B). We found that the radioactivity distribution

of both tracers was not homogeneous in Ad5.tk.sst$_2$-infected tumors, probably because the virus did not distribute evenly in the tumor. High and more homogeneous tracer radioactivity was found in the CA20948 and 9L-tk tumors, the sst$_2$- and HSV-tk-positive controls, respectively. We did not find an increased uptake in saline-injected U87MG tumors after injection of both tracers, indicating that the uptake of the tracers in the Ad5.tk.sst$_2$-infected tumors was mediated by the expression of the targeted proteins.
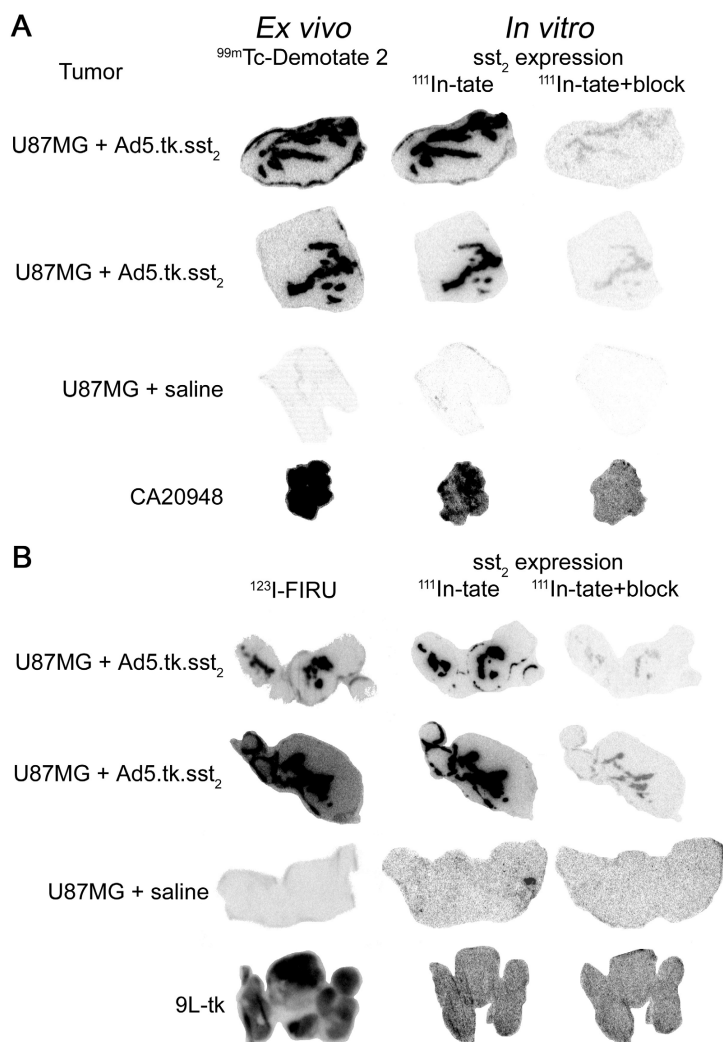
**Fig. 5** *Ex vivo* autoradiography images showing the intra-tumoral distribution of [^{99m}Tc]Demotate 2 (A) and [^{123}I]FIRU (B) as well as *in vitro* autoradiography images showing [^{111}In-DOTA^0,Tyr^3]octreotate binding in the adjacent tumor sections. Two representative Ad5.tk.sst$_2$ infected U87MG tumors, CA20948, 9L-tk and saline injected U87MG tumors are shown for each radiolabelled tracer.

Fig. 5 also shows the *in vitro* autoradiographies of sections adjacent to those used for *ex vivo* autoradiography. These data shows sst_2-mediated binding in these tissues, resembling the pattern of sst_2 and HSV-tk expression in the *ex vivo* autoradiography. In addition, the binding of $[^{111}In\text{-}DOTA^0,Tyr^3]$octreotate could be blocked in all Ad5.tk.sst_2-infected tumor sections and in that of the sst_2-positive controls: rat brain tissues (data not shown) and CA20948. No receptor binding of $[^{111}In\text{-}DOTA^0,Tyr^3]$octreotate was seen in the non-infected U87MG tumors and the HSV-tk-positive control, which do not express sst_2 on their cell membranes.

Two series of tumor sections from different tumor levels revealing the pattern of both $[^{99m}Tc]$Demotate 2 and $[^{123}I]$FIRU radioactivity using *ex vivo* autoradiography are depicted in Fig. 6. Again, it could be shown that sst_2 and HSV-tk genes were not homogeneously expressed following Ad5.tk.sst_2 infection. We found a striped pattern, probably representing the needle tracks of the viral injection.
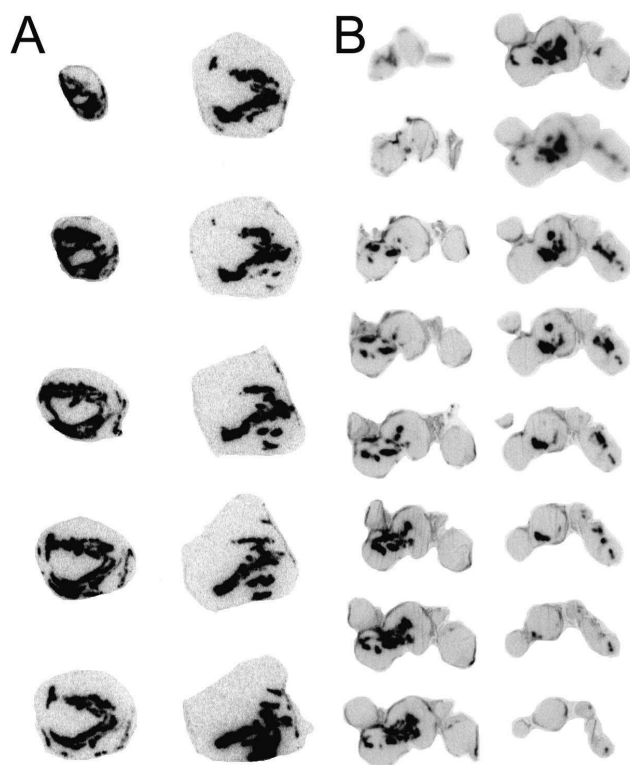
Fig. 6 *Ex vivo* autoradiography of different sections taken throughout two Ad5.tk.sst_2 infected U87MG tumors. Tumor sections show radioactivity of $[^{99m}Tc]$Demotate 2 (A) and $[^{123}I]$FIRU (B). The distance between each section is 250 μm.
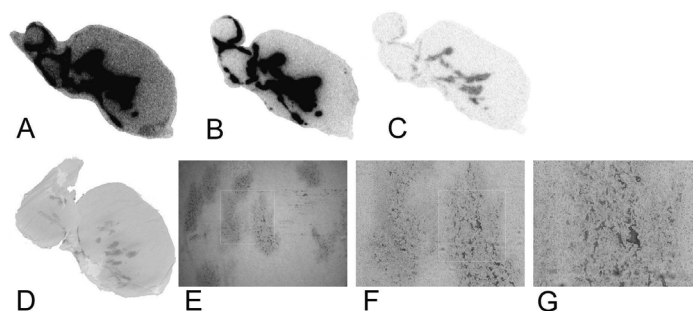
Fig. 7 *Ex vivo* autoradiography four hours after injection of 3 MBq of [^{123}I]FIRU (A), *in vitro* autoradiography using 10^{-10} M [^{111}In-DOTA^0,Tyr^3]octreotate (B), or [^{111}In-DOTA^0,Tyr^3]octreotate plus an excess of octreotide (C) and immunohistochemistry (D-G) staining using rabbit-anti-HSV-tk primary antibody, at different magnifications; D: section overview (no magnification), E: 40x, F: 100x, G: 200x. See Color Figures, p. 160.

Immunohistochemistry

Fig. 7 shows *ex vivo* and *in vitro* autoradiographs and HSV-tk-immunohistochemistry sections of an Ad5.tk.sst$_2$-infected U87MG tumor at increasing magnification. Only U87MG tissue that was infected with Ad5.tk.sst$_2$ showed both HSV-tk and sst$_2$ expression as can be seen from the matching autoradiography and the immunohistochemistry results.

Discussion

One of the challenges of gene therapy in clinical studies is the current lack of quantitative information about the expression of the genes of interest and their products, such as enzymes or receptors, after vector administration to the tumor cells[9]. In this study, we used a novel animal SPECT/CT imaging system and we showed that during pre-clinical studies this can be a most useful tool for non-invasive imaging of reporter genes, such as sst$_2$ and HSV-tk, expressed after Ad5.tk.sst$_2$ infection *in vivo*. We were also able to quantify the radioactivity in the tumors using the imaging data, which was previously shown for rat kidneys [6] and is now shown feasible for tumors as well.

We used a subcutaneous human glioma tumor model in nude mice that was injected with a non-replicating Ad5.tk.sst$_2$ viral vector, followed by intravenous injection three days later of radiolabeled tracers to show transgene expression. The results of *in vivo* SPECT imaging using [^{99m}Tc]Demotate 2 and [^{123}I]FIRU for sst$_2$ and HSV-tk expression, respectively, showed a non-homogeneous uptake of both tracers in the Ad5.tk.sst$_2$-infected tumors. The striped and spotted pattern of the radioactivity of these tracers revealing sst$_2$ and HSV-tk expression can be explained by the fact that the viral vector was injected directly into the tumor and that we used a non-replicating viral vector. This heterogeneous gene expression was also shown by Buchsbaum et al. in an A-427 tumor infected with an adenoviral vector carrying the sst$_2$

gene and after injection of ^{99m}Tc-P2045[36]. In an earlier study we investigated the viral spread in solid tumor tissue and compared single and multiple injections with convection enhanced delivery (CED), i.e. slow infusion of the virus[37]. Using all delivery modalities, spread of the viral vector was low in glioma tumor tissues, although multiple injections resulted in enhanced distribution when compared to CED or single injection.

The results of our longitudinal study indicate that sst_2 expression decreased over time in Ad5.tk.sst$_2$ infected tumors. Hemminki and co-workers were able to detect sst_2 expression for at least 15 days after RGDTKSSTR infection in Hey ovarian cancer cells *in vivo* using a gamma camera[38]. This is longer than in our study, which can be explained by the fact that the Hey tumors were infected twice during these 15 days. We also expect that the use of a replicating viral vector will increase the long-term gene expression in our study. Nevertheless, similar to our findings, Hemminki et al. found that sst_2 expression decreased over time, measured with region of interest analysis.

Biodistribution results showed an increased [^{99m}Tc]Demotate 2 radioactivity in the livers of viral infected U87MG-bearing animals compared to the saline injected animals. This phenomenon was observed in less than half of the animals in this group. It is conceivable that in these animals a blood vessel had been punctured during intra-tumoral infection with subsequent infection of the liver by the viral particles. This, however, has no impact on the amount of radioactivity in the Ad5.tk.sst$_2$ infected tumors (data not shown). In addition, the biodistribution results also show that there is hardly any difference in uptake of radioactivity between infected and non-infected U87MG tumors after injection with [^{123}I]FIRU, while SPECT images do show such differences. Unfortunately, at this stage we cannot explain the discrepancy between these results. One possible explanation could be that we injected a higher amount radiolabeled FIRU mass in the SPECT studies compared to that in the biodistribution studies, because of the higher radioactivity levels needed for SPECT studies. We plan to investigate this phenomenon in more detail in future experiments.

The non-homogeneous expression of reporter genes in the viral infected tumors which was found with SPECT imaging, was confirmed by the *ex vivo* and *in vitro* autoradiographs of Ad5.tk.sst$_2$-infected U87MG tumor sections. This can be one of the explanations of the lower levels of therapeutic efficacy in clinical gene therapy trials[9]. To increase the effectiveness of viral based gene therapy, the need for a more homogeneous transgene expression is evident. Several methods to increase intra-tumoral spread of adenoviruses have been published, including pre-treatment with protease[39] and elastase[40] and the use of relaxin-expressing adenoviruses[41]. Results from these studies show that connective tissue and the extracellular matrix play a role in reducing the viral spread in tumors.

Ex vivo autoradiography also showed that the pattern of both [^{99m}Tc]Demotate 2 and [^{123}I]FIRU uptake corresponded with sst_2 expression according to the adjacent *in vitro* autoradiographs. *In vitro* autoradiography studies were performed with three purposes: 1) to show that uptake of [^{99m}Tc]Demotate 2 was receptor-specific using a blockade with an excess of

unlabeled peptide, 2) to show that the binding pattern of both tracers in these tumor sections was similar and resembled the expression of sst_2 in these tissues because of viral gene expression and not because of inflammation and 3) to show that both sst_2 and HSV-tk were simultaneously expressed in infected tumor tissue. Immunohistochemistry confirmed that the pattern of HSV-tk expression was similar with the pattern of sst_2 expression, indicating that both genes were expressed simultaneously after infection with Ad5.tk.sst_2. We therefore consider that sst_2 expression in these tissues is probably not due to inflammation in the tumor after the viral infection, but due to the viral gene transfer.

In our studies, we found that both genes can be used to visualize the location of gene expression following Ad5.tk.sst_2 gene transfer. Sst_2 imaging can be used when the sst_2 expression in the surrounding tissue is low, while in tissues with high sst_2-expression imaging with HSV-tk substrates will be preferable. It is published that normal human brain tissue shows expression of sst[42] and we therefore recommend that post-infection imaging in GBM tissue would be performed using HSV-tk gene expression. We were able to show that FIRU radiolabeled with ^{123}I is suitable for SPECT imaging. In addition, other nucleosides, such as FHBG or FIAU, can be used for visualization of HSV-tk expression in sst_2-rich areas. While FIAU is not known for crossing the blood-brain-barrier (BBB)[43], this nucleoside can still be used for HSV-tk expression imaging studies when the BBB is disrupted, which is often the case in GBM patients. Depending on the radionuclide, these nucleosides can be used for PET[16] as well as SPECT imaging[44], with high uptake in HSV-tk expressing tissue. Provided that sst_2 expression in the tissue surrounding the tumor is low, radiolabeled somatostatin analogs are our preferred choice for *in vivo* imaging. They have the advantage of high and specific membrane binding and uptake in sst_2-expressing tissue[45], the radiolabeling can be performed routinely at high specific activity[30].

The use of this dual transgene expressing viral vector offers the possibility to apply a combination with both sst_2 radionuclide therapy and HSV-tk/GCV suicide therapy, which is expected to have a higher tumoricidal effect than each of the therapeutic methods alone. Boucher et al. combined GCV treatment with 5-fluorocytosine (5-FC) administration in a double suicide gene therapy modality[46]. They found that the sequential incubation of DU145 human prostate cancer cells with 5-FC and GCV increased cytotoxicity *in vitro*. We plan to perform a combination therapy in U87MG infected tumors *in vivo* with peritoneally injected GCV and systemically injected ^{177}Lu or ^{90}Y labeled [DOTA^0,Tyr^3]octreotate to show improved therapeutic effect when these compounds are used together. In our case, it might be more interesting to use an ^{90}Y-labeled compound in a therapy study, since ^{90}Y emits β-particles with higher energy (2.3 MeV) and longer path length (12 mm) compared to ^{177}Lu (0.49 MeV and 2 mm, respectively). Taken into account the non-homogeneous expression of sst_2 in Ad5.tk.sst_2 infected tumors, it can be expected that more damage to the tumor cells would be induced using ^{90}Y.

Zinn et al. showed simultaneous imaging of both sst_2 and HSV-tk expression in transfected A-427 human non-small cell lung cancer cells using gamma camera imaging[11]. They concluded that this double transgene approach in gene transfer allows dual isotope detection with a gamma camera to show simultaneous *in vivo* monitoring of the expression of more than one transgene. They also found that sst_2 expression imaging *in vivo* using ^{99m}Tc-P2045 showed excellent sensitivity and linearity related to the dose of the adenovirus, which was in contrast with the HSV-tk expression, which was not reliably detected using ^{131}I-FIAU. They state that the HSV-tk system may have inherent problems for *in vivo* imaging due to the difference in delivery to the HSV-tk-expressing cells, compared to sst_2 (diffusion instead of receptor binding and internalization), making the latter more interesting at least for imaging. Our biodistribution results showed that ^{123}I-FIRU in viral-infected tumor tissue was not significantly increased compared to non-infected tissue, indicating that ^{123}I-FIRU is not exclusively taken up in cells that are expressing the HSV-tk gene. These results differ from the results reported by Nanda et al. who found a slightly higher uptake in IG.AdApt. TK infected tumors at 4 hours p.i.[19]. This discrepancy might be caused by a different time period after viral infection (2 days reported by Nanda et al. compared to 3 days in our study). However, we believe that, although the mechanism of delivery is different compared to sst_2 binding and internalization, imaging of HSV-tk expression using ^{123}I-FIRU is feasible *in vivo*.

This study is one of the first in using animal SPECT/CT imaging for the detection and quantification of viral gene expression after Ad5.tk.sst_2 gene transfer in human glioma tumor-bearing mice. We performed viral infections intra-tumorally in U87MG tumors that did not express HSV-tk or sst_2 prior to the introduction of the viruses representing the patient situation. We conclude that intra-tumoral *in vivo* infection using Ad5.tk.sst_2 resulted in the simultaneous and non-homogenous expression of both HSV-tk and sst_2 and that these reporter genes can be used for imaging viral gene expression using radiolabeled HSV-tk and sst_2 substrates. Infected tumors showed only limited long-term expression of transgenes *in vivo*. Non-invasive imaging techniques, such as SPECT/CT, can be applied for monitoring and quantification of gene expression following vector-based gene transfer and subsequent treatment of cancer.

References

1 Massoud TF, Gambhir SS. Molecular imaging in living subjects: seeing fundamental biological processes in a new light. *Genes Dev 2003*; **17:** 545-580.

2 Beekman FJ, van der Have F *et al.* U-SPECT-I: a novel system for submillimeter-resolution tomography with radiolabeled molecules in mice. *J Nucl Med 2005*; **46:** 1194-1200.

3 Schramm NU, Ebel G *et al.* High-resolution SPECT using multipinhole colliation. *IEEE Trans Nucl Sci 2003*; **50:** 315-320.

4 Chatziioannou A, Tai YC, Doshi N, Cherry SR. Detector development for microPET II: a 1 microl resolution PET scanner for small animal imaging. *Phys Med Biol 2001*; **46:** 2899-2910.

5 Ritman EL. Molecular imaging in small animals--roles for micro-CT. *J Cell Biochem Suppl 2002*; **39:** 116-124.

6 Forrer F, Valkema R *et al.* In vivo radionuclide uptake quantification using a multi-pinhole SPECT system to predict renal function in small animals. *Eur J Nucl Med Mol Imaging 2006*; **33:** 1214-1217.

7 Verwijnen SM, Sillevis Smith PA *et al.* Molecular imaging and treatment of malignant gliomas following adenoviral transfer of the herpes simplex virus-thymidine kinase gene and the somatostatin receptor subtype 2 gene. *Cancer Biother Radiopharm 2004*; **19:** 111-120.

8 Surawicz TS, Davis F *et al.* Brain tumor survival: results from the National Cancer Data Base. *J Neurooncol 1998*; **40:** 151-160.

9 Rainov NG, Ren H. Gene therapy for human malignant brain tumors. *Cancer J 2003*; **9:** 180-188.

10 Hemminki A, Belousova N *et al.* An adenovirus with enhanced infectivity mediates molecular chemotherapy of ovarian cancer cells and allows imaging of gene expression. *Mol Ther 2001*; **4:** 223-231.

11 Zinn KR, Chaudhuri TR *et al.* Gamma camera dual imaging with a somatostatin receptor and thymidine kinase after gene transfer with a bicistronic adenovirus in mice. *Radiology 2002*; **223:** 417-425.

12 Rainov NG. A phase III clinical evaluation of herpes simplex virus type 1 thymidine kinase and ganciclovir gene therapy as an adjuvant to surgical resection and radiation in adults with previously untreated glioblastoma multiforme. *Hum Gene Ther 2000*; **11:** 2389-2401.

13 Trask TW, Trask RP *et al.* Phase I study of adenoviral delivery of the HSV-tk gene and ganciclovir administration in patients with current malignant brain tumors. *Mol Ther 2000*; **1:** 195-203.

14 Moolten FL. Drug sensitivity ("suicide") genes for selective cancer chemotherapy. *Cancer Gene Ther 1994*; **1:** 279-287.

15 Tjuvajev JG, Chen SH *et al.* Imaging adenoviral-mediated herpes virus thymidine kinase gene transfer and expression in vivo. *Cancer Res 1999*; **59:** 5186-5193.

16 Jacobs A, Voges J *et al.* Positron-emission tomography of vector-mediated gene expression in gene therapy for gliomas. *Lancet 2001*; **358:** 727-729.

17 de Vries EF, van Waarde A *et al.* [(11)C]FMAU and [(18)F]FHPG as PET tracers for herpes simplex virus thymidine kinase enzyme activity and human cytomegalovirus infections. *Nucl Med Biol 2000*; **27:** 113-119.

18 Wiebe LI, Knaus EE, Morin KW. Radiolabelled pyrimidine nucleosides to monitor the expression of HSV-1 thymidine kinase in gene therapy. *Nucleosides Nucleotides 1999*; **18:** 1065-1066.

19 Nanda D, de Jong M *et al.* Imaging expression of adenoviral HSV1-tk suicide gene transfer using the nucleoside analogue FIRU. *Eur J Nucl Med Mol Imaging 2002*; **29:** 939-947.

20 Green LA, Nguyen K *et al.* A tracer kinetic model for 18F-FHBG for quantitating herpes simplex virus type 1 thymidine kinase reporter gene expression in living animals using PET. *J Nucl Med 2004*; **45:** 1560-1570.

21   de Jong M, Breeman WA *et al.* Comparison of (111)In-labeled somatostatin analogues for tumor scintigraphy and radionuclide therapy. *Cancer Res 1998*; **58:** 437-441.

22   Kwekkeboom DJ, Kooij PP *et al.* Comparison of 111In-DOTA-Tyr3-octreotide and 111In-DTPA-octreotide in the same patients: biodistribution, kinetics, organ and tumor uptake. *J Nucl Med 1999*; **40:** 762-767.

23   Virgolini I, Britton K *et al.* In- and Y-DOTA-lanreotide: results and implications of the MAURITIUS trial. *Semin Nucl Med 2002*; **32:** 148-155.

24   Kwekkeboom DJ, Bakker WH *et al.* [177Lu-DOTAOTyr3]octreotate: comparison with [111In-DTPAo]octreotide in patients. *Eur J Nucl Med 2001*; **28:** 1319-1325.

25   Teunissen JJ, Kwekkeboom DJ, Krenning EP. Staging and treatment of differentiated thyroid carcinoma with radiolabeled somatostatin analogs. *Trends Endocrinol Metab 2006*; **17:** 19-25.

26   Maina T, Nock B *et al.* [99mTc]Demotate, a new 99mTc-based [Tyr3]octreotate analogue for the detection of somatostatin receptor-positive tumours: synthesis and preclinical results. *Eur J Nucl Med Mol Imaging 2002*; **29:** 742-753.

27   Longnecker DS, Lilja HS *et al.* Transplantation of azaserine-induced carcinomas of pancreas in rats. *Cancer Lett 1979*; **7:** 197-202.

28   Bernard BF, Krenning E *et al.* Use of the rat pancreatic CA20948 cell line for the comparison of radiolabelled peptides for receptor-targeted scintigraphy and radionuclide therapy. *Nucl Med Commun 2000*; **21:** 1079-1085.

29   Vincent AJ, Vogels R *et al.* Herpes simplex virus thymidine kinase gene therapy for rat malignant brain tumors. *Hum Gene Ther 1996*; **7:** 197-205.

30   Breeman WP, Van Der Wansem K *et al.* The addition of DTPA to [(177)Lu-DOTA(0),Tyr(3)]octreotate prior to administration reduces rat skeleton uptake of radioactivity. *Eur J Nucl Med Mol Imaging 2003*; **30:** 312-315.

31   Breeman WAP, deBlois EH, Krenning EP. Effects of quenchers on the radiochemical purity of 111In-labeled peptides. *J Nucl Med 2007*; **48, suppl 2:** 73P.

32   Fallaux FJ, Bout A *et al.* New helper cells and matched early region 1-deleted adenovirus vectors prevent generation of replication-competent adenoviruses. *Hum Gene Ther 1998*; **9:** 1909-1917.

33   de Visser M, van Weerden WM *et al.* Androgen-dependent expression of the gastrin-releasing Peptide receptor in human prostate tumor xenografts. *J Nucl Med 2007*; **48:** 88-93.

34   Melis M, Krenning EP *et al.* Localisation and mechanism of renal retention of radiolabelled somatostatin analogues. *Eur J Nucl Med Mol Imaging 2005*; **32:** 1136-1143.

35   Ter Horst M, Nanda N *et al.* [123I]FIRU, a tracer for the 'molecular imaging' of HSV1-tk suicide gene transfer. *Submitted 2007*.

36   Buchsbaum DJ. Imaging and therapy of tumors induced to express somatostatin receptor by gene transfer using radiolabeled peptides and single chain antibody constructs. *Semin Nucl Med 2004*; **34:** 32-46.

37   ter Horst M, Verwijnen SM *et al.* Locoregional delivery of adenoviral vectors. *J Nucl Med 2006*; **47:** 1483-1489.

38   Hemminki A, Zinn KR *et al.* In vivo molecular chemotherapy and noninvasive imaging with an infectivity-enhanced adenovirus. *J Natl Cancer Inst 2002*; **94:** 741-749.

39   Kuriyama N, Kuriyama H *et al.* Protease pretreatment increases the efficacy of adenovirus-mediated gene therapy for the treatment of an experimental glioblastoma model. *Cancer Res 2001*; **61:** 1805-1809.

40   Maillard L, Ziol M *et al.* Pre-treatment with elastase improves the efficiency of percutaneous adenovirus-mediated gene transfer to the arterial media. *Gene Ther 1998*; **5:** 1023-1030.

41   Kim JH, Lee YS *et al.* Relaxin expression from tumor-targeting adenoviruses and its intratumoral spread, apoptosis induction, and efficacy. *J Natl Cancer Inst 2006*; **98:** 1482-1493.

42   Reubi JC, Cortes R *et al.* Distribution of somatostatin receptors in the human brain: an autoradiographic study. *Neuroscience 1986*; **18:** 329-346.

43 Jacobs A, Braunlich I *et al.* Quantitative kinetics of [124I]FIAU in cat and man. *J Nucl Med 2001*; **42:** 467-475.

44 Choi SR, Zhuang ZP *et al.* SPECT imaging of herpes simplex virus type1 thymidine kinase gene expression by [(123)I]FIAU(1). *Acad Radiol 2005*; **12:** 798-805.

45 De Jong M, Valkema R *et al.* Somatostatin receptor-targeted radionuclide therapy of tumors: preclinical and clinical findings. *Semin Nucl Med 2002*; **32:** 133-140.

46 Boucher PD, Im MM, Freytag SO, Shewach DS. A novel mechanism of synergistic cytotoxicity with 5-fluorocytosine and ganciclovir in double suicide gene therapy. *Cancer Res 2006*; **66:** 3230-3237.

PART 5

Summary and Concluding Remarks

Summary and Concluding Remarks

Despite advances in neurosurgery, radiotherapy and chemotherapy, malignant gliomas cannot be cured and each year, 450 people die from this disease in The Netherlands (25,000 deaths per year in the European Union and Northern America). After initial treatment, all malignant gliomas eventually recur. 80% of these tumors recur within 2-3 cm margin of the original tumor on CT/MRI and they only rarely metastasize outside the skull. Nevertheless, due to an infiltrative growth pattern, radical surgical excision with oncological margins is not possible. The locoregional nature of malignant gliomas and their poor prognosis make these tumors excellent models to study gene therapy approaches. An additional advantage is the lack of replication of normal neurons and glial cells, which discriminates tumor cells in the brain from the surrounding normal tissue.

In this thesis, we describe the development of a new replication competent adenovirus driven by a glial fibrillary acidic protein (GFAP) promoter. Furthermore, we present work on the imaging and delivery of adenovirus to brain tumors.

Transcriptional targeting of adenoviral vectors

Conditionally replicative adenoviruses (CRAds) were introduced to improve oncolytic efficacy compared to non-replicating adenoviral vectors. Ideally, viral replication in tumor cells will result in cytolysis and subsequent spread of progeny throughout the tumor. The use of tumor selective replication is achieved through either of two alternative strategies. The first strategy involves the introduction of mutations in viral genes to abrogate the interaction of the encoded proteins with cellular proteins necessary to complete the viral life cycle in normal cells, but not in tumor cells. In the second strategy, a tumor- or tissue-specific promoter controls the expression of an essential early adenovirus gene. GFAP is an intermediate filament that is highly and selectively expressed in glial cells at both the mRNA and protein level. In addition, immunohistochemistry studies have confirmed high expression levels of GFAP protein in malignant gliomas, although the intensity of the staining can be very heterogeneous[1]. This makes the GFAP promoter (called gfa2 promoter) an interesting candidate to employ in a tissue-specific promoter driven CRAd against malignant gliomas.

In **Chapter 2.1** we investigated the possibility of increasing the transcriptional activity of the human gfa2 promoter by inserting one or three additional copies of putative GFAP enhancer regions (A, B and D region). Transfection of a GFAP positive cell line with plasmids containing the GFAP promoter with three additional copies of the enhancer region (gfa2(B)$_3$ and gfa2(ABD)$_3$) revealed respectively 68-fold and 84-fold higher LacZ expression than the parental gfa2 promoter.

We then infected various cell lines with replication-deficient adenoviral vectors, containing the LacZ marker gene, driven by the gfa2 or the enhanced promoters. The latter promoters

gave LacZ expression levels that were approximately 10-fold higher than those with the parental gfa2 promoter, while retaining specificity for GFAP-expressing cells.

The enhanced promoters were also tested in transgenic mice, but surprisingly, no or only very low expression of marker genes was noticed, probably due to toxicity.

Finally, we injected the adenoviral vectors carrying the enhanced promoters into nude mouse brain and showed that LacZ expression was limited to GFAP-positive cells. From this, we conclude that gfa2 enhanced promoters are useful for production of short-term, glia-specific, high expression levels of transgenes in an adenoviral context.

In **Chapter 2.2**, we used the gfa2(B)$_3$ promoters to drive expression of E1A in glia spe-cific CRAd (Ad5-gfa2(B)3-E1). Ad5-gfa2(B)3-E1 was constructed by replacing the nLacZ sequence from the pShuttle plasmid with the adenoviral E1 region.

First, we tested the expression levels of the early adenovirus genes E1A and E1B by Western blotting. Following infection of a GFAP-positive cell line (U251) with Ad5-gfa2(B)3-E1, the expression of E1A and E1B was 75% and 30% respectively of the levels obtained after wtAd5 infection. However, following infection of the GFAP negative cell line SK-BR3 with Ad5-gfa2(B)3-E1, E1A and E1B expression was nearly undetectable.

Secondly, we investigated the efficacy and specificity of Ad5-gfa2(B)3-E1 replication and cytotoxicity in vitro. Infection of a panel of GFAP-positive and GFAP-negative cell lines with Ad5-gfa2(B)3-E1 showed efficient elimination of GFAP positive cells by Ad5-gfa2(B)3-E1, in some cell lines as efficiently as wtAd5, while the elimination was attenuated in GFAP negative cell lines.

Thirdly, in vivo experiments were performed in xenograft bearing nude mice. Treatment of GFAP-positive SNB-19 tumors with Ad5-gfa2(B)3-E1 resulted in significant slowing of tumor growth, although less than after treatment with wtAd5. No such effect was observed in GFAP-negative A549 subcutaneous tumors.

Finally, we showed that the attenuation of the oncolytic efficacy of Ad5gfa2(B)3-E1 *in vivo*, compared to wtAd5, probably resulted from the deletion of E3 in the former. For virotherapy, the conservation of E3 will certainly induce a significant increase in the antitumor efficacy of CRAds[2]. However, as described by Nanda et al.[3] the insertion of Herpes Simplex-thymidine kinase in E3 in a replication competent adenovirus allows ganciclovir (GCV) mediated "suicide"gene-therapy resulting in enhanced tumor grow reduction. For safety issues, it is probably advisable to delete E3 and insert a suicide gene. In the future, a recently described immune competent large animal model for GBM[4] may be used to shed more light on the safety and the host immune responses to gene therapy vectors. However, a caveat of this model is that human adenoviruses replicate inefficiently in canine versus human tissue[5,6].

To circumvent this, Smith et al. developed a "syngeneic" canine CRAd based on canine adenovirus type 2 (CAV2)[7].

Delivery of adenovirus

In **Chapter 3** the limited tissue penetration of adenoviral vectors after injection into gliomas tissue is addressed. Tissue or tumor penetration can be improved by using CRAds, as discussed in **Chapter 2.2**. In **Chapter 3**, we attempted to improve tissue penetration further by exploring a new delivery method, convection-enhanced delivery (CED). CED is based on continuous infusion of drugs via intracranial catheters, enabling convective distribution of high drug concentrations over large volumes of the target tissue. In **Chapter 3**, we compared intratumoral distribution of adenoviral vectors following CED with single injection (SI) versus multiple injection (4x, MI).

Nude mice bearing subcutaneous glioma xenografts were injected with replication deficient adenoviruses carrying the human somatostatine receptor subtype 2 (sst_2) marker gene (Ad5.tk.sstr) by CED, MI or SI. Three days later, the radiolabeled tracer (^{99}Tc-Demotate) was injected intravenously to visualize and quantitate sst_2 tracer uptake by γ-camera, biodistribution and *ex vivo* autoradiography measurements.

The radioactivity in the xenografts and volume of distribution following CED were comparable to that after SI. In contrast, MI resulted in a stronger signal on γ-camera and a significant, 2-fold higher accumulation of radioactivity compared to CED and SI. Furthermore, following MI the transduced tumor volume and the maximum area of transduction were increased 2-3 fold compared to both SI and CED. Therefore, in the clinic MI is probably the most effective delivery method for the large adenoviral particles in malignant gliomas.

Imaging of adenovirus mediated transgene expression

1-(2-fluoro-2-deoxy-β-D-ribofuranosyl)-5-iodouracil (FIRU), has previously been described for the non-invasive imaging of HSV1-tk gene expression[8]. The main advantages were: 1) FIRU accumulated as well as or better than the other compounds tested in constitutively HSV-tk expressing cells; and 2) FIRU was less toxic.

In **Chapter 4.1**, we used single-photon emission computed tomography (SPECT) for the imaging properties of ^{123}I -FIRU. Nude mice bearing constitutively HSV1-tk expressing xenografts (9L-tk cells) were injected with ^{123}I labeled FIRU and four hours later the HSV1-tk expression was clearly visualized in the xenografts.

Furthermore, the cytotoxicity of FIRU was compared to related compounds (ganciclovir (GCV), 1-(2-fluoro-2-deoxy-β-D-arabinofuranosyl)-5-iodouracil (FIAU) and 1-(2-fluoro-2-deoxy-β-D-ribofuranosyl)-5-(*E*)-(2-iodovinyl)-uracil (IVFRU). FIRU was 7 logs less toxic than FIAU in HSV1-tk expressing cells and 1-2 logs in non-HSV1-tk expressing dividing cells. In addition, no toxicity was shown in mice and rats receiving up to 200 times the projected

clinical dose of FIRU. Although, toxicity of tracer amounts will not be pharmacologically rel-
evant in the clinical setting, these data favor FIRU for imaging of HSV1-tk gene expression.

Lastly, biodistribution and early kinetics studies of FIRU in 9L and 9L-tk tumor bearing mice
showed four hours after injection a maximum tracer uptake of 23 % ID/g tissue in 9L-tk
tumors (range 16.6-32.4 %ID/g), which is high compared to uptake in muscle (<2 %), thyroid
(2.2 %), stomach (6.2 %), blood (<2 %) and brain (<2 %). Early kinetics studies demonstrated
initial phase and terminal phase half-lives of respectively 0.8 h and 1.3 h (blood); 0.1 h and
4 h (muscle); and 0.5 h and 6.7 h (non-HSV1-tk expressing 9L tumor), indicating rapid renal
clearance of the tracer from the body. In 9L-tk tumors, FIRU accumulates for about one
hour, followed by a slower decrease of radioactivity with a half-life of 11.3 h. In summary, the
favorable imaging and toxicity profile make radiolabeled FIRU a promising agent for imaging
of HSV1-tk gene transfer in clinical studies.

In **Chapter 4.2**, we further studied the imaging properties of FIRU following adenovirus
mediated HSV-tk expression. A non-replicating adenovirus expressing the sst_2 receptor as
well as HSV-tk (Ad5.tk.sstr) was injected intratumorally into nude mice bearing s.c. human
glioma xenograft (U87MG). After three-six days, allowing sst_2 and HSV-tk expression, mice
were injected intravenously with either ^{99}Tc-Demotate/[^{111}In-DTPA^0]octreotide or ^{123}I-FIRU
to target sst_2 or HSV-tk respectively. Using SPECT/CT, we could non-invasively image sst_2
and HSV-tk expression. Sst_2 expression could even be imaged and quantified, up to a week
after infection. Although both tracers were clearly imaged it was to a lesser extent than in
non-infected 9L-tk+ xenografts or in the constitutively sst_2 expressing rat pancreatic tumor
xenografts (CA20948). The non-infected 9L-tk+ or CA20948 xenografts showed in contrast
no uptake of ^{99}Tc-Demotate or ^{123}I-FIRU respectively.

Next, we performed *ex vivo* autoradiography on tumor sections to determine the tracer
uptake. We found tracer uptake adjacent to the injection tract instead of the whole tumor as
in the positive controls, explaining the difference. To ensure that the *ex vivo* autoradiography
was induced by virus infected cells, we have performed (after decay of radioactivity) *in vitro*
autoradiography and immunohistochemistry on adjacent tumor sections. These tumor slices
showed corresponding patterns of sst_2 or HSV-tk expression.

Future studies
The optimal animal model to evaluate CRAds would be an orthotopic model in immunocom-
petent animals, allowing for CRAd replication in both the tumor and the host.

Unfortunately, no animal model suits these conditions. To evaluate the oncolytic potency of
CRAds in tumors, vectors are commonly injected into human xenografts in immunodeficient

mice, which are not permissive for human adenoviral replication. Furthermore, to evaluate the toxicity and immunobiology in host tissue, CRAds can be injected into cotton rats. The cotton rat is a rodent species that is semipermissive for human adenovirus and can be used as an animal model to evaluate oncolytic adenoviral vectors[9]. A major limitation of the cotton rat is, however, the lack of a tumor model.

The next step for our group is to construct a gfa2 based CRAd with a therapeutic and imaging gene. Construction of a CRAd expressing both a therapeutic gene as well as an imaging gene is not possible due to lack of space in E3. Since HSV-tk can be used as imaging as well as therapeutic gene, it is probably the most suitable candidate to be cloned into the next generation CRAd (Ad5gfa2(B)3-HSV-tk).

The preclinical evaluation of Ad5gfa2(B)3-HSV-tk in immunodeficient mice bearing human tumor xenografts will provide information on maximal transgene expression and subsequently the best time for "suicide" cell killing. Experiments in cotton rats will provide further information on the biodistribution and the toxicity of the CRAd and on the immune response against it. In addition, HSV-tk/GCV as a fail-safe mechanism to prevent or control systemic spread and replication of the virus can be examined. Depending on these results translation into a clinical trial can be made.

To investigate the future role of CED in gene-therapy delivery, experiments have to be performed in large animal brains instead of mouse xenograft tumors, since this will match the human situation more closely. Furthermore, the role for stereotactic insertion of a catheter to carry out CED and gene-therapy in patients with an inoperable GBM can be reevaluated in a large orthotopic animal model, such as the canine model[4,7].

References

1 Cosgrove M, Fitzgibbons PL *et al.* Intermediate filament expression in astrocytic neoplasms. *Am J Surg Pathol 1989*; **13:** 141-145.

2 Suzuki K, Alemany R, Yamamoto M, Curiel DT. The presence of the adenovirus E3 region improves the oncolytic potency of conditionally replicative adenoviruses. *Clin Cancer Res 2002*; **8:** 3348-3359.

3 Nanda D, Vogels R *et al.* Treatment of malignant gliomas with a replicating adenoviral vector expressing herpes simplex virus-thymidine kinase. *Cancer Res 2001*; **61:** 8743-8750.

4 Candolfi M, Kroeger KM *et al.* Adenoviral-mediated gene transfer into the canine brain in vivo. *Neurosurgery 2007*; **60:** 167-177; discussion 178.

5 Ternovoi VV, Le LP *et al.* Productive replication of human adenovirus type 5 in canine cells. *J Virol 2005*; **79:** 1308-1311.

6 Winters WD, Young RJ. Incomplete human adenovirus replication in canine tumour cells and serological evidence of infections in tumour-bearing canine pets. *J Comp Pathol 1980*; **90:** 197-207.

7 Smith BF, Curiel DT *et al.* Administration of a conditionally replicative oncolytic canine adenovirus in normal dogs. *Cancer Biother Radiopharm 2006*; **21:** 601-606.

8 Nanda D, de Jong M *et al.* Imaging expression of adenoviral HSV1-tk suicide gene transfer using the nucleoside analogue FIRU. *Eur J Nucl Med Mol Imaging 2002*; **29:** 939-947.

9 Toth K, Spencer JF *et al.* Cotton rat tumor model for the evaluation of oncolytic adenoviruses. *Hum Gene Ther 2005*; **16:** 139-146.

Samenvatting

Ondanks ontwikkelingen in de neurochirurgie, radiotherapie en chemotherapie is het niet mogelijk om patiënten met maligne gliomen (o.a. glioblastomen) te genezen. Ieder jaar overlijden hieraan 450 patiënten in Nederland (25.000 sterfgevallen per jaar in Europa en Noord-Amerika). Ondanks initiële behandeling krijgen alle patiënten uiteindelijk een recidief. Bij 80% van hen ligt dit binnen een marge van 2-3 cm van de oorspronkelijke tumor op CT/MRI. Zelden is er sprake van een uitzaaiing buiten de schedel. Vanwege het infiltratieve groeipatroon is radicale chirurgische resectie, met oncologische marges, niet mogelijk. De locoregionale aard van maligne gliomen en de slechte prognose maken deze tumoren tot geschikte kandidaten voor gen-therapie. Een bijkomend voordeel is het ontbreken van replicatie in normale neuronen en gliale cellen, terwijl replicatie wel optreedt bij tumor cellen.

In dit proefschrift wordt de ontwikkeling van een replicatie competent adenovirus onder de controle van een glial fibrillary acidic protein (GFAP) promoter beschreven. Verder wordt ingegaan op nieuwe ontwikkelingen in de verspreiding en beeldvorming (imaging) van adenovirale vectoren in hersentumoren.

Transcriptional targetting van adenovirale vectoren

Conditioneel replicerende adenovirussen (CRAds) zijn geïntroduceerd om de oncolytische effectiviteit ten opzichte van niet-replicerende adenovirale vectoren te verbeteren. In de ideale situatie leidt virale replicatie in een tumorcel tot cel lysis en aansluitend verspreiding van de virale kopieën door de tumor. Er zijn twee strategieën voor het bereiken van tumor selectieve replicatie. De eerste strategie maakt gebruik van het aanbrengen van mutaties in virale genen om interacties tussen virale- en cellulaire eiwitten op te heffen, die essentieel zijn voor het voltooien van een normale virale replicatie cyclus in normale cellen, maar niet in tumor cellen. De tweede strategie betreft een tumor- of weefsel specifieke promoter. Bij deze strategie controleert de promoter de expressie van essentiële vroege adenovirale genen, noodzakelijk voor adenovirale replicatie. GFAP is een intermediair filament dat selectief tot expressie komt in gliale cellen, zowel op mRNA- als op eiwit niveau. Hiernaast hebben immunohistochemische studies aangetoond dat het GFAP eiwit hoog tot expressie komt in maligne gliomen, alhoewel de kleuring erg heterogeen is qua intensiteit[1]. Al met al kan de GFAP promoter een interessante kandidaat zijn om te gebruiken in een CRAd tegen maligne gliomen.

In **hoofdstuk 2.1** onderzoeken we de mogelijkheid om de transcriptie activiteit van de humane gfa2 promoter te versterken door het toevoegen van één of drie extra kopieën van veronderstelde GFAP versterker regionen (A, B en D regionen). Transfectie van een GFAP positieve cellijn met plasmiden, die de GFAP promoter met drie extra kopieën van de versterker regio (gfa2(B)$_3$ en gfa2ABD)$_3$) bevatten, toonde respectievelijk 68- en 84-voudig hogere LacZ expressie ten opzichte van de oorspronkelijke gfa2 promoter.

Vervolgens hebben we diverse cellijnen geïnfecteerd met replicatie deficiënte adenovirale vectoren, waarbij de expressie van het LacZ marker gen onder de controle staat van de gfa2 promotor of één van de versterkte promotoren. De versterkte promotoren gaven LacZ expressie niveaus die ongeveer tien maal hoger waren dan de oorspronkelijke gfa2 promoter, terwijl ze hun specificiteit behielden voor GFAP positieve cellen. De versterkte promotoren werden ook getest in transgene muizen waarbij, tot onze verbazing, geen of alleen lage expressie van marker genen werd waargenomen, waarschijnlijk als gevolg van toxiciteit. Tenslotte hebben we adenovirale vectoren, die versterkte promotoren bevatten, geïnjecteerd in het brein van naakte muizen. Deze experimenten toonden dat LacZ expressie beperkt blijft tot cellen die GFAP tot expressie brengen. Op grond van deze data hebben we de conclusie getrokken dat gfa2 versterkte promotoren geschikt zijn om gedurende een korte periode, glia specifiek en hoge expressie niveaus van transgenen in een adenovirale context te genereren.

In **hoofdstuk 2.2** hebben we de gfa2(B)$_3$ promotor gebruikt om E1A tot expressie te brengen in een glia specifieke CRAd (Ad5-gfa2(B)$_3$-E1). Ad5-gfa2(B)$_3$-E1 werd gemaakt door de nLacZ sequentie te vervangen in de pShuttle door de adenovirale E1 regio. Als eerste hebben we met dit virus de expressie niveaus van de vroege adenovirale genen, E1A en E1B, onderzocht op Western blot. Na infectie van een GFAP-positieve cellijn (U251) met Ad5-gfa2(B)$_3$-E1 werden expressie niveaus van E1A en E1B gemeten. Deze waren, respectievelijk, 75% en 30 % van de waarden die gemeten werden na infectie met wild type Adenovirus serotype 5 (wtAd5, de in de natuur voorkomende vorm van dit adenovirus). Hiernaast werd ook een GFAP-negatieve cellijn (SK-BR3) geïnfecteerd met Ad5-gfa2(B)$_3$-E1 waarna er praktisch geen E1A en E1B expressie waargenomen werd.

Ten tweede hebben we de effectiviteit en specificiteit in replicatie en cytotoxiciteit van Ad5-gfa2(B)$_3$-E1 in vitro onderzocht. Na infectie van een panel GFAP-positieve en GFAP-negatieve cellijnen met Ad5-gfa2(B)$_3$-E1 werden de GFAP-positieve cellen efficiënt geëlimineerd door Ad5-gfa2(B)$_3$-E1, in sommige cellijnen zelfs even efficiënt als door wtAd5, terwijl de eliminatie in GFAP-negatieve cellijnen was verminderd.

Tevens hebben we in vivo experimenten uitgevoerd bij naakte muizen met subcutane tumor (GFAP positief en GFAP-negatief). Behandeling van GFAP-positieve tumoren met Ad5-gfa2(B)$_3$-E1 zorgde voor een significante reductie van tumorgroei, alhoewel minder dan na behandeling met wtAd5. In de GFAP-negatieve tumoren werd dit effect niet waargenomen.

Tenslotte hebben we aangetoond dat het verminderde oncolytische effect van Ad5-gfa2(B)$_3$-E1 ten opzichte van wtAd5 mogelijk verklaard wordt door het ontbreken van de E3 regio in Ad5-gfa2(B)$_3$-E1. Voor virotherapeutische behandeling zal het behoud van de E3 regio

waarschijnlijk resulteren in toename van het oncolytisch effect van CRAds[2]. Hiernaast heeft Nanda et al.[3] beschreven dat de insertie van het Herpes Simplex thymidine kinase gen in de E3 regio van een replicatie competent adenovirus, waarna ganciclovir (GCV) gemedieerde "suicide"gen-therapie volgde, ook geresulteerd heeft in een toegenomen tumorgroei reductie. Vanuit veiligheids perspectief is het vermedelijk raadzaam om de E3 regio te verwijderen en een suicide gen hiervoor in de plaats te zetten. In de toekomst kan een recent beschreven immuun competent groot diermodel voor GBM[4] worden gebruikt om meer inzicht te verkrijgen over de veiligheid en immuun respons van de gastheer op gentherapeutische vectoren. Een kanttekening die bij dit model geplaatst kan worden is dat het humane adenovirus minder efficiënt repliceert in honden- dan in humaan weefsel[5,6]. Om dit probleem te vermijden heeft Smith et al. een syngene honden CRAd ontwikkeld die gebaseerd is op het honden-adenovirus type 2 (CAV2)[7].

Verspreiding van adenovirus (Delivery of adenovirus)

In **hoofdstuk 3** wordt de beperkte weefsel penetratie van adenovirus na injectie in glioma weefsel onderzocht. Weefsel of tumor penetratie kan enerzijds worden verbeterd d.m.v. een CRAd, zoals reeds besproken werd in **hoofdstuk 2.2**. In dit hoofdstuk proberen we de weefsel penetratie te verbeteren door gebruik te maken van een nieuwe verspreidingsmethode, convection-enhanced delivery (CED). CED is gebaseerd op de continue infusie van medicatie via intracraniële katheters, waardoor m.b.v. continue positieve druk gedurende een lange periode een hoge therapie/medicatie concentratie in een groot volume verspreid kan worden over het bedoelde weefsel. In **hoofdstuk 3** hebben we de intratumorale verspreiding van adenovirus via CED vergeleken met enkelvoudige injectie (SI) en meervoudige injecties (4x, MI).

Nadat de subcutane gliale tumoren in naakte muizen een bepaald volume bereikt hadden werden ze geïnjecteerd met een niet-replicerend adenovirus dat het humane somatostatine receptor subtype 2 (sst_2) gen (Ad5.tk.sstr) bevatte m.b.v. de CED, MI of SI injectie methode. Drie dagen later werd een radioactief gelabelde tracer (^{99}Tc-Demotate) intraveneus toegediend om de binding/opname van de tracer aan sst_2 te visualiseren en te kwantificeren m.b.v. γ-camera, biodistributie en *ex vivo* autoradiografie.

De radioactiviteit in de subcutane tumoren en het verspreidingsvolume na CED was vergelijkbaar met SI. In tegenstelling tot SI en CED werd na MI een sterker signaal waargenomen m.b.v de γ-camera en een significante, 2 maal verhoogde stapeling van radioactiviteit gemeten. Tevens werd er na MI in de geïnfecteerde tumor een 2-3 maal groter volume en een groter maximaal verspreidingsoppervlak van het virus waargenomen t.o.v. SI en CED. Hieruit concluderen we dat, in de kliniek, MI waarschijnlijk de meest effectieve manier van verspreiding is van grote adenovirussen binnen maligne gliomen.

Imaging van door adenovirus geïnduceerde transgeen expressie

1-(2-fluoro-2-deoxy-β-D-ribofuranosyl)-5-iodouracil (FIRU), is recent beschreven als tracer voor het niet-invasief imagen van de HSV-tk gen expressie[8]. De belangrijkste voordelen zijn: 1) FIRU stapelt even goed cq. beter dan andere tracers in cellen die HSV-tk op een stabiel niveau tot expressie brengen; en 2) FIRU is minder toxisch.

In **hoofdstuk 4.1**, hebben we single-photon emission computed tomography (SPECT) gebruikt om de imaging eigenschappen van ^{123}I –FIRU te testen. Naakte muizen met subcutane tumoren, die HSV-tk (9L-tk cellen) tot expressie brengen, werden geïnjecteerd met ^{123}I gelabeled FIRU. Vier uur later werden de dieren gescand waarbij de subcutane tumoren duidelijk gevisualiseerd konden worden.

Hiernaast hebben we de cytotoxiciteit van FIRU vergeleken met gerelateerde verbindingen (ganciclovir (GCV), 1-(2-fluoro-2-deoxy-β-D-arabinofuranosyl)-5-iodouracil (FIAU) en 1-(2-fluoro-2-deoxy-β-D-ribofuranosyl)-5-(*E*)-(2-iodovinyl)-uracil (IVFRU). FIRU was 7 log minder toxisch dan FIAU in HSV-tk tot expressie brengende cellen en 1-2 log in cellen die HSV-tk niet tot expressie brengen. In een aanvullend experiment waarbij muizen en ratten tot 200 maal de equivalente klinische FIRU dosis toegediend kregen werd geen toxiciteit waargenomen. Ofschoon de toxiciteit van de toegepaste tracer hoeveelheden niet farmacologisch relevant zullen zijn voor de kliniek pleiten deze gegevens voor FIRU om HSV-tk gen expressie te imagen.

Tenslotte toonden biodistributie en vroege kinetische studies van FIRU bij 9L en 9L-tk tumor dragende muizen, vier uur na injectie, een maximale tracer opname van 23 % ID/g weefsel in 9L-tk tumoren (range 16.6-32.4 %ID/g), welke hoog is vergeleken met opname in spier (<2 %), schildklier (2.2 %), maag (6.2 %), bloed (<2 %) en hersenen (<2 %). Vroeg kinetische studies toonden initiële fase en terminale fase half-waarde tijden van respectievelijk 0.8 h en 1.3 h (bloed); 0.1 h en 4 h (spier); 0.5 h en 6.7 h (9L tumoren die HSV1-tk niet tot expressie brengen), welke duiden op snelle renale tracer klaring. In 9L-tk tumoren, stapelt FIRU zich gedurende een uur, waarna een langzame afname van de radioactiviteit volgt met een half-waarde tijd van 11.3 h. Samengevat: het gunstige imaging en toxiciteits profiel van radioactief gelabeled FIRU maken het tot een veelbelovende tracer voor het imagen van HSV-tk gen expressie in klinische trails.

In **hoofdstuk 4.2**, hebben we de imaging eigenschappen van FIRU verder bestudeerd in een adenovirale context waarbij het HSV-tk gen tot expressie gebracht wordt. Een niet-repli-cerend adenovirus dat zowel de sst$_2$ receptor als HSV-tk tot expressie brengt (Ad5.tk.sstr) werd intratumoraal geïnjecteerd bij naakte muizen die subcutane humane gliale tumoren (U87MG) droegen. Na drie-zes dagen, waarin sst$_2$ en HSV-tk tot expressie gebracht werd in geïnfecteerd weefsel, werden de muizen intravenous geïnjecteerd met ^{99}Tc-Demotate/[^{111}In-DTPA^0]octreotide of ^{123}I-FIRU met als doel sst$_2$ of HSV-tk, respectievelijk. Met behulp

van SPECT/CT waren we in staat om, niet invasief, sst_2 en HSV-tk expressie te imagen. Sst_2 expressie kon zelfs worden geimaged en gekwantificeerd tot een week na injectie. Alhoewel beide tracers duidelijk konden worden gevisualiseerd in de geïnfecteerde tumoren was dit in een mindere mate dan in niet geïnfecteerde 9L-tk+ tumoren (xenografts) of in subcutane rat pancreas tumoren die continu in hoge mate sst_2 tot expressie brengen (CA20948). De niet geïnfecteerde 9L-tk+ of CA20948 tumoren toonden daarentegen geen opname van ^{99}Tc-Demotate of ^{123}I-FIRU, respectievelijk.

Vervolgens hebben we *ex vivo* autoradiografie uitgevoerd op tumor coupes. Hierbij hebben we radioactiviteit opname rondom het naald traject gevonden i.p.v. de gehele tumor, zoals bij de positieve controles. Het verschil bij de SPECT opnames tussen de geïnfecteerde tumoren en de positieve controles kan hiermee worden verklaard. Om er zeker van te zijn dat de waargenomen radioactiviteit bij de *ex vivo* autoradiografie afkomstig is van geïnfecteerde cellen hebben we (na het verval van de radioactiviteit) *in vitro* autoradiografie en immunohistochemie uitgevoerd op naast gelegen coupes. Deze tumoren toonden een corresponderend patroon van sst_2 of HSV-tk expressie.

Toekomstige studies

Het optimale model om een CRAd in te testen is een orthotopisch model bij immuuncompetente dieren, waarbij de CRAd zich kan repliceren in zowel de tumor als de gastheer. Helaas voldoet geen enkel model aan deze condities. Om het oncolytisch vermogen van CRAds te beoordelen worden de vectoren normaal gesproken getest door ze te injecteren in humane tumoren bij immuun deficiënte muizen, die niet ontvankelijk zijn voor humane adenovirale replicatie. Hiernaast kunnen CRAds worden geïnjecteerd in cotton ratten (Sigmodon hispidus) om de toxiciteit en immunobiologie te onderzoeken in gastheer weefsel. De cotton rat is een knaagdier soort dat *semipermissive* is voor het humane adenovirus en kan worden gebruikt als diermodel voor het beoordelen van oncolytische adenovirale vectoren[9]. De grootste beperking van de cotton rat is het ontbreken van een tumor model.

De volgende stap voor onze groep is het construeren van een gfa2 gebaseerde CRAd dat zowel een therapeutisch als een imaging gen bevat. Het probleem waar we hier tegenaan lopen is dat de ruimte in E3 niet groot genoeg is om er zowel een therapeutisch - als imaging gen in te construeren. Aangezien HSV-tk zowel als imaging en als therapeutisch gen kan worden gebruikt is dit waarschijnlijk de meest geschikte kandidaat voor de volgende generatie CRAds (Ad5gfa2(B)3-HSV-tk).

De preklinische evaluatie van Ad5gfa2(B)3-HSV-tk in een immunodeficiënte muis met subcutane humane tumoren kan informatie verschaffen over de maximale transgen expressie en hieruit volgend, de beste tijd voor "suïcide" cel dood. Experimenten in cotton ratten kunnen informatie verschaffen over de biodistribution en toxiciteit van de CRAd en over de

opgewekte immuun respons. Bovendien kan de rol van HSV-tk/GCV als veiligheidsmechanisme ter voorkoming van of als controle bij systemische verspreiding en replicatie van het virus worden onderzocht. Afhankelijk van deze resultaten kan nagedacht worden over de translatie naar een klinische trial.

Om de toekomstige rol van CED in gentherapie te onderzoeken moeten er experimenten uitgevoerd worden in breinen van grote dieren in plaats van subcutane xenografts in muizen, aangezien dit beter overeenkomt met de humane situatie. Tenslotte, de rol voor de stereotactische plaatsing van een katheter in het brein om CED en gentherapie uit te voeren bij patiënten met een inoperabel GBM kan worden geëvalueerd in een groot orthotopisch diermodel, zoals het honden model[4,7].

Referenties

1   Cosgrove M, Fitzgibbons PL *et al.* Intermediate filament expression in astrocytic neoplasms. *Am J Surg Pathol 1989*; **13:** 141-145.

2   Suzuki K, Alemany R, Yamamoto M, Curiel DT. The presence of the adenovirus E3 region improves the oncolytic potency of conditionally replicative adenoviruses. *Clin Cancer Res 2002*; **8:** 3348-3359.

3   Nanda D, Vogels R *et al.* Treatment of malignant gliomas with a replicating adenoviral vector expressing herpes simplex virus-thymidine kinase. *Cancer Res 2001*; **61:** 8743-8750.

4   Candolfi M, Kroeger KM *et al.* Adenoviral-mediated gene transfer into the canine brain in vivo. *Neurosurgery 2007*; **60:** 167-177; discussion 178.

5   Ternovoi VV, Le LP *et al.* Productive replication of human adenovirus type 5 in canine cells. *J Virol 2005*; **79:** 1308-1311.

6   Winters WD, Young RJ. Incomplete human adenovirus replication in canine tumour cells and sero-logical evidence of infections in tumour-bearing canine pets. *J Comp Pathol 1980*; **90:** 197-207.

7   Smith BF, Curiel DT *et al.* Administration of a conditionally replicative oncolytic canine adenovirus in normal dogs. *Cancer Biother Radiopharm 2006*; **21:** 601-606.

8   Nanda D, de Jong M *et al.* Imaging expression of adenoviral HSV1-tk suicide gene transfer using the nucleoside analogue FIRU. *Eur J Nucl Med Mol Imaging 2002*; **29:** 939-947.

9   Toth K, Spencer JF *et al.* Cotton rat tumor model for the evaluation of oncolytic adenoviruses. *Hum Gene Ther 2005*; **16:** 139-146.

Dankwoord

Op de omslag staat zoals gewoonlijk één naam vermeld, maar velen hebben bijgedragen aan dit proefschrift. Bij de verschillende hoofdstukken zijn meerdere personen al bedankt voor hun bijdrage bij het verrichte onderzoek. Bij deze wil ik iedereen bedanken die heeft bijgedragen aan dit proefschrift. Een aantal van hen wil ik in het bijzonder noemen.

Prof. Dr. P.A.E. Sillevis Smitt, beste Peter, als drijvende kracht achter het gentherapie onderzoek bij glioblastomen heb je mij de mogelijkheid gegeven om dit promotieonderzoek uit te voeren. Bedankt hiervoor. Hiernaast heeft je streven naar perfectie, gecombineerd met je enthousiasme en gedrevenheid voor onderzoek geresulteerd in de totstandkoming van dit proefschrift en heeft het tevens een belangrijke bijdrage geleverd aan mijn wetenschappelijke vorming. Je snelle feedback op experimenten en manuscripten zorgde voor een prettige begeleiding.

Prof. Dr. Ir. M. de Jong, beste Marion, bedankt voor de mogelijkheden die je hebt gecreëerd op de afdeling nucleaire geneeskunde. Je input en snelle feedback hebben gezorgd voor een prettige samenwerking.

Dr. H.C.G.M. de Leeuw, beste Bertie, bedankt voor het bijspijkeren van de hiaten in mijn lab kennis. Van "Labtourist" heb je me snel tot "Labexpert" gebracht. Je kennis van de moleculaire biologie heeft enorm bijgedragen aan de kwaliteit van dit proefschrift. Meerdere malen zag je nog brood in door mij verloren gewaande data en moedigde je me aan om mijn eigen ideeën uit te werken. Ik voel me zeer vereerd om je eerste promovendus te mogen zijn.

Hiernaast wil ik de leden van de kleine commissie, de professoren Dirven, Krenning en Hoeben hartelijk danken voor de snelle beoordeling van het manuscript. Beste Rob Hoeben, bedankt voor de nuttige bijdrage bij de interpretatie van de data en de virus productie.

Ik wil ook de overige leden van de commissie bedanken, te weten de professoren Avezaat, Bangma, van den Bent, Kros, Klein en Dr. Scholte, voor het leveren van oppositie tijdens de verdediging. Max Kros en Martin van den Bent, bedankt voor jullie bijdrage tijdens de werkbesprekingen. Jan Klein, bedankt dat je als mijn opleider Anesthesiologie plaats hebt genomen in de commissie. De onderzoekstijd die je me gegeven hebt heeft me vleugels gegeven.

Heel veel dank ben ik verschuldigd aan mijn collega's van het neuro-oncologie lab:

Mark Rodijk, dank voor het vele werk, je gezelligheid, humor en niet te vergeten de lekkere beats. Eric Brouwer, als computer goeroe en hulp bij de laatste experimenten was je een onmisbare schakel in het geheel. Elza Duijm, als kamergenote zorgde je voor een vrolijke noot, ook in tijden dat we lekkage hadden. Pim French, met je sceptische blik zorgde je ervoor dat ik extra kritisch bleef. Esther Hulsenboom, ik kon altijd vertrouwen op je kunde en een complete voorraad op het lab. Mathilde Kouwenhoven, je gedrevenheid om jouw FISH-je te klaren heb ik bewonderd. Theo Luider, bedankt voor de coördinatie van het lab. Jeroen van Kampen, bedankt voor je zoektocht naar GCV-TP, de hooiberg was vrij groot! Arjenne Romeijn bedankt voor je werk achter de schermen. Elize ter Steege, Setareh Shamsili, Ping-Pin Zen, Suzanne van Weelden, Lennard Dekker en Ria van Straten dank ik voor mijn prettige tijd op het lab. Mieke Timmermans bedankt voor de hulp met de immunohistochemie en de perfecte foto.

Alle proefdierexperimenten heb ik uitgevoerd in het CIL bij mijn collega's van het nucleair geneeskunde lab. Ver weg, in de catacomben van de universiteit, hebben jullie je domein. Gelukkig heeft jullie gezelligheid en enthousiasme hier niet onder te lijden!

Ten eerste wil ik Suzanne Verwijnen bedanken. Als collega-onderzoeker hebben we intensief en plezierig samengewerkt. Nadat je me snel en kundig ingewijd hebt in de wereld van de "proefdier- nucleaire geneeskunde" hebben we vele experimenten samen uitgevoerd, hetgeen geleid heeft tot twee mooie boekjes. Gefeliciteerd met je recent behaalde promotie. Bert Bernard, altijd bereid voor overleg en het geven van legio goede adviezen, bedankt voor je positieve kijk op mijn experimenten. Monique de Visser, je gezellige lach fleurde de stilte altijd op. Gefeliciteerd om, net als Suzanne, als moeder je promotie af te ronden. Marleen Nelis, Ria van den Berg, Magda Bijster en Ron Brigoos: bedankt voor de ontspannen tea-breaks en de vele hulp bij de experimenten. Flavio Forrer, thanks for your help. Wout Breeman en Eric de Bloois: de stipte labelingen zorgden altijd voor een spetterend signaal. Ambroos Reijs bedankt voor je helpende hand bij het publicabel maken van de plaatjes.

Natuurlijk wil ik ook mijn paranimfen, Ylian Liem en Timo Baks bedanken. Onze "werkbesprekingen" in de koffiebar hebben gezorgd voor een nog hechtere vriendschap. Lieve Ylian, bedankt voor je statistische hulp, maar vooral voor je gezelligheid en je oprechte interesse. Je promotie komt er ook snel aan! Timo, het onderzoek is net als surfen. Na wat dobberen in de Caribbean, hangen we nu ook in de trapeze met ons hoofd in het water!

Familie de Ronde, bedankt voor jullie rotsvaste vertrouwen.

Lieve ouders en Paulien, bedankt voor de support tijdens mijn studie en onderzoek. Ook al was mijn onderzoek voor jullie abracadabra, jullie luisterend oor en relativeringsvermogen hebben me geholpen om door te zetten naar dit mooie eindresultaat.

Lieve Manon. Het onderzoek is afgelopen! Bedankt voor alle mogelijkheden en hulp die je me gegeven hebt. Je liefde steunde me om mijn promotie af te ronden. Zonder jou was het niet gelukt! Bedankt, ik hou van je.

Sponsoring

Curriculum Vitae

De schrijver van dit proefschrift werd op 20 april 1976 geboren te Enschede. In 1994 behaalde hij het VWO diploma aan het "Kottenpark College" te Enschede. Na het behalen van zijn propedeuse Chemische Technologie aan de Universiteit Twente te Enschede startte hij in 1995 met de studie geneeskunde aan de Erasmus Universiteit te Rotterdam. In 1999 behaalde hij het doctoraal examen en in 2001 het artsexamen cum laude. Datzelfde jaar begon hij als arts-assistent op de afdeling Neurochirurgie in het Erasmus MC te Rotterdam. Van mei 2003 tot en met december 2005 was hij werkzaam op het laboratorium Neuro-oncologie van het Erasmus MC met het onderzoek dat wordt beschreven in dit proefschrift. Na een half jaar gewerkt te hebben als arts-assistent op de Intensive Care van het Erasmus MC is hij sinds juni 2006 werkzaam binnen de Anesthesiologie. Op 1 oktober 2006 is hij gestart met de opleiding tot anesthesioloog in het Erasmus MC.

Publicatielijst

Van den Brink WA, **Ter Horst M**, van den Heuvel A, et al: Brain oxygenation is marginally impaired in experimental closed head injury*. (Thesis van den Brink WA: Head injury, from man to model 2000)*

Van den Brink WA, van Haagen OBHAM, van Rooijen A, **Ter Horst M**, et al.: Secondary hypoxia augments behavioral deficits in experimental closed head injury *(Thesis van den Brink WA: Head injury, from man to model 2000)*

De Leeuw HCGM, Su M, **Ter Horst M**, Iwata S, Rodijk M, Hoeben RC, Messing A, Sillevis Smitt PAE, Brenner M. Increased Glia-Specific Transgene Expression With Glial Fibrillary Acidic Protein Promoters containing Multiple enhancer Elements, Journal of Neuroscience Research 2006;*83*:744-753

Ter Horst M, Verwijnen S, Brouwer E, Hoeben RC, de Jong M, de Leeuw HCGM, Sillevis Smitt PAE. Locoregional Delivery of Adenoviral Vectors, Journal of Nuclear Medicine, 2006;*47*:1483-1489

Brouwer E, Havenga MJ, Ophorst O, de Leeuw B, Gijsbers L, Gillissen G, Hoeben RC, **Ter Horst M**, Nanda D, Dirven C, Avezaat CJ, Goudsmit J, Sillevis Smitt PAE. Human adenovirus type 35 vector for gene therapy of brain cancer: improved transduction and bypass of pre-existing anti-vector immunity in cancer patients, Cancer Gene Ther. 2007;*14(2):*211-9.

Ter Horst M, Brouwer E, Verwijnen S, Rodijk M, de Jong M, Hoeben RC, de Leeuw HCGM, Sillevis Smitt PAE. A Targeting Malignant Gliomas with a Glial Fibrillary Acidic Protein (GFAP)-Selective Oncolytic Adenovirus, Journal of Gene Medicine,2007, *In Press*

Ter Horst, Nanda D, Morin K, Verwijnen V, Kros M, Forrer F, de Jong M, Knaus E, Wiebe L,Sillevis Smitt PAE. [^{123}I]FIRU, a tracer for the 'molecular imaging' of HSV1-tk suicide gene transfer, Submitted

Verwijnen S, **Ter Horst M**, Sillevis Smitt PAE, Hoeben RC, Forrer F, Müller C, Breeman W, Krenning E, de Jong M. Molecular imaging following adenoviral gene transfer visualizes sst_2 and HSV1-tk expression, Submitted
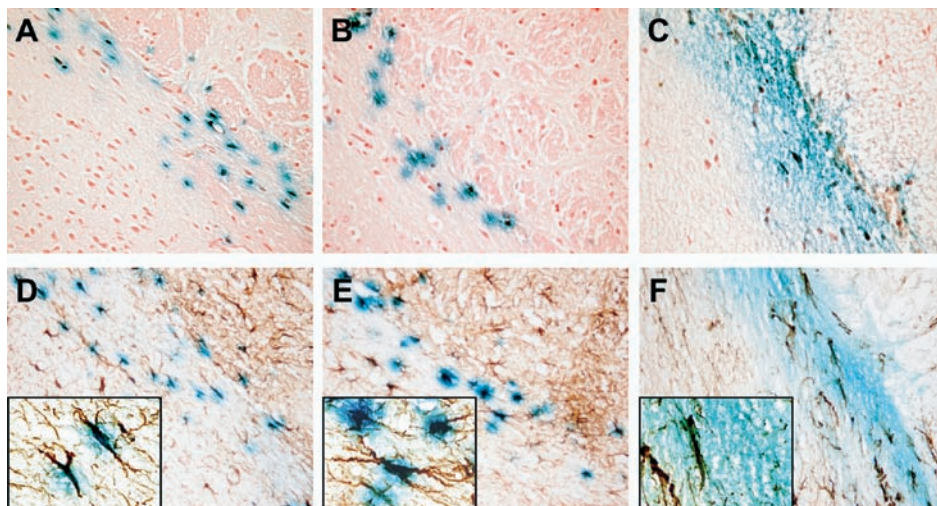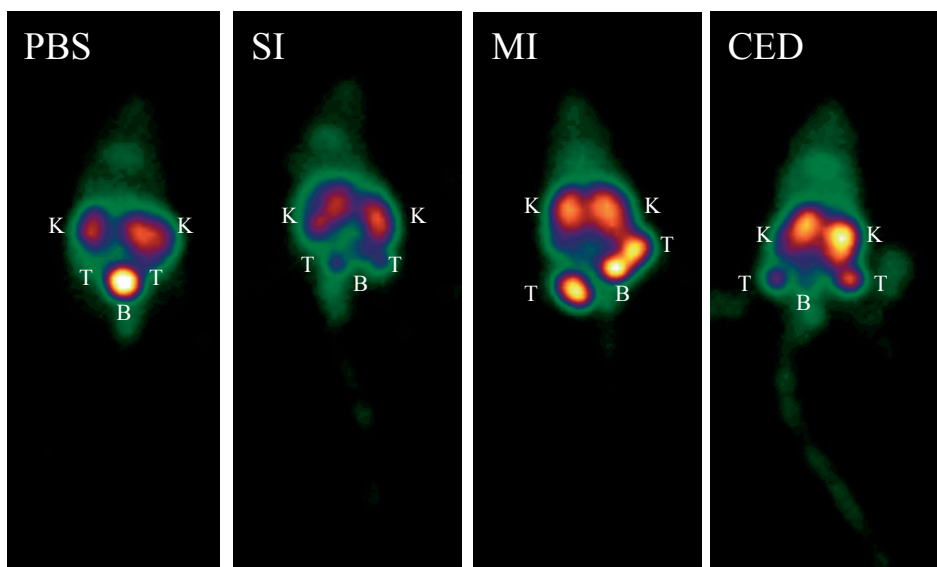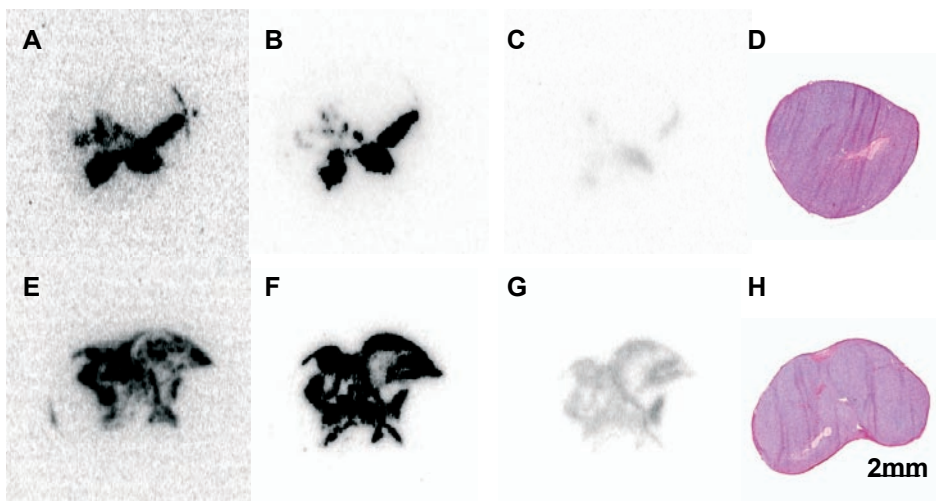
Color figures
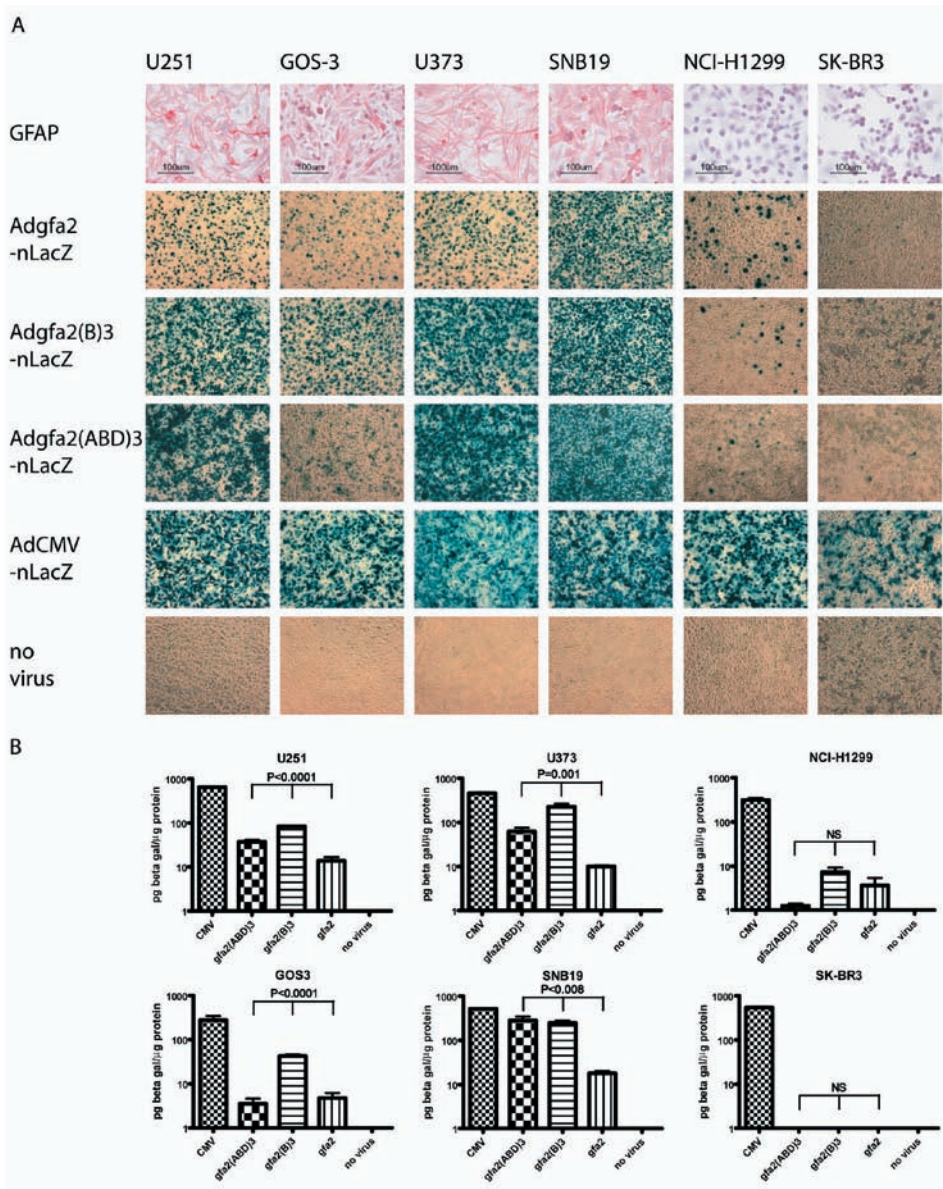
Chapter 2.1, Fig. 4 Activity of gfa2 and enhanced promoters in an adenoviral context. **A:** X-gal staining 48 hours after infection with either adenoviral gfa2 or enhanced promoter constructs at a concentration of 100 pfu/cell. **B:** The β-galactosidase expression, following infection with the adenoviral vectors, was then measured by the Galacto-Light method.

Chapter 2.1, Fig. 5 β-galactosidase expression in mouse brain following injection of adenoviral vectors. Adgfa2nLac (**A, D**), Adgfa2(B)$_3$nLac (**B, E**), or AdCMVnLac (**C, F**) was injected into the basal ganglia of nude mice (1x10^5 pfu). X-gal staining was performed 3 days after injection. Independent sections were either counterstained using nuclear fast red (red; **A, B, C**) or stained using polyclonal anti-GFAP (brown, **D-F**). After injection with both gfa2-based vectors. blue staining is observed in GFAP-positive astrocytes (**D, E**). Only after injection of AdCMVnLac, additional blue staining of neurons is observed (**F**). **A-F:** ×20; insets: ×100 amplification of a selected regions.

Chapter 3, Fig. 2 γ-Camera images of NMRI *nu/nu* mice. Mice bearing U87MG xenografts 3.5 h after intravenous administration of 0.5 µg ^{99m}Tc-Demotate 2 (100 MBq). Three days before imaging, tumors had been injected with PBS (left) or 1.5x10^9 pfu Ad5.tk.sstr administered either with CED, SI, or (4x; MI). Both tumors in each animal received the same treatment. Images are representative and demonstrate that MI results in better tracer uptake than CED and SI. B = bladder; K = kidney; T = tumor.

Chapter 3, Fig. 3 Autoradiographs of Ad5.tk.sstr injected U87MG xenografts by single injection (A-D) or by multiple injection (E-H). Ex vivo autoradiographs were performed 4 h after injection of 99mTc-Demotate 2 (A and E). In vitro autoradiographs were performed on adjacent slides with 125I-DOTA-Tyr3-octreotate (B and F). Binding was displaced by excess unlabeled octreotide (C and G). Adjacent tumor sections were visualized with hematoxilin-eosin staining (D and H). Representative sections demonstrate that the area of viral distribution is larger in sections from tumors injected with MI compared with SI.
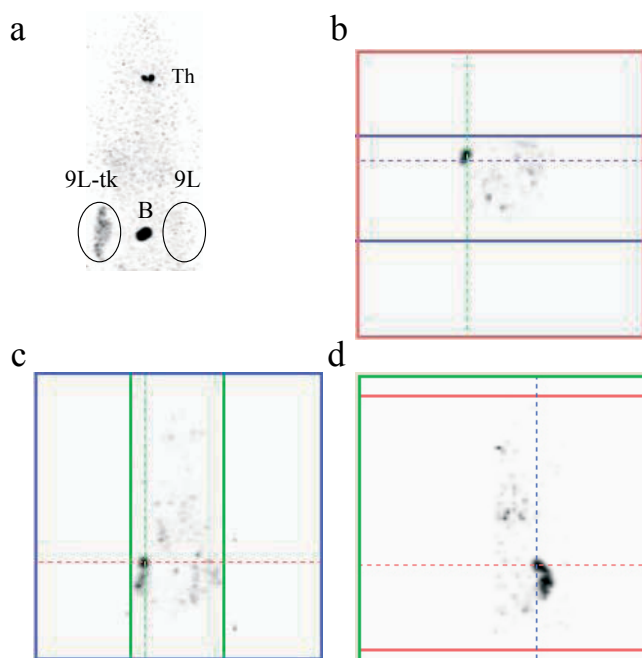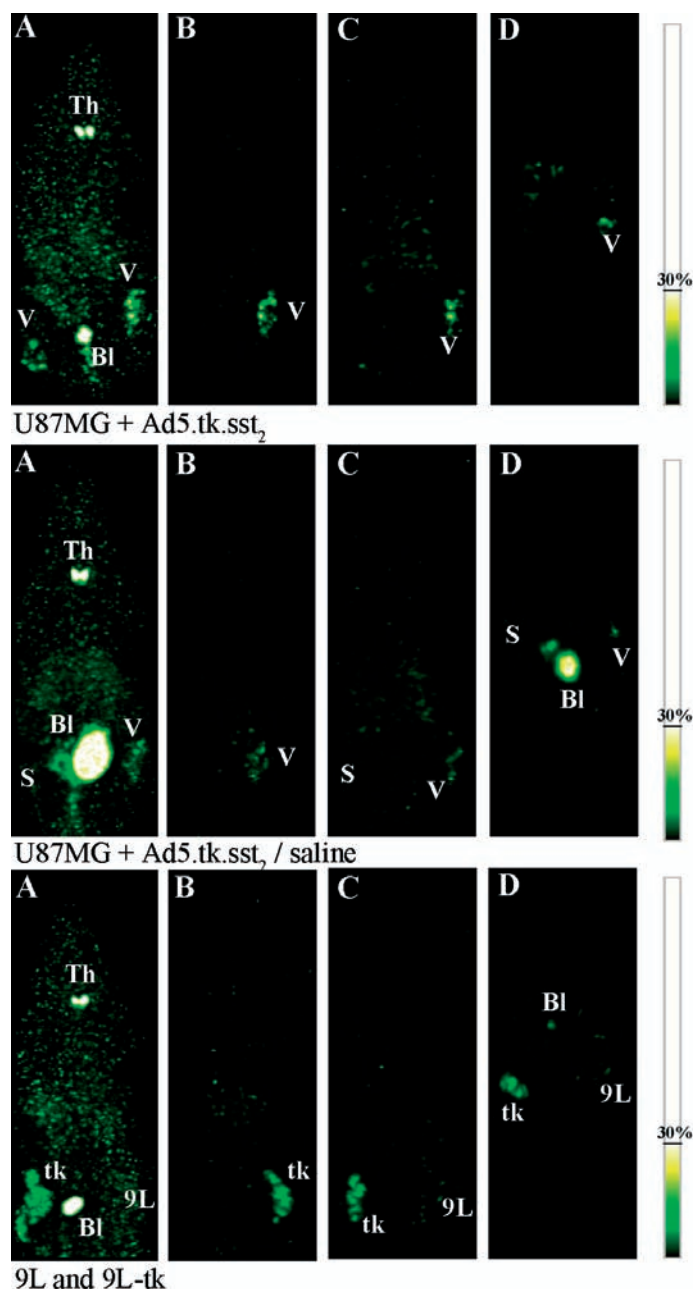
Chapter 4.1, Fig. 4 Small animal SPECT image using [^{123}I]FIRU as reporter probe. 3D-reconstruction of the whole mouse acquired by multipinhole SPECT is shown in (a). The transaxial (b), coronal (c) and saggital (d) slices of the mouse clearly visualize the HSV-tk positive tumor (9L-tk+) in the left flank. The HSV-tk negative tumor (9L) in the right flank remained at back-ground level. Th thyroid; B bladder.
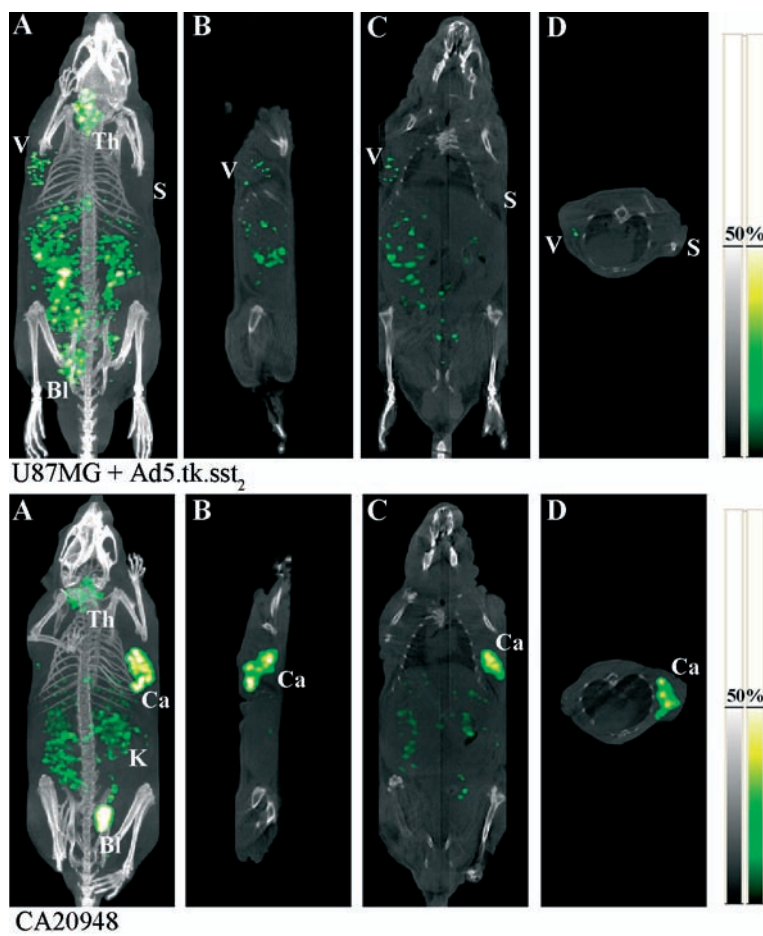
	U87MG + Ad5.tk.sst$_2$	U87MG + saline	CA20948
^{99m}Tc activity (kBq)	0.0275	0.0002	0.1295
measured volume (mm^3)	104	137	158
Uptake (kBq/mm^3)	0.2637	0.00113	0.8189

Chapter 4.2, Fig. 1 Animal SPECT/CT scans. The upper panel shows a mouse bearing one Ad5. tk.sst$_2$ infected U87MG tumor and one saline-injected U87MG tumor. The lower panel shows a sst$_2$-positive CA20948 tumour-bearing mouse. Both where scanned 4 hours p.i. of 100 MBq (1 µg) [^{99m}Tc] Demotate 2. Maximum intensity projection images (A), sagittal (B), coronal (C) and transversal (D) slices are shown at the height of the tumor. Images are representative examples of n=3 animals per group. Grey scale = CT image, Color scale = SPECT image, slice thickness=0.30 mm. (Th=thyroid, Bl=bladder, K=kidney, V=viral-infected U87MG tumor, S=saline-injected U87MG tumor, Ca=CA20948 tumor). The table shows quantification results of these images.

Chapter 4.2, Fig. 2 Animal SPECT scans of Ad5.tk.sst$_2$ infected or saline injected U87MG and 9L-tk/9L tumor bearing mice injected with 40 MBq/0.6 µg [^{123}I]FIRU, 4 hours p.i. of the radiolabelled tracer. Whole body images (A), coronal (B), sagittal (C) and transversal (D) slices are shown at the height of the tumor, slice thickness=0.30 mm. Images are examples of n=3 animals per group. (Th=thyroid, Bl=bladder, V=viral-infected U87MG tumor, S=saline injected U87MG tumor, tk=9L-tk tumor, 9L=9L tumor)
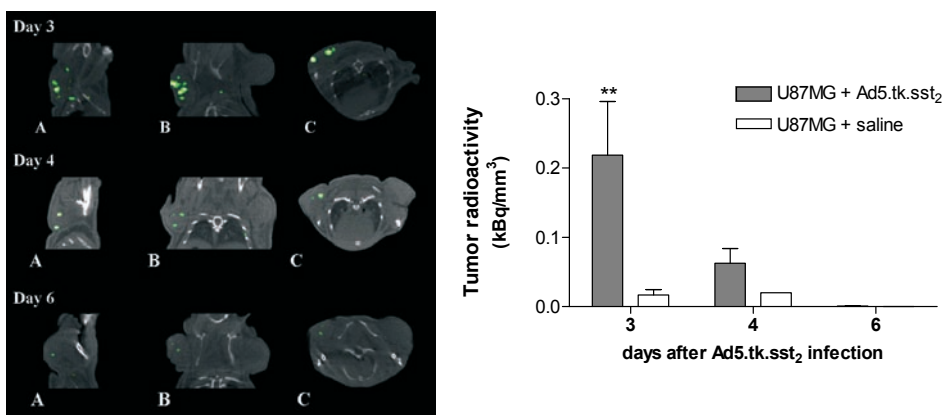
Chapter 4.2, Fig. 3 Longitudinal study in a mouse bearing one Ad5.tk.sst$_2$ infected and one saline injected U87MG tumor. On day 3, 4 and 6 after infection the mouse was injected with either 100 MBq/1 µg [^{99m}Tc]Demotate 2 (on day 3) or [^{111}In-DTPA^0]octreotide (on days 4 and 6); SPECT and CT images were made. SPECT images are shown at the height of the tumor, slice thickness=0.30 mm. The graph shows the quantification results of at least n=2 animals. (sagittal (A), coronal (B) and transversal (C) slices are shown). Data is expressed as mean ± SEM kBq/mm^3. ** P<0.01.
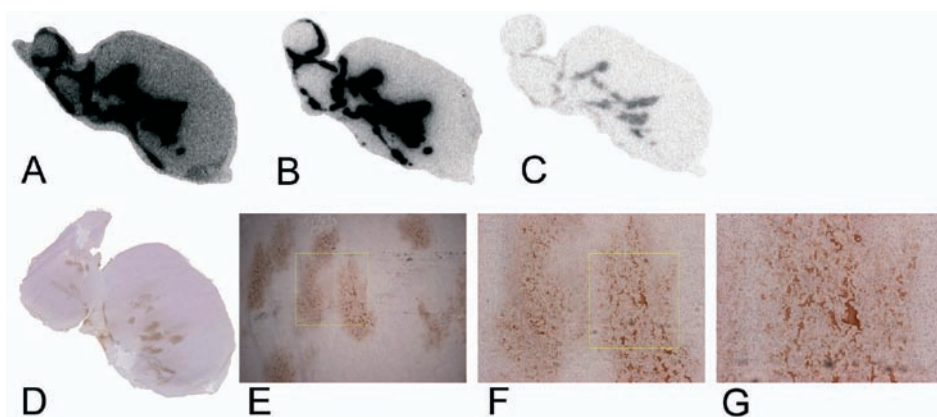
Chapter 4.2, Fig. 7 *Ex vivo* autoradiography four hours after injection of 3 MBq of [^{123}I]FIRU (A), *in vitro* autoradiography using 10^{-10} M [^{111}In-DOTA^0,Tyr^3]octreotate (B), or [^{111}In-DOTA^0,Tyr^3]octreotate plus an excess of octreotide (C) and immunohistochemistry (D-G) staining using rabbit-anti-HSV-tk primary antibody, at different magnifications; D: section overview (no magnification), E: 40x, F: 100x, G: 200x.